Lost Alpha Gamma Rays Monitor (LRM)

Feasibility study and conceptual design for the Lost Alpha Monitor (LAM). Phase I.

S. Soare[1], V.L. Zoita[1], V. Braic[1], R. Costa Pereira[2], T. Craciunescu[1], D. Falie[1], V. Golonorod'ko[3], V. Kiptily[4], I. Lengar[5], V. Yavorskij[3], I. Zychor[7], N. Balshaw[4], D. Croft[4], A. Cufar[5], M. Curuia[1], A. Fernandes[2], J. Figueiredo[6], Y. Krivchenkov[4], N. Lam[4], C. Marren[4], S. Mianowski[7], V. Riccardo[4], K. Schoepf[3], Z. Stancar[5], L. Swiderski[7], V. Thompson[4]

[1]Institute of Atomic Physics (IAP), Bucharest, Romania
[2]Instituto de Plasmas e Fusão Nuclear, Instituto Superior Técnico (IST), Universidade de Lisboa, Spain
[3]University of Innsbruck, Fusion@Österreichische Akademie der Wissenschaften (OEAW), Austria
[4]Culham Centre for Fusion Energy (CCFE), Culham Science Centre, Abingdon, UK
[5]Slovenian Fusion Association (SFA), Jozef Stefan Institute, Reactor Physics Department, Ljubljana, Slovenia
[6]EUROfusion Consortium, JET, Culham Science Centre, Abingdon, UK
[7]National Centre for Nuclear Research (NCBJ), Institute of Plasma Physics and Laser Microfusion (IPPLM), Warsaw, Poland

SUMMARY

The main objective of the Lost Alpha Gamma Rays Monitor (LRM) project is the development of a new diagnostics technique for the investigation of escaping fast particles (including alpha particles) in JET. The method is based on the detection of the gamma radiation induced by the escaping particles on a target external to the plasma. For a beryllium target this reaction is $^{9}Be(\alpha, n\gamma)^{12}C$. The implementation on JET of the Lost Alpha Monitor technique would make possible simultaneous measurement of both confined and lost alphas using the same nuclear reaction and possibly the same detectors.

The project objectives include calculations of alpha particle fluxes on the target, calculations of the target gamma-ray emission, radiation transport calculations, radiation system design, manufacture and installation, development of gamma-ray detectors, design, manufacture and installation of a data acquisition system, and the development of data processing to obtain plasma parameters.

The initial project proposal contained a simple low cost technical solution: insert a beryllium target into the Field-of-View of one of the JET gamma-ray camera (KN3) channels. Detect and analyse the gamma-ray emission using existing diagnostics devices or devices to be developed within another EUROfusion WPJET4 project.

Soon after the start of the LRM project it was realised that in order to implement on JET the simple physical principle of the Lost Alpha Monitor (LAM) one needs a rather complex technically challenging diagnostics equipment. The implementation on JET was further hindered by the existence of large quantities of carbon in the form of the divertor CFC tiles. Fast neutron interaction with this carbon leads to a high level of background gamma radiation of the same energy as that from the (α, Be) reaction inside the plasma.

The report on Feasibility Study and Conceptual Design, Phase I, contains detailed presentations of several technical solutions developed and evaluated for the LAM diagnostics. Two different locations on JET were considered: one on the horizontal KN3 gamma-ray camera in octant one and another on the KJ5 soft X-ray camera in octant four. Two design options were investigated for the KN3 location and four design options for the KJ5 location.

One of the KJ5 design options was developed up to the level of conceptual design. Its evaluation showed that the design and construction of such a system would have needed financial resources several times larger than those allocated to the LRM project.

The LRM project included also a first phase of numerical work done in support of the diagnostics design. The results of the numerical work had a direct impact on the design of the LAM/KA4 diagnostics.

Together with the financial evaluation, the results of the numerical work have also been used to decide upon the continuation of the LRM project.

The EUROfusion WPJET4 Project Board decided on 03.07.2015 to close down the LRM project as no technical solution that could be designed and constructed with the available resources could be found.

CONTENTS

1. Introduction.

1.1 Necessity of the new diagnostics development

Future deuterium-tritium experiments on JET are expected to produce significant population of alpha particles at plasma parameters approaching as closely as possible the ITER values. The confinement of fast particles produced in fusion reactions is of crucial importance for future fusion devices like ITER and DEMO.

Fast particles (including alpha particles) have been studied on JET by a set of diagnostics that provided information both on confined and escaping particles.

The JET diagnostics dedicated to confined alpha particle studies are the KN3 gamma-ray cameras and the KM6 gamma-ray spectrometers [1]. The KN3 gamma-ray cameras (two cameras, vertical and horizontal, with 9 and 10 lines of sight, respectively) provide the spatial distribution of the gamma-ray emission sources in the JET plasma.

The JET plasma is viewed by gamma-ray spectrometers which provide horizontal and vertical measurements of the alpha particles via gamma ray emission spectrometry of the nuclear reaction $^{9}Be(\alpha, n\gamma)^{12}C$ in the plasma core.

The JET diagnostics dedicated at the moment to lost alpha particle studies are the thin foil Faraday cup (FC) array [2] and a scintillator probe (SP) [3].

The Faraday Cup array (KA2 JET diagnostics) detects the current of escaped fast ions at multiple poloidal locations, the detectable energy range for alpha particles being about 1–5 MeV.

The Scintillator Probe (KA3 JET diagnostics) detects lost fast ions and provides information on the lost ion pitch angle and gyro-radius.

A new method to monitor escaped alpha particles has been proposed [4-6] and it was based on $^{9}Be(\alpha, n\gamma)^{12}C$ nuclear reaction which is the same as the one used for the confined alpha particle measurements with JET gamma-ray spectrometers mentioned above. Alpha particles escaping the plasma would bombard a dedicated Be target having suitable geometry and materials placed at a specific location. Gamma-rays from the $^{9}Be(\alpha, n\gamma)^{12}C$ reaction would be detected by a detector placed within a radiation structure that would provide adequate collimation and shielding from both the neutrons and the background gamma radiation.

If the application on JET of this new diagnostics (called KA4 to fit into the standard JET nomenclature) is successful, this technique could be extended for application on ITER and other fusion machines.

Modelling of the escaped fusion alpha-particles is a very important issue for the interpretation of the alpha-particle experiments on JET. The envisaged modelling of the DT alpha source will be based on the 3D in constant-of-motion space Fokker-Planck code FIDIT incorporating fast ion transport induced by Coulomb collisions in JET-like tokamaks with weak TF ripples [7]. The current version of FIDIT is suitable for simulating time-dependent distributions of fast ions in realistic plasma equilibria and for plasma parameters provided by the JET database. The code FIDIT was previously used for predictive modelling of confined and lost alpha particles in JET scenarios with

monotonic and current hole equilibria [8]. FIDIT calculations of the distribution of beam tritons rendered a satisfactory explanation of the current hole effect on the spatial profiles of neutron emission in JET TTE experiments [9] and served as a validation of the code. The simulation of the time evolution of gamma-ray emission generated by alphas with energies above 1.7 MeV in JET TTE, as presented in [10], had been based on the numerical solution of a simplified 3D COM Fokker-Planck equation neglecting the diffusive transport. Both the present version of FIDIT and also a new version, which will include collisional diffusion, are supposed to be used for modelling the time-dependent distributions of beam deuterons produced during D blips in tritium plasmas, as well as of DT fusion alphas in the envisaged DT campaigns.
In addition the Monte-Carlo code DOLFI (computationally effective numerical approach for calculating Distributions of Lost Fast Ions) is to be developed, which will be used for interpretive and predictive modelling the distribution of anomalous loss (additional to first orbit losses) of alpha particles in JET accounting for 3D effects of magnetic fields and the real shape of the plasma facing surface. Such simulations are important for identifying the various mechanisms of alpha particle losses in JET and, on the other hand, for predicting alpha particle heat loads and loss fluences on the first wall.
Neutron and photon radiation transport calculations were proposed to be carried out in order to evaluate the radiation field at the position of the KA4 detector using the MCNP code with large volume radiation sources. MCNP calculations using point radiation sources were proposed to be performed in order to evaluate the shielding factors for the KA4 radiation collimator and shield.

1.2. LRM project evolution

The initial proposal for the Lost alpha gamma-Ray Monitor (LRM) project was based on a rather straightforward upgrade of the KN3 gamma-ray camera (see chapter 4.1). In order to test as soon as possible the LAM/KA4 working principle a prototype phase was proposed in the structure of the LRM project.
Major technical difficulties and high costs that would not allow for the implementation of the new LAM/KA4 technique within the KN3 gamma-ray cameras were identified soon after the start of the project. It was thus decided (at LRM Project Board Meeting of 02.09.2014) that alternative locations for the Lost Alpha Monitor target should be identified and assessed during a feasibility study at the beginning of the project. The best location will be selected and proposed to be developed up to the Conceptual Design phase. The proposal would be subject to a Gate Review that would be held at the end of March 2015.
A very considerable amount of design work carried out during four months (Oct. 2014 – Jan. 2015) has lead to a complete re-structuring of the LRM project, as presented at the WPJET4 Project Board Meeting of 03.02.2015.
A new location for the KA4 diagnostics was identified in octant 4, behind the KJ5 Soft X-ray camera (see chapter 4.2).
The LAM/KA4 octant 4 location had two options defined by the solution for the Be target. A first option would use one of the TAE antenna protection tiles as the KA4

target. The other option would use a dedicated Be target proposed to be located in the Field-of-View (FoV) of the KJ5 channel #4.

The first option 1 has been extensively developed during the four months mentioned above and it had at the end of Jan. 2015 most of the elements of a conceptual design. Further development were considered to be done depending on the outcome of a series of numerical calculations aimed at the comparison of various gamma radiation contributions at the location of the KA4 detector.

The results of the numerical calculations (see chapter 7) have been evaluated during a Project Technical Meeting on March 31st, 2015 [11]. The main conclusion was that the parasitic gamma-radiation due to a fast neutron inelastic scattering reaction within the CFC divertor tiles was expected to be much stronger than the estimated Be target gamma-ray emission.

The work done by IAP on the development of a technique to deal with the high level of parasitic 12C gamma radiation was discontinued. This technique would have made possible the processing of LAM data for levels of parasitic gamma radiation as high as ten times the target radiation [12]. However the implementation of this technique would have lead to a significant change in the project aim as defined in the initial project proposal.

The high value of the carbon-emitted parasitic gamma radiation could be avoided by designing a dedicated Be target placed in one of the KJ5 channels not seeing the CFC divertor tiles. Solutions for the dedicated target have been proposed and evaluated during the following three months, April-June 2015.

The results were presented at the WPJET4 Project Board Meeting of 03.07.2015. Since no technical solution that could be designed and constructed with the available resources could be found the Project Board decided to close down the LRM project.

2. Specific LAM/KA4 project requirements

2.1 LAM/KA4 System Description

A new gamma-ray technique to measure escaped alpha-particles was proposed to be developed within the LRM project. This new JET KA4 diagnostics was initially proposed to be based on the nuclear reaction $^{9}Be(\alpha,\gamma n)^{12}C$ used for the JET gamma-ray spectrometers. Other nuclear reactions have been considered but the work reported here is based on the use of a Be target and gamma-ray emission.

Escaped alpha particles with energies in excess of 1.7 MeV interacting with a bulk Be target will produce 4.44-MeV gamma-radiation. Measurements of the gamma radiation will provide the rate of fast alpha particle losses. Eventually the alpha particle monitor will provide a local value of the lost fast particle flux (number of lost particles per unit surface and time).

A schematic diagram for the LAM principle is presented in Figure 2.1.

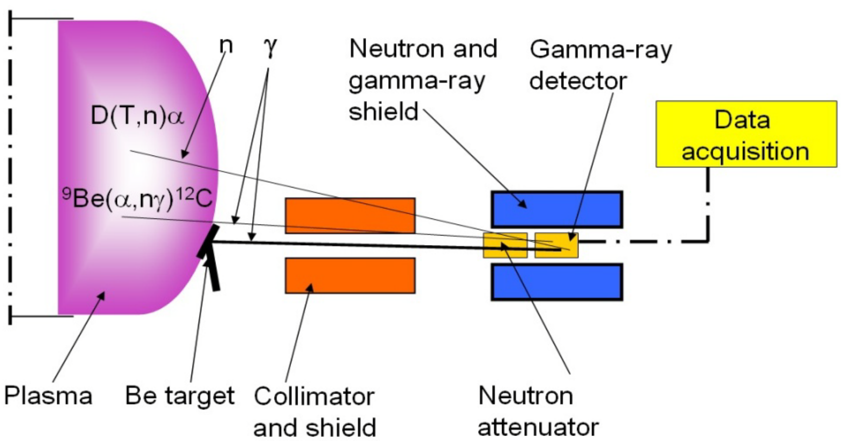

Figure 2.1: schematic diagram for the LAM principle

The JET LAM/KA4 diagnostics shall consist of the following components:

-Lost Alpha Monitor (LAM) radiation system, whose main components are the alpha particle target and the radiation collimator and shield.

-Two gamma-ray detectors

-Data acquisition hardware for two detection channels

-Data acquisition software (KA4 dedicated data acquisition software)

-KA4 data processing procedure to derive local values of the lost particle flux (PPF's)

The design solution for the Lost Alpha Monitor would be selected from a set of solutions developed and evaluated during a Feasibility Study together with dedicated Conceptual Design activities.

The KA4 diagnostics development project was proposed to consist of the following activities:

-Definition of the physical conditions for particle-target interactions as well as radiation transport and detector response. The work would comprise calculations on fast particle orbits, lost particle fluxes, target gamma-ray emission, gamma-ray detector response

-Design, manufacture and installation of the KA4 radiation system (alpha particle target and radiation collimator and shield)

-Design, manufacture and installation of two gamma-ray detectors based on the CeBr3 scintillator

-Design, manufacture and installation of a data acquisition system for the two KA4 gamma-ray detectors

-Procedure for obtaining estimates of lost particle fluxes from the gamma radiation emitted by the monitor target

2.2 Boundary conditions

- Relationship to the JET long term plan

The LRM project milestone schedule is based on the Reference scenario of the JET long term plan [13].

- Interface with the Gamma Ray and Neutron Camera Upgrade

The first option for the Lost Alpha Monitor is to use gamma-ray detectors and associated data acquisition to be developed within the “Gamma Ray and Neutron Camera Upgrade (GCU)” EUROFusion project.

- Interface with the KJ5 Soft X-ray Camera in octant 4

The second option for the location of the LAM diagnostics is behind the KJ5 SXR upper camera (octant 4). The SXR camera radiation shield is to be used as pre-collimator for the KA4 radiation collimator.

- Remote handling compatibility

Some of the components of the LAM radiation system (e.g., target and the target carrier) should be compatible with remote handling.

- Vacuum vessel interface

For some of the components of the LAM radiation system (e.g., target and the target carrier) the design information is to be retrieved from site surveys or provided by JET Drawing Office. Information on target available location may need new surveys and/or site inspection.

2.3 Functional requirements

- Target shape, dimensions and location for efficient lost particle collection

The LAM/KA4 target shape, dimensions and location should be optimised such that it would provide the highest possible value for the target gamma-ray emission.

- Radiation collimation and shielding for LAM detectors

The radiation collimation and shielding for the LAM detectors should be optimised such that it would provide the highest possible value for the signal-to-background ratio.

- Neutron attenuation

Neutron attenuators should be placed in front of the KA4 detectors in order to reduce the value of the fast neutron flux by a factor of approximately 100.

2.4 Technical project requirements

The technical requirements for the LRM project include numerical simulation works related to the estimation of fast particle fluxes, target induced gamma radiation and detector response, development of a Lost Alpha Monitor target from concept design to a device installed on JET. Development of a data processing procedure to extract information on lost alpha particles from the monitor data is also within the scope of the LRM project.

A. Requirements for the LAM radiation system:

- LAM target shape, dimensions and materials
- LAM target location and available space (space envelope)
- LAM radiation collimator and shield: location, dimensions, materials
- Installation and maintenance procedure. Remote handling requirements.

B. Requirements for the lost alpha particles flux calculation

- Particle orbit calculations should provide the energy distribution for the escaping fast particles
- Lost particle flux calculations should provide estimates of the expected fast particle flux at a specified target position.

C. Requirements for the target gamma-ray emission calculation

- Together with item B, above, develop a KA4 synthetic diagnostic based on FIDIT and DOLFI codes

D. Requirements for the KA4 data acquisition

-Develop a data acquisition system for the signals provided by two CeBr3 gamma-ray detectors.

E. Requirements for the radiation (neutron and photon) calculations

- Evaluation of parasitic photon flux at the KA4 detector location;
- Evaluation of neutron flux at the KA4 detector location
- Evaluation of shielding factors for the KA4 radiation collimator and shield

3. Review of proposed LAM/KA4 locations

The initial LRM proposal was based on locating the LAM/KA4 diagnostics on channel #10 of the KN3 horizontal gamma-ray camera. This location had to be abandoned for the reasons presented below (see chapter 4.1.1).

A number of alternative potential locations on JET have been looked for and investigated along the following lines:
- Look for locations equivalent to the position of the 5th (lowest) pylon of the KA2 (FC) diagnostics
- Look for locations of components removed or to be removed before the DT campaign (e.g., Be evaporators)
-Look for locations of diagnostics to be removed before the DT campaigns (e.g., vertical soft X-ray camera, KL7 IR camera)
-Look for the possibility to piggyback on another existing diagnostics (e.g., upper horizontal soft X-ray camera)

The possibility of finding a location that would not need a dedicated Be target was also investigated at length, e.g.:
-Look at the gamma-ray emission from the lower part of an outer poloidal limiter
-Look at the gamma-ray emission from another bulk Be component (e.g., the TAE antenna protection tiles)

These investigations lead to a second potential location for the LAM/KA4 diagnostics: behind the upper horizontal KJ5 soft X-ray camera in octant 4.

3.1 KN3 horizontal gamma-ray camera

This was the first choice for the implementation on JET of the LAM/KA4 diagnostics. The proposal was based on the assumption that channel # 10 (Figure 3.1) of the horizontal KN3 camera is practically of no use for the tomographic reconstruction of the neutron emission profile. To the knowledge of the authors of the present report, in all neutron tomographic reconstructions the emission level in channel #10 is taken as zero. Actually even the emission level in channel #9 could be safely neglected. This is going to be even more justified for high power high beta DT discharges.

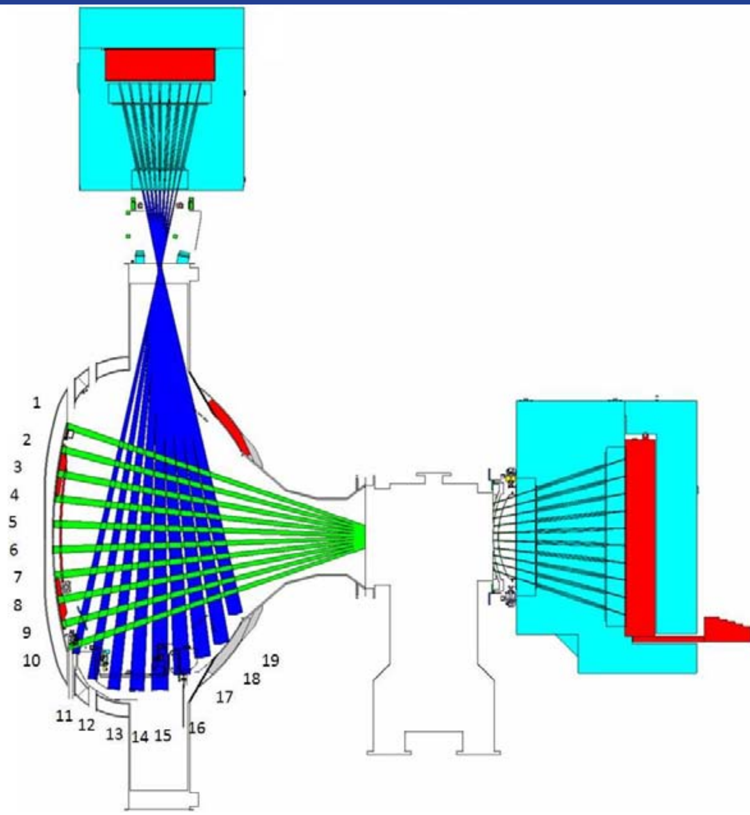

Figure 3.1: JET KN3 gamma-ray cameras showing the horizontal (1 to 10) and vertical (11 to 19) channels

3.2 KJ5 upper horizontal soft X-ray camera in octant 4

The proposed location for the LAM/KA4 diagnostics on the KJ5 soft X-ray camera in octant 4 is shown in Figure 3.2. The LAM/KA4 radiation collimator and shield is proposed to be installed behind the upper horizontal KJ5 soft X-ray camera and above the KM9 MPRu neutron spectrometer.

The upper SXR camera in Octant 4 had initially 8 channels (Figure 3.3). Channel #1 has never been used for X-ray measurement. Channels #2 and #3 have become inoperative after the installation of the Octant 4 TAE antenna. Thus the use of channels #1-3 for the KA4 diagnostics would have no impact on the operation of the KJ5 soft X-ray camera.

For this location the KA4 Line-of-Sight (LoS) and Field-of-View (FoV) are basically determined by the KJ5 radiation collimator and shield, which acts as a pre-collimator for the KA4 diagnostics. The KJ5 construction does not allow any change in the L0S or FoV.

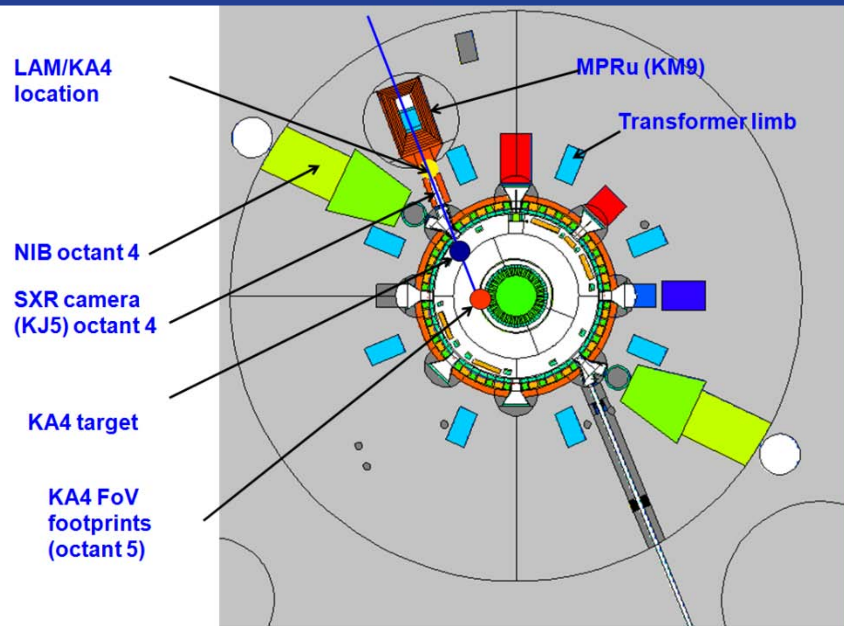

Figure 3.2: Location of the LAM/KA4 diagnostics on the KJ5 soft X-ray camera in octant 4

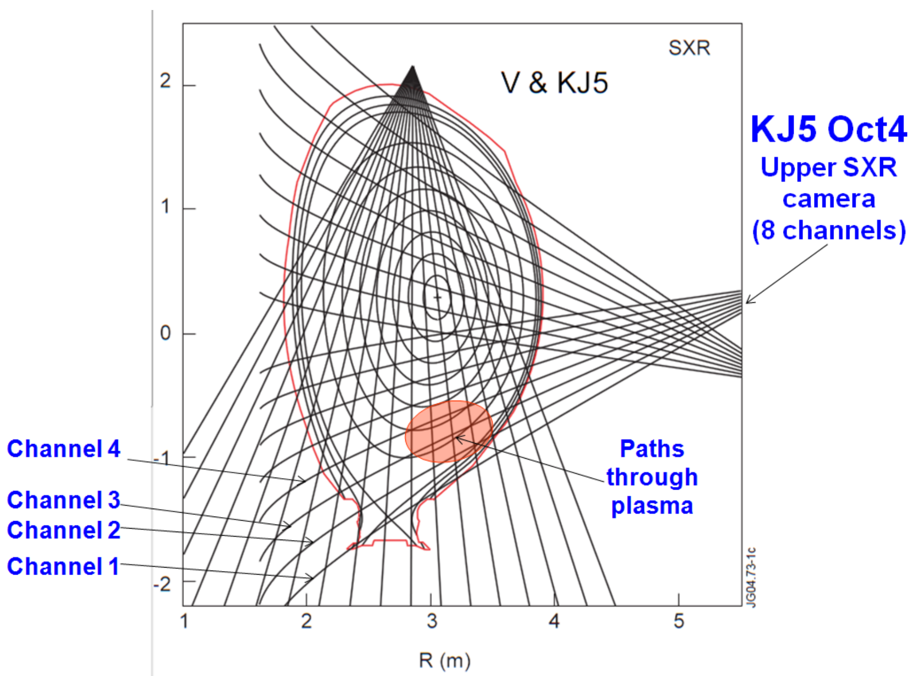

Figure 3.3: KJ5 upper Soft X-ray camera

As already seen from an old figure of KJ5, octant 4, Figure 3.4, channels #1-3 hit, at the end of their Line-of-Sight, the inner divertor tiles made of W-coated CFC. It can also be seen that, to a first approximation, channel #4 does not see any CFC.

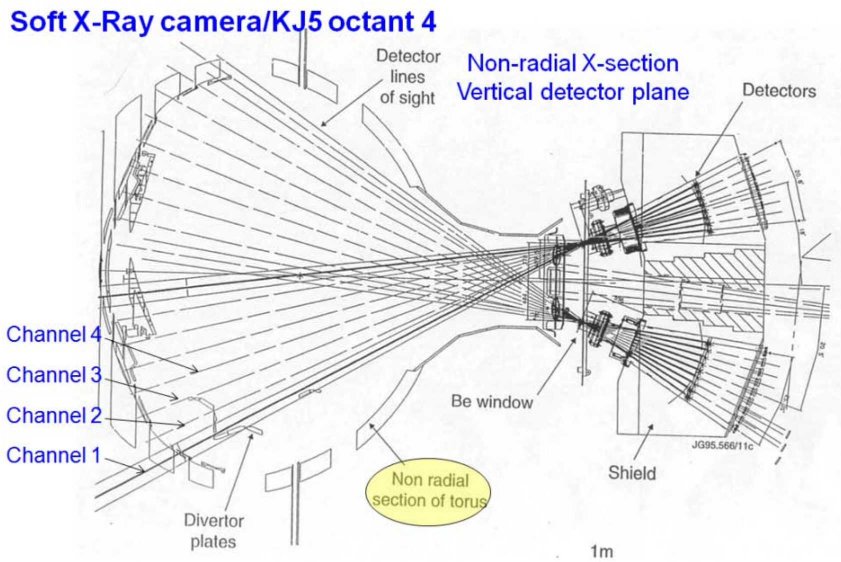

Figure 3.4: KJ5 upper soft X-ray camera (non-radial cross-section)

Regarding a possible use of channel #4 from Figure 3.5 one can see that at least for high beta plasmas, channel #4 would see only a weak soft X-ray emission from the plasma and neglecting its contribution would not affect the X-ray tomographic reconstruction.

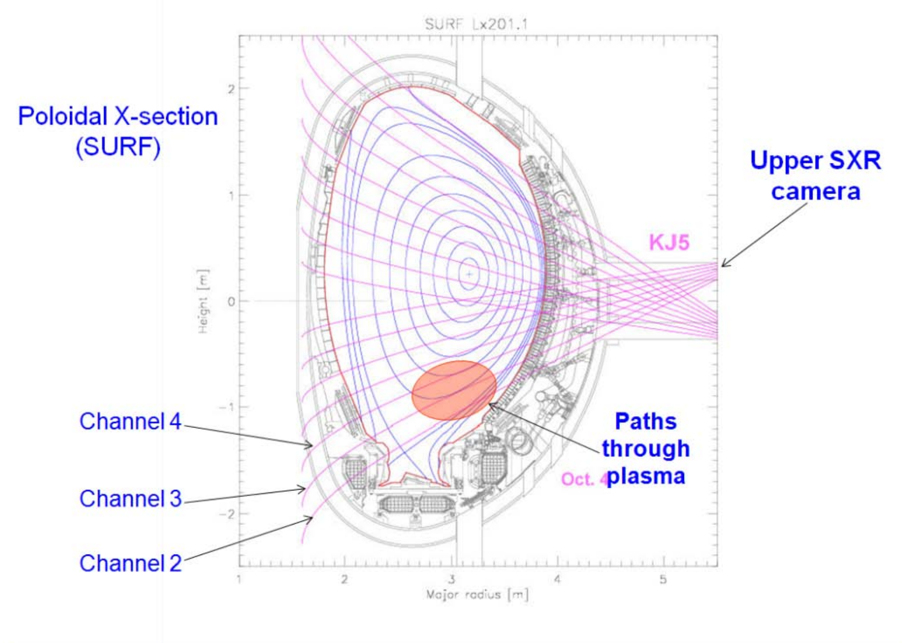

Figure 3.5: KJ5 upper soft X-ray camera with magnetic surfaces

The following alternative design solutions for the KJ5 location of the LAM/KA4 diagnostics have been evaluated within the feasibility study:

1. Detector location
   1.1. Inside a dedicated radiation collimator-shield
   1.2. Inside the KJ5 radiation collimator-shield (allowed/possible for channels #1-3, KJ5 slightly affected if channel #4 is chosen)
2. Target
   2.1. TAE Be protection tile
   2.2. Dedicated target (Only possible for KJ5 channel no. 4)
3. Target material
   3.1. Beryllium
   3.2. Boron (Only possible for a dedicated target. See ANNEX 4)
4. Target emitted radiation
   4.1. Gamma-rays
   4.2. Neutrons (Not considered in detail. See ANNEX 4).

3.2.1 KA4 FoV's@TAE antenna

In order to assess the diagnostics potential of the KJ5 location the Fields-of-View at the target (the TAE antenna protection tile) have been defined and evaluated. Figures 3.6-3.9 show the results.

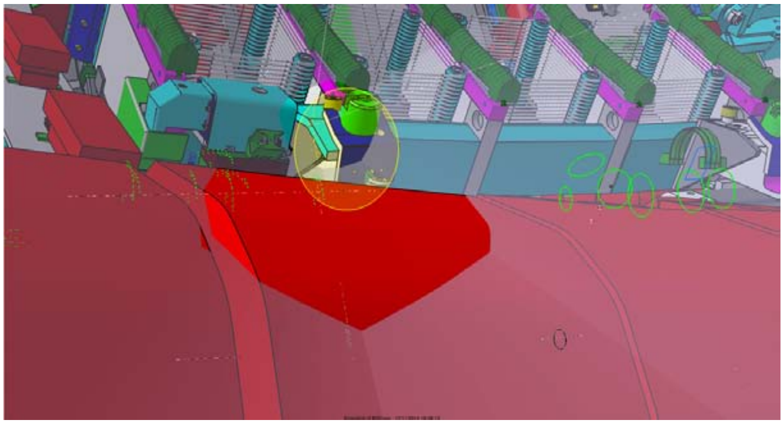

Figure 3.6: KA4 target: TAE tile surface in the channel 1 Field-of-View

The result shown in Figure 3.6 is that channel #1 Field-of-View does not cross the TAE protection tile. Thus channel #1 cannot be used to look at the target. It could be used as a reference channel.

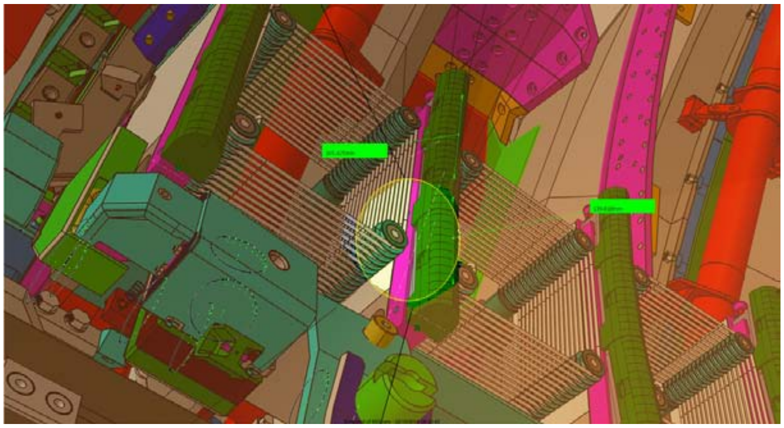

Figure 3.7: KA4 target: TAE tile surface in the channel 2 Field-of-View

The result shown in Figure 3.7 is that channel #2 Field-of-View crosses the lower end of the TAE protection tile. Channel #2 can thus be used for the LAM/KA4 diagnostics.

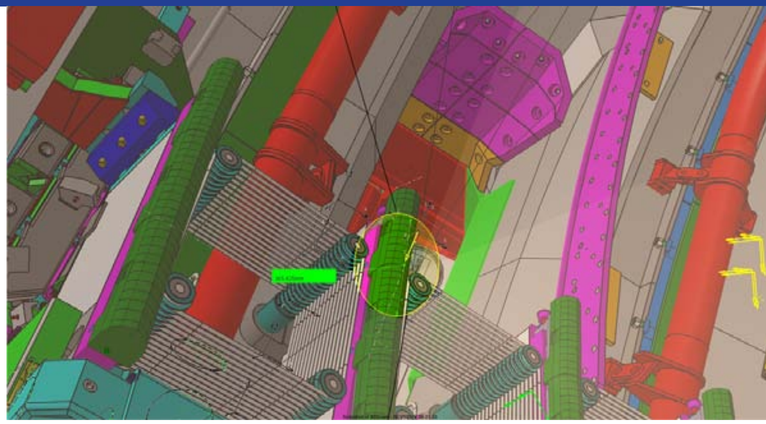

Figure 3.8: KA4 target: TAE tile surface in the channel 3 Field-of-View

The result shown in Figure 3.8 is that channel #3 Field-of-View crosses the upper half of the TAE protection tile. Channel #3 can thus be used for the LAM/KA4 diagnostics.

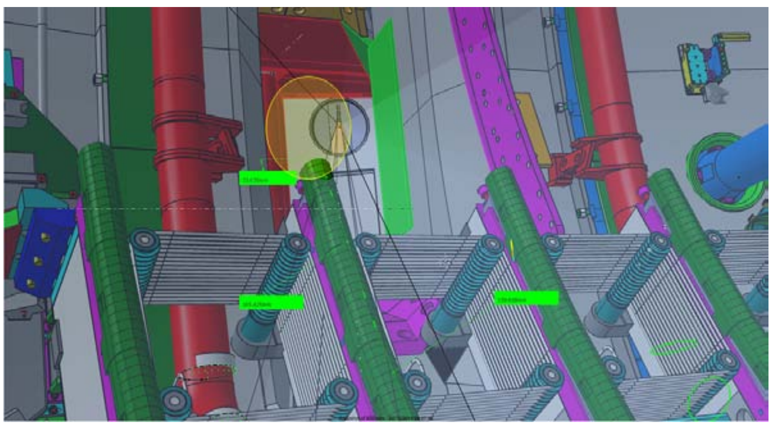

Figure 3.9: KA4 target: TAE tile surface in the channel 4 Field-of-View

The result shown in Figure 3.9 is that channel #4 Field-of-View crosses a small part of the target at the upper end of the TAE protection tile.

3.2.2 KA4 FoV footprints

Further assessment of the diagnostics potential of the KJ5 location was done by defining and evaluating the foot prints of the KJ5 Fields-of-View on the divertor CFC tiles. Figures 3.10-3.13 show the results.

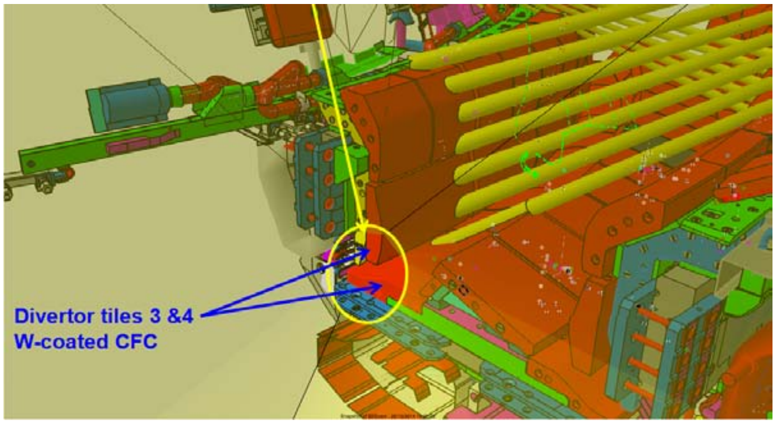

Figure 3.10: Channel 1 FoV footprint on OCT5

Figure 3.10 shows that channel #1 sees parts of the W-coated CFC divertor tiles #3 and #4.

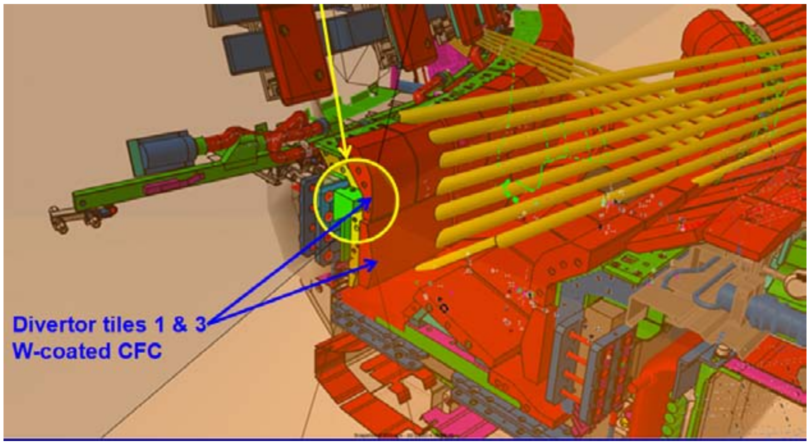

Figure 3.11: Channel 2 FoV footprint on OCT5

Figure 3.11 shows that channel #2 sees parts of the W-coated CFC divertor tiles #1 and #3.

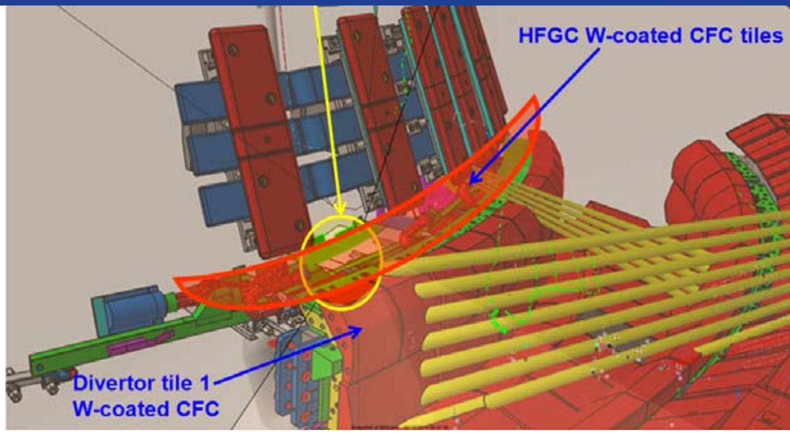

Figure 3.12: Channel 3 FoV footprint on OCT5

Figure 3.12 shows that channel #3 sees a small part of the W-coated CFC divertor tile #1 and a full size HFGC W-coated CFC tile.

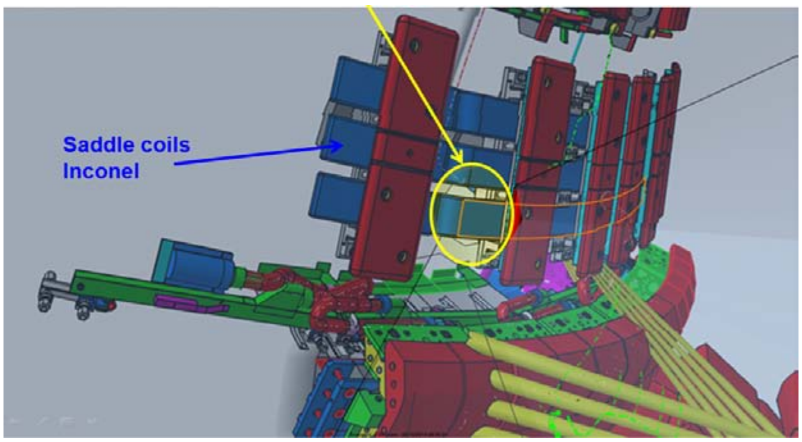

Figure 3.13: Channel 4 FoV footprint on OCT5

Figure 3.13shows that channel #4 does not see any of the W-coated CFC divertor tiles. Its footprint is on the inner saddle coils (made of Inconel).

4. Review of alternative design solutions for the LAM radiations system

4.1 KA4 on KN3

4.1.1 KA4 on KN3 Ch. 10

The Be target was proposed to be placed in the field of view of channel #10 of the JET horizontal gamma-ray camera in the limiter shadow (to avoid overheating) and between channels #17 and #18 of the vertical camera (left available for other use) (Figure 4.1) as their field of view intersect orbits of the confined alpha particles. The KA4 target is a Be disc of 100 mm radius. KN3 channel #9 is to be used as the reference. Except for the target, all the other LAM/KA4 components would be provided by the gamma-ray camera.

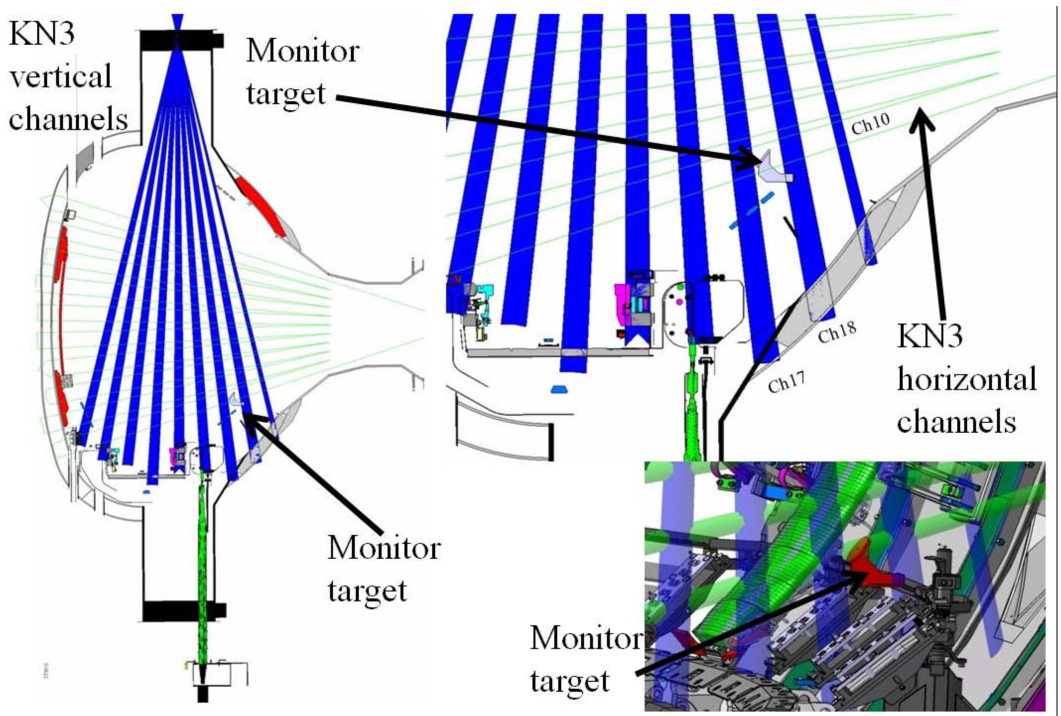

Figure 4.1: LAM target location on the KN3 channel 10

For this location of the LAM/KA4 target an approximate and very conservative estimation of the expected count rate was presented in [6]. Only the lowest level of losses (the first orbit and cone losses) were taken into account for 2.5-3 MA discharges with a DT rate of 10^{19} alphas/s. The diagnostics configuration (target, Field-of-View, detector) was that of the KN3 channel 10. The estimated count rate for the 4.44 MeV gamma-rays was about of 1 kHz. The expected total gamma-ray background, integrated over the energy range up to 9 MeV, was estimated to be at the same level. This shows a satisfactory margin for the expected signal-to-background ratio, taking into account that MHD events could cause an extremely high alpha-particle loss rate.

The first design option (Ch. 10) for the KN3 location of the KA4 diagnostics had to be dropped for the following reasons:

- Clash with the KN3 neutron camera use in DT experiments. Channel #10 was considered essential for DT experiments by the JET neutron group. A Be target inserted into the FoV of in channel 10 was considered not acceptable. A possible solution based on a retractable target was considered to be too expensive for the available project budget. This would have made it possible to insert the Be target into the channel #10 FoV only for dedicated fast particle losses experiments.
- The matter of the recess of the target with respect to the apex of the Octant 1 limiter remained an outstanding issue regarding the location of the LAM target on KN3 channel #10.
- Potential clash with RH equipment. This matter is presented in detail in Annex 1.1 (EAG report of May 26th 2014), including a couple of possible design solutions that would mitigate or avoid this clash.

4.1.2 KA4 on KN3 Ch. 9

As seen in Figure 4.2 the FoV of channel #10 sees one of the CFC divertor tiles (the HFGC tile).

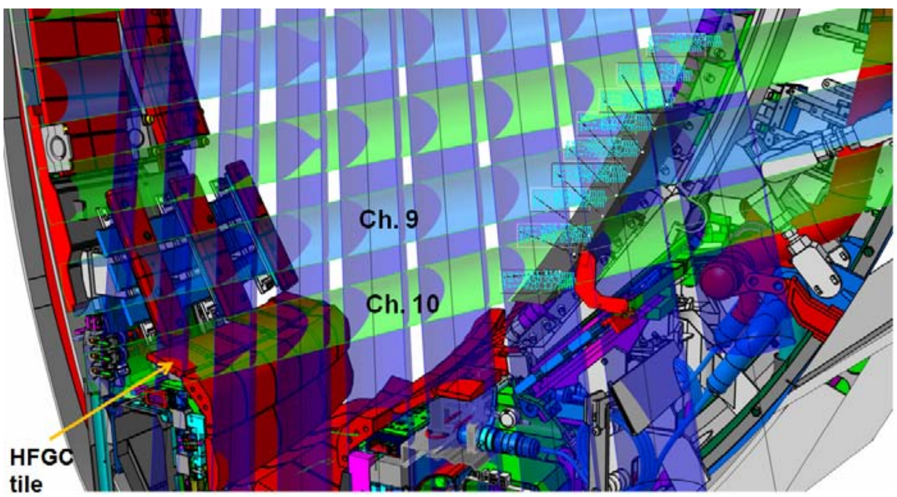

Figure 4.2: KA4 design option on KN3, channel #9

Therefore the option of using channel #9 (which does not see any of the CFC tiles) for the KA4 diagnostics was briefly considered within the feasibility study. It was not further developed as it had the other issues mentioned for the channel #10 option.

4.2 KA4 on KJ5

Various design options have been considered and evaluated for the KJ5 location of the LAM/KA4 diagnostics. Figure 4.3 shows a schematic diagram of the KJ5 location containing all the components of the alternative technical solutions.
As shown in Figure 4.3 there are two alternative options for the location of the KA4 detectors: inside the old KJ5 radiation shield or inside a new KA4-dedicated radiation collimator and shield.
Regarding the KA4 target three different solutions have been considered:

- -One of the TAE antenna protection tiles
- -Extension of a TAE antenna protection tile
- -A dedicated Be target placed above one of the TAE antenna protection tile

Two different solutions have been developed for the KA4 data acquisition system (DAQ). The initial project proposal (DAQ1) developed by IST is based on the IPFN ATCA data acquisition digitizers and it is presented below (see chapter 7). An alternative solution (DAQ2) based on window comparators was developed by IAP for the acquisition and processing of data in the case of a high level of background gamma radiation [12].

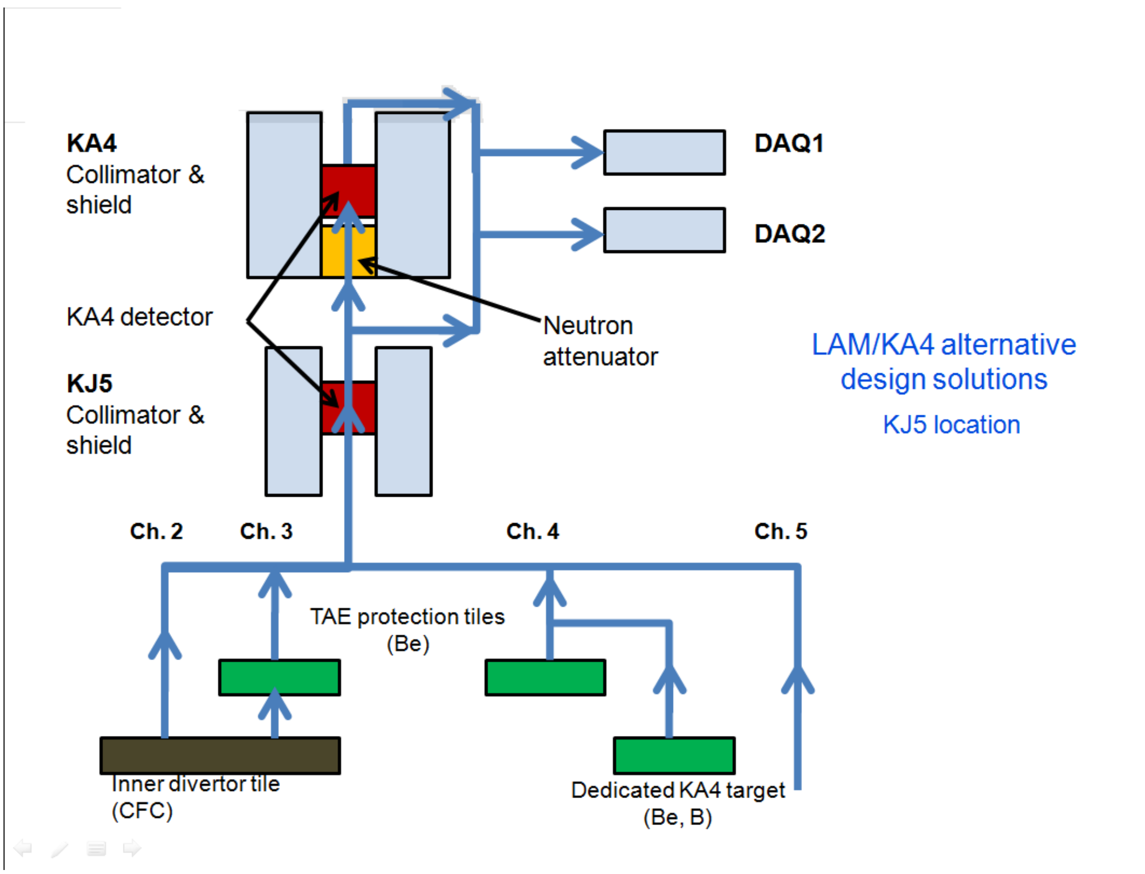

Figure 4.3: LAM/KA4 alternative design solutions on the KJ5 location

4.2.1 KA4 on KJ5: Option 1

Option 1 for the KA4 location on KJ5 (Figure 4.4) has the following structure:
-Channel #2 is used as the reference channel
-Channel #3 has the Be target in its FoV
-The KA4 gamma-ray detectors are placed within a new radiation collimator and shield, behind neutron attenuators
-KA4 DAQ is based on the IPFN ATCA data acquisition digitizers
KJ5 Option 1 is complex, expensive and it does not provide a solution for the high level of parasitic gamma radiation.

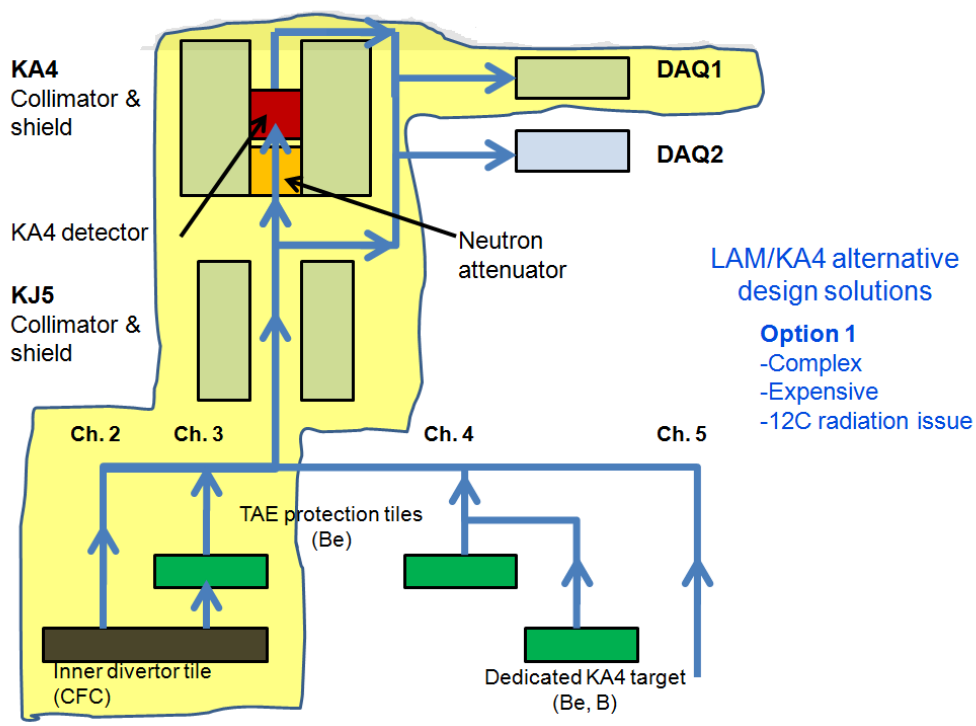

Figure 4.4: KA4 on KJ5: Option 1

4.2.2 KA4 on KJ5: Option 2
Option 2 for the KA4 location on KJ5 (Figure 4.5) has the following structure:
-KA4 target is an extension of one of the TAE antenna protection tiles
-Channel #5 is used as the reference channel
-Channel #4 has the Be target in its FoV
-The solution for the detectors, radiation shield and DAQ is the same as for Option 1.
KJ5 Option 2 is the most complex, and the most expensive technical solution.

The extension of one of the TAE antenna protection tiles turned out to be technically very challenging if not impossible (see EAG report in Annex 1.2).

Option 2 has a high impact on the KJ5 soft X-ray upper camera as it uses two out of its five remaining working channels.

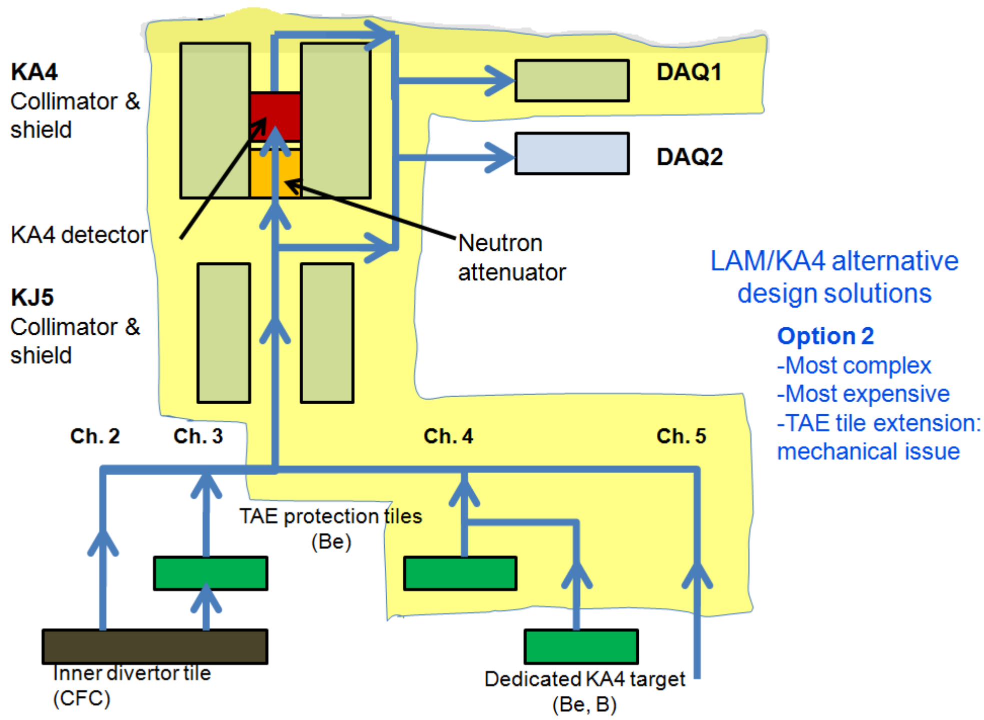

Figure 4.5: KA4 on KJ5: Option 2

4.2.3 KA4 on KJ5: Option 3

Option 3 for the KA4 location on KJ5 (Figure 4.6) has the following structure:

-Channel #2 is used as the reference channel

-Channel #3 has the Be target in its FoV

-The KA4 gamma-ray detectors are placed within the old KJ5 radiation collimator and shield. No neutron attenuators could be accommodated within the KJ5 shield.

-KA4 DAQ is based on the IAP window comparators solution

KJ5 Option 3 is the simplest KA4 technical solution and it has also the lowest cost. This solution could be designed and constructed within the available LRM project budget. However, choice of this solution would lead to a significant change in the project aim as defined in the initial project proposal.

The basic idea behind this solution is that the parasitic 12C gamma-ray emission is proportional to the neutron yield (for a fixed amount of CFC in the KA4 detector FoV).

For transient events (e.g., MHD events), the neutron yield and the fast particle losses have different time evolutions (Figure 4.7). Gamma-ray signals from Ch. 2 and Ch. 3

detectors are collected by DAQ2 through window comparators. Only a narrow energy band containing the 4.4 MeV line is recorded.

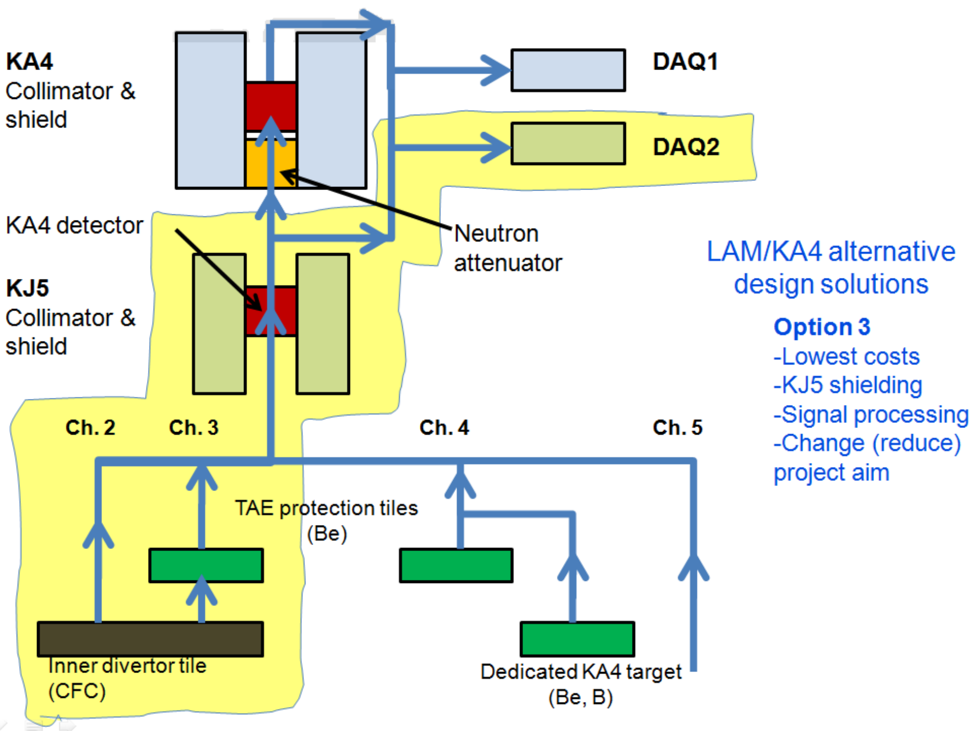

Figure 4.6: KA4 on KJ5: Option 3

Signals from the two channels are processed by a dedicated algorithm. In its simplest form, the output will be the difference between the two channels. Adequate data processing techniques can deal efficiently with differences of about 10%.
The result is a technique that could provide real-time monitoring of particle losses.

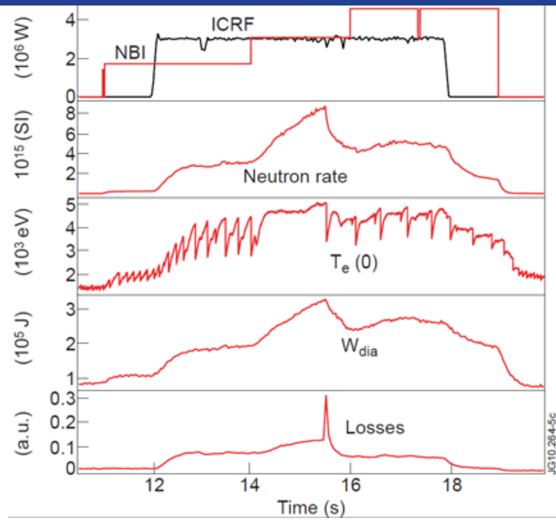

Figure 4.7: Particle losses in a JET discharge with a monster sawtooth

4.2.4 KA4 on KJ5: Option 4

Option 4 for the KA4 location on KJ5 (Figure 4.7) has the following structure:

-A dedicated Be KA4 target placed above one of the TAE antenna protection tiles

-Channel #5 is used as the reference channel

-Channel #4 has the Be target in its FoV

-The KA4 gamma-ray detectors are placed within the old KJ5 radiation collimator and shield. No neutron attenuators could be accommodated within the KJ5 shield.

-KA4 DAQ is based on the IPFN ATCA data acquisition digitizers

The main issue for Option 4 is the design and construction of a dedicated Be target. Otherwise this solution is simpler than Option 1 and although it has a lower cost it could still not be done within the allocated LRM project budget. Option 4 (like Option 2) has a high impact on the KJ5 soft X-ray upper camera as it uses two out of its five remaining working channels.

The four design options for the KJ5 location have been developed to different levels of details within the feasibility study. Option 1 had the most advanced design and in the end had all the elements of a conceptual design. Some components developed for Option 1 were used also for the other design options (e.g., the new KA4 radiation collimator and shield).

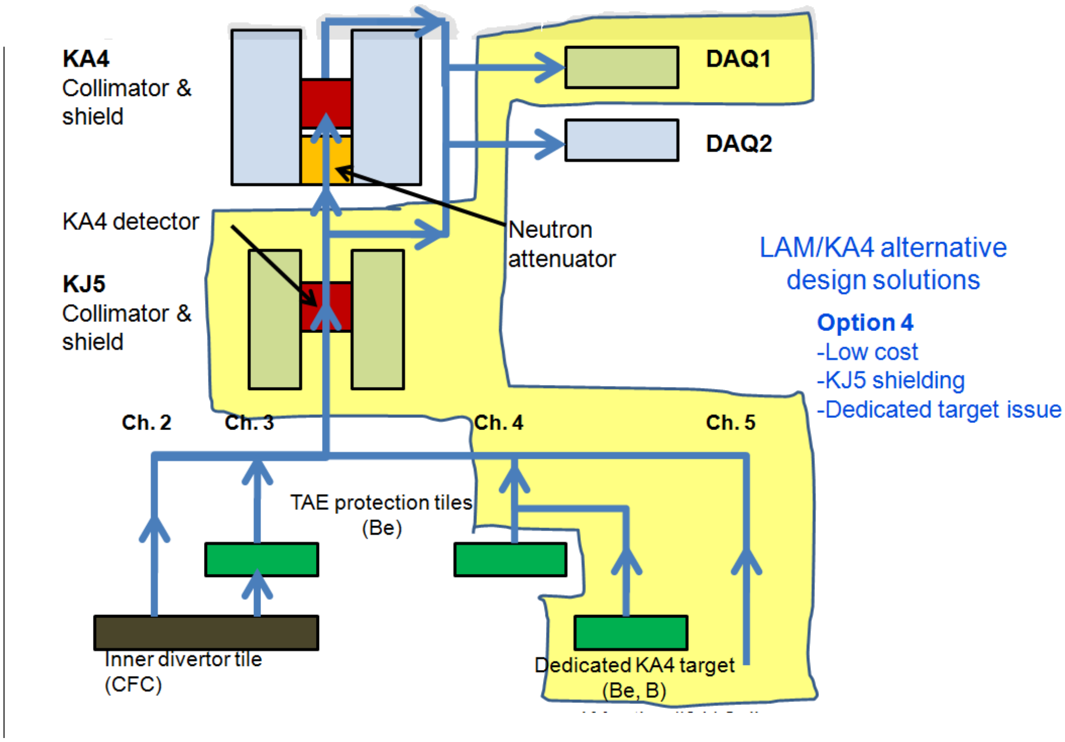

Figure 4.8: KA4 on KJ5: Option 4

5. Conceptual design of the LAM radiation system

5.1. Introduction

In the LRM project schedule the conceptual design should have been done after an evaluation of the various design solutions and the selection of the optimum solution. The evolution of the project (see chapter 1.2) prompted the project team to develop in advance of the project schedule a conceptual design for one the technical solutions that seemed to satisfy from the technical point of view most of the project requirements.

Design activities for the following components of the LAM/KA4 diagnostics are included in the LRM project work plan:

- KA4 radiation system (alpha particle target and radiation collimator and shield)
- Neutron attenuators
- Gamma-ray detectors
- Data acquisition system for two KA4 gamma-ray detectors

This chapter presents the conceptual design for the LAM radiation system, the LAM neutron attenuators and a support structure for the assembly containing the radiation collimator and shield, the neutron attenuators and the gamma-ray detectors. Elements for the conceptual design of the KA4 detectors and data acquisition are presented in chapters 6 and 7.

The LAM conceptual design has been developed for Option 1 of the KJ5 location (see chapter 4.2.1).

This design option is presented schematically in Figure 4.4 and it has the following main features:

- The working channel that has the Be target in its FoV is channel 3 of the KJ5 diagnostics. The gamma-ray detector of this channel sees the Be target, i.e., part of the protection tile of the TAE antenna.
- KJ5 channel #2 is used as the reference channel
-The KA4 gamma-ray detectors are placed within a new radiation collimator and shield, behind LiH neutron attenuators
-The two gamma-ray detectors are based on the CeBr3 scintillator
-KA4 DAQ is based on the IPFN ATCA data acquisition digitizers

In this design option both gamma-ray detectors have divertor CFC tiles in their FoV.

An overall view of the LAM/KA4 diagnostics containing all its hardware components (except for the DAQ) is shown in Figure 5.1.

The radiation collimator and shield is located behind the KJ5 radiation shield, the minimum distance between the two shields being 439 mm. The KJ5 radiation shield is used as a pre-collimator for the KA4 diagnostics. The dimensions of the KJ5 collimator determine the dimension (solid angle) of the FoV for the KA4detectors. It should be kept in mind that the KJ5 collimator cannot be changed.

The KA4 radiation collimator and shield houses the two KA4 gamma-ray detectors (see details in Figure 5.2). A LiH neutron attenuator is placed in front of each gamma-ray detector. The detector in channel #3 views the LAM target through the KJ5 stainless steel collimator. The detector FoV at the target (the TAE protection tile) is shown in Figure 3.8. The distance between the LAM target and the gamma-ray detector is 5706 mm.

5.2. KA4/LAM radiation collimator and shield

The KA4/LAM radiation collimator and shield structure is shown in Figure 5.4.
The radiation (neutron and gamma-rays) shield is made up of alternating plates of high density polyethylene (HDPE) and lead (Figure 5.4). The radiation collimator is made of a slab of stainless steel into which the channels for the detectors and neutron attenuators are drilled (Figure 5.5). The dimensions of the active structure (without the shield casing) of the LAM radiation shield are 1000x1420x1300 mm^3.

5.3. KA4/LAM target

The LAM/KA4 target is one of the TAE antenna protection tiles (Figure 5.6). The upper part of the Be tile (about 2/3) falls into the FoV of the detector in channel #3 (Figure 3.8).

5.4 LAM/KA4 neutron attenuators

The KA4/LAM neutron attenuators are based on the technology developed by IAP for the upgrade of the JET tangential gamma-ray spectrometer (KM6T) diagnostics [14].
The 30 mm diameter of the LAM neutron attenuator happens to be a fortunate choice determined by:
-the available solid angle at the entrance of the LAM/KA4 radiation shield
-the diameter of the neutron attenuator prototype developed by IAP (INOE)
The fact that the attenuator prototype technology can be used for the LAM/KA4 diagnostics represents a significant financial saving for the LRM project.
Regarding the length of the attenuator room has been provided within the LAM radiation shield for an attenuator length up to 750 mm. This should be enough even for the highest foreseeable JET DT neutron yields. However, the actual dimension (length) should be checked by MCNP calculations.

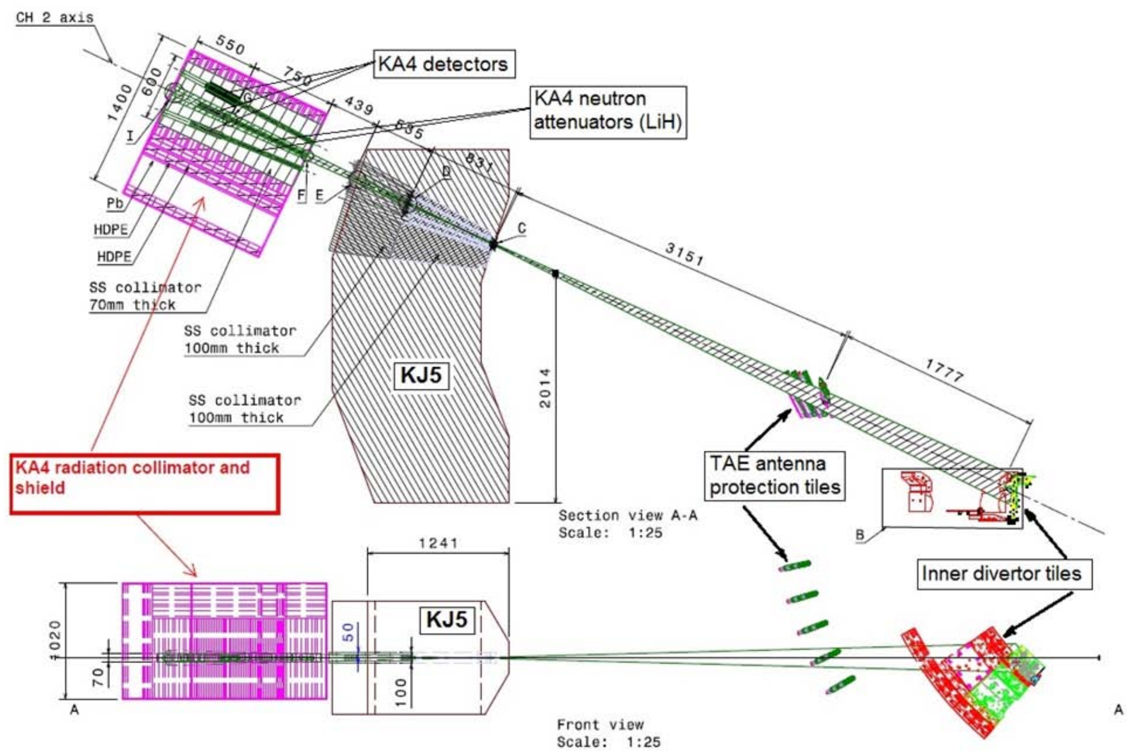

Figure 5.1: KA4 radiation system. Top: vertical cross-section containig channel #2, 3, and 4. Bottom: “horizontal” cross-section through channel #2.

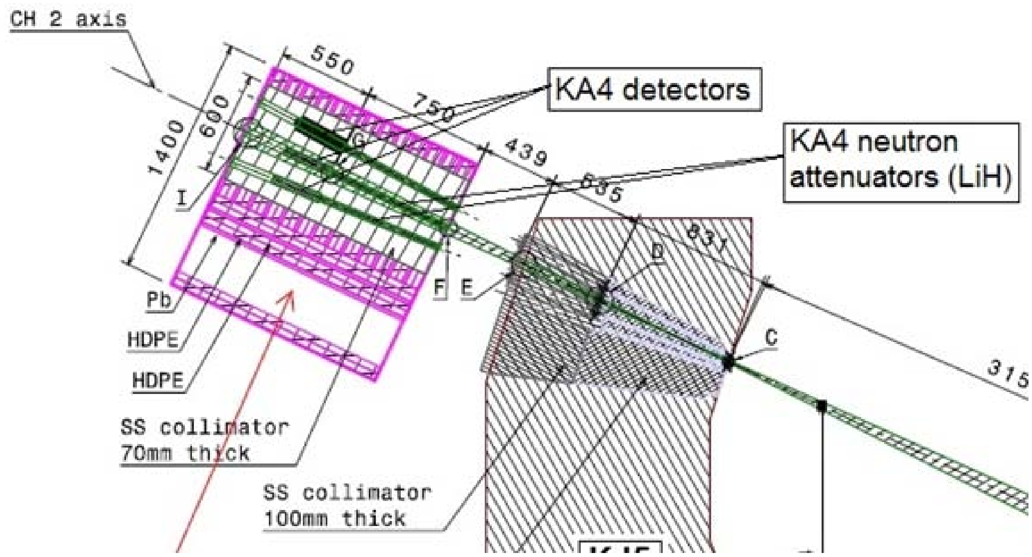

Figure 5.2: KA4 radiation collimator and shield showing also the KA4 detectors and the KA4 neutron attenuators in channels #2 and 3.

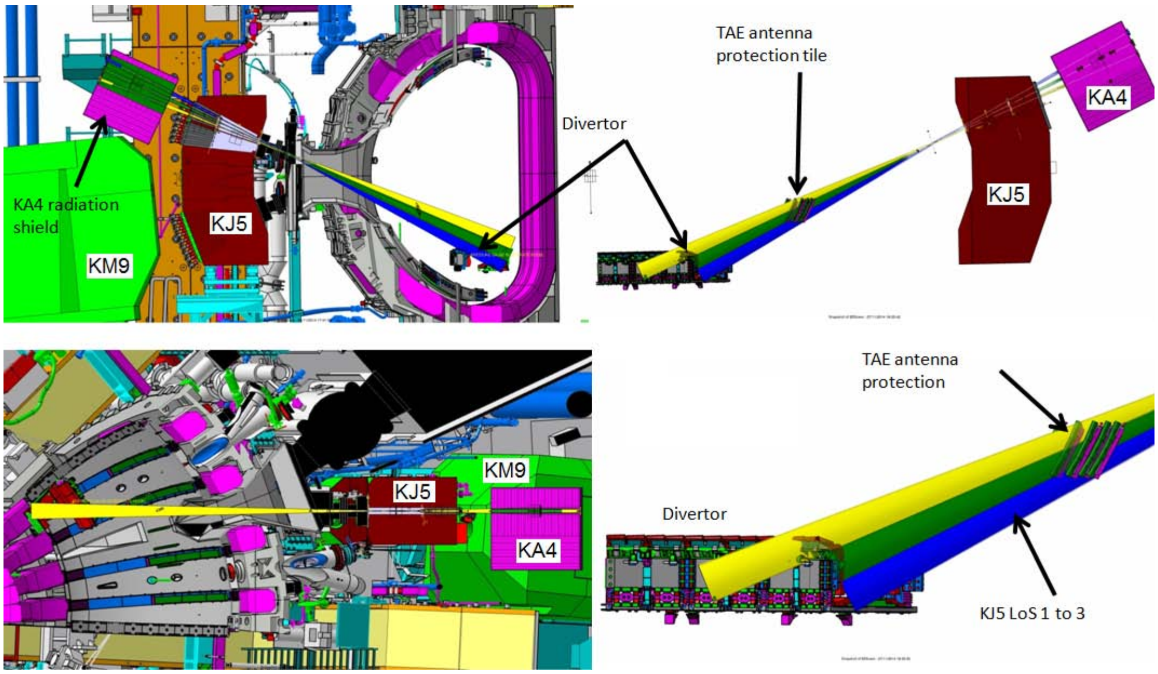

Figure 5.3: KA4 radiation collimator and shield showing its position with respect to the adjacent JET diagnostics: KJ5 soft X-ray camera and KM9 magnetic proton recoil spectrometer. The FoV's for channels #1, 2, and 3 are also shown crossing the TEA antenna protection tiles and ending on the inner divertor tiles.

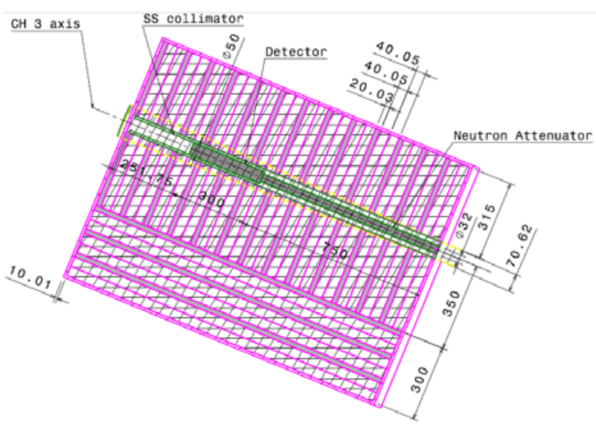

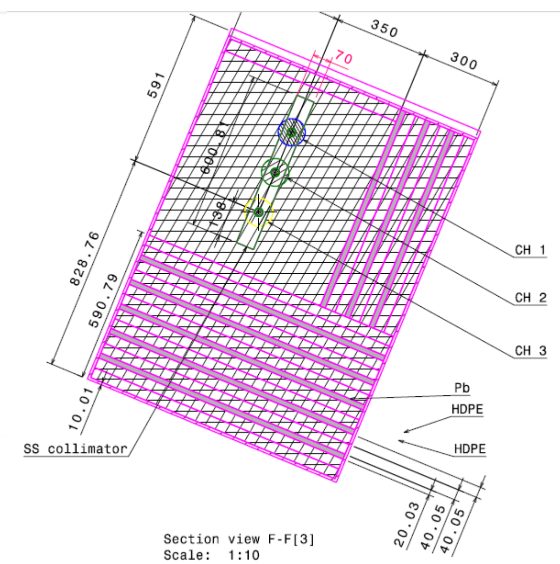

Figure 5.4: Radiation collimator and shield structure

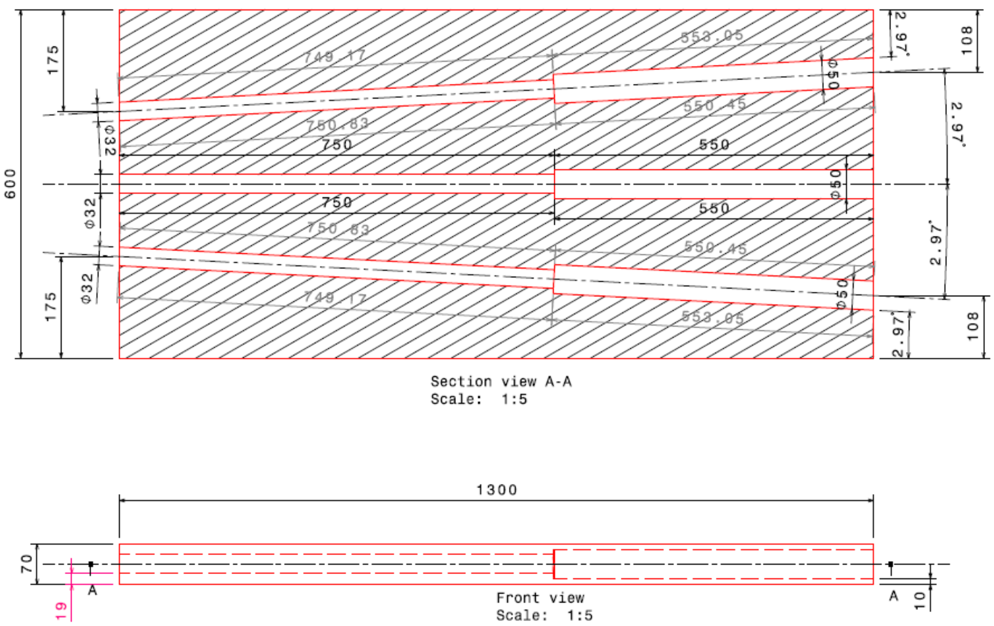

Figure 5.5: KA4 collimator

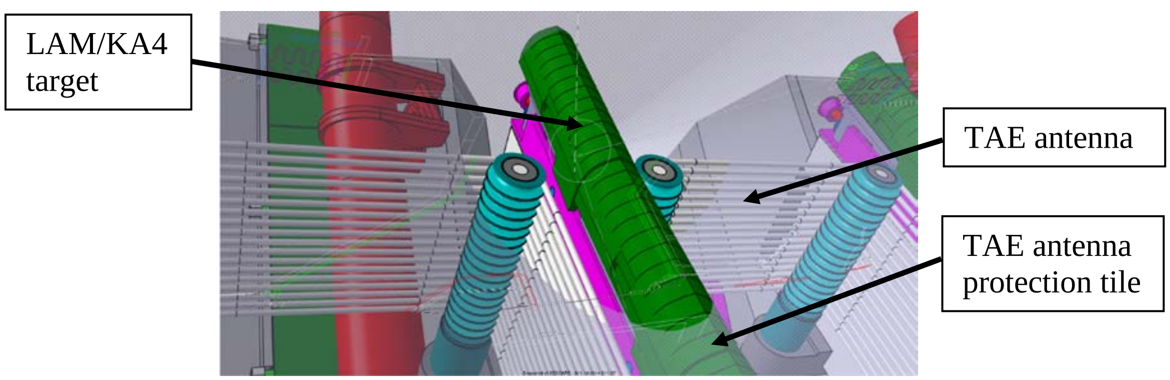

Figure 5.6: LAM/KA4 target (highlighted in green)

5.5. LAM/KA4 support structure

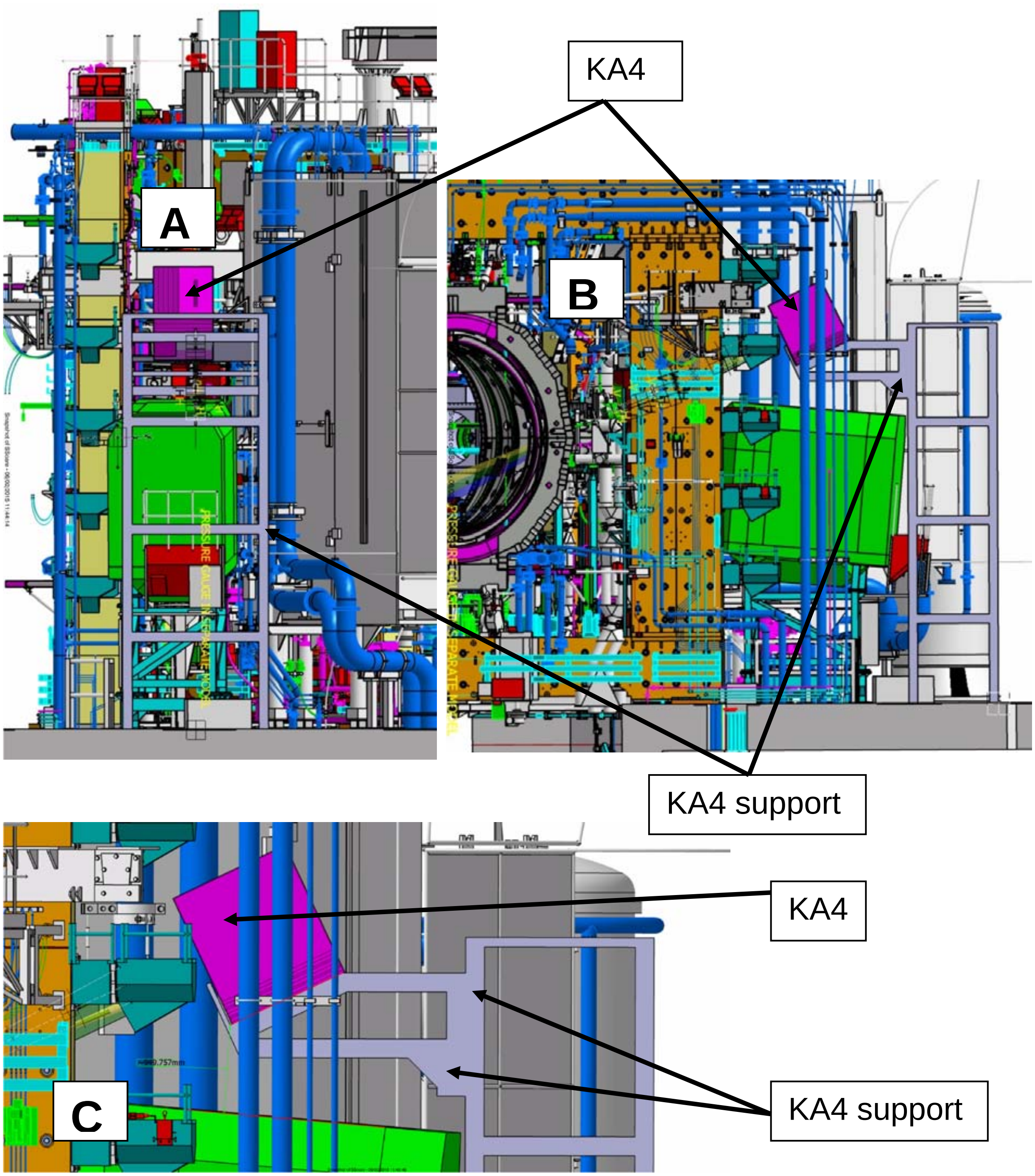

Figure 5.6: KA4 support: A: rear view; B: side view; C: detail of side view

The entire assembly of the radiation collimator and shield including the two gamma-ray detectors and the two neutron attenuators is held into place by a support structure shown in Figure 5.6. Figure 5.6 shows the support structure for an alternative position of the radiation collimator and shield. This is further away from the KJ5 radiation shield than the recommended position shown in Figure 5.3. Even at its closest distance from the KJ5 shield, the KA4 assembly is positioned at safe clearances with respect to the two adjacent diagnostics: KJ5 and KM9.

6. LAM/KA4 detectors

(For details on the response of the gamma-ray detector, see ANNEX 3)

The following design options have been proposed and evaluated for the LAM/KA4 detector module:

- Scintillator: CeBr3 (1” or 2” diameter x 1” or 2” height)
- Photodetector: Photomultiplier tube (PMT) with low sensitivity to magnetic field (e.g. Metal Channel dynode or Fine Mesh dynode)
    - additional magnetic shielding (e.g. ~20 mm Permalloy), could be possibly constructed as a part of the detector casing

The proposed design was tested at IPPLM/NCBJ on a detector with the following structure:

- $CeBr_3$ scintillator, crystal size Ø25x25 mm
- PMT, H8711-200, Metal Channel dynode, PMT outer size 30x30x45 mm

The results are presented in Figure 6.1 and show a slightly nonlinear response of the PMT at high energies (5-6 MeV). This does not perturb monitoring at LAM energy range of interest (around 4.4 MeV).

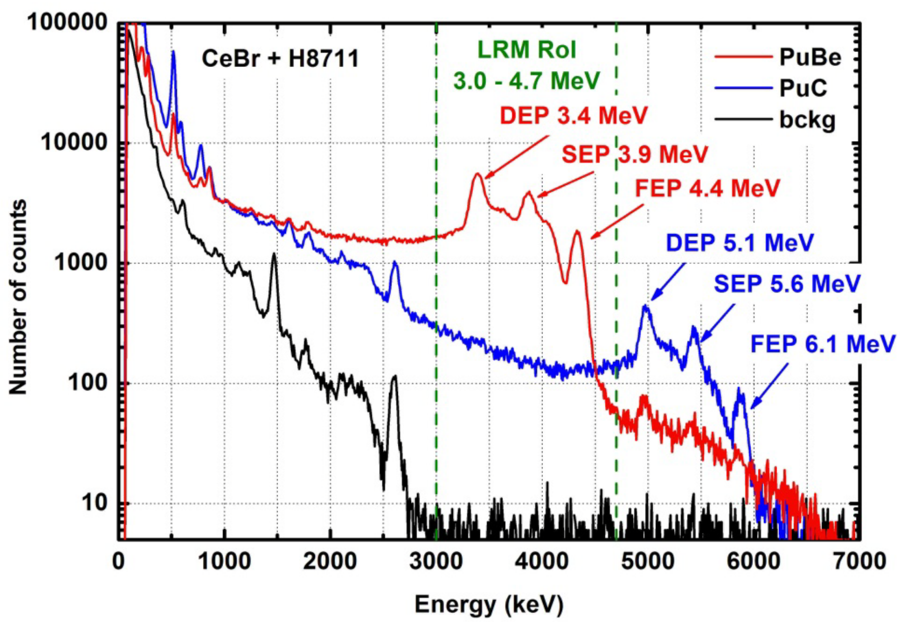

Figure 6.1: Response of a $CeBr_3$ scintillator tested at IPPLM/NCBJ

Table below show the recommended scintillator dimensions for the LAM/KA4 detector.

$CeBr_3$ scintillator	average count number	count number at 1.5 MeV	count number at 4.4 MeV	count number at 6.1 MeV
1”x1”	**1.0**	**1.0**	**1.0**	**1.0**
2”x2”	**4.1**	**4.3**	**4.6**	**5.0**
3”x3”	8.1	8.8	9.4	10.8

7. LAM/KA4 Data acquisition and processing (DAQ)

7.1 Introduction
The data acquisition system for the Lost Alpha Gamma Rays Monitor (KA4/LAM) will acquire data from two detectors based on the CeBr3 scintillator.
Two solutions have been proposed:
-one solution (DAQ1) is based on the IPFN ATCA data acquisition platform
-another solution (DAQ2, developed by IAP) uses window comparators [12]

7.2 DAQ solution based on ATCA data acquisition platform
The IPFN ATCA data acquisition platform includes digitizers which sample up to 400 MSPS@14-bit, provide 500 MByte/channel inboard storage and complex triggering algorithms.
Although the digitizer board features eight 14-bit channels sampling up to 400 MS/s, only two channels will be acquired, profiting of 2 GB of inboard memory.
Figures 7.1 and 7.2 show the acquisition module and the controller. Similar systems have been successfully installed on JET gamma-ray diagnostics during JET-EP2 enhancements, reflectometry diagnostics on the IPP.CR COMPASS and on the USP TCA/Br tokamaks.


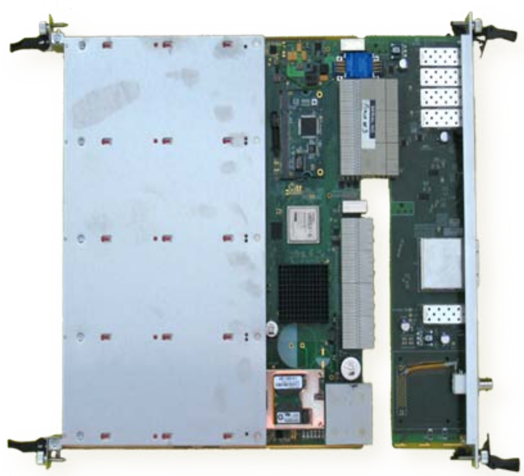

Figure 7.1 (LHS): 8 Channel 400 MSPS Digitizer. TRP-400 V1.0
Figure 7.2 (RHS): ATCA Controller

Data Acquisition System Specifications
Input characteristics:

- Eight analogue ADC channels per board at 400 MSPS using AD5474 from TI™.
- Resolution: 14 bits;
- Input Range: ±1.1 V @ 50 Ω;
- 8 channels AC coupled (with a pass-band of 5kHz to 100 MHz) or DC coupled (introduces ~200 mV of input offset);
- 50 Ω input on Lemo coaxial plug (EPL.00.250.NTN).

Acquisition Configuration:

-Two Blocks (block #1, block #2) of 4 channels each per board. Each block can be acquired simultaneously but data is retrieved from each block separately.
- Programmable acquisition rate: 400, 200, 160, 100, 80, 50 MHz;
- Acquisition modes (acquisition up to memory filling):
    - Raw data, maximum of 2 channels/block when operating at 400 MHz;
    - Segmented data (burst mode);
    - Processed data: advanced algorithms customized for the incoming signals may be implemented, if requested.

Trigger source:

The trigger source can be originated from:

- Software trigger;
- Hardware trigger:
    - Front panel unipolar Lemo plug (EPL.00.250.NTN): external LVTTL (3.3V) trigger, 5V tolerant; Polarity: ascending edge.
    - Rear panel differential Lemo plug (LEMO_EPL_0S_302_HLN): compliant to RS-485 standard interface (5V) - Trigger from the Control Trigger and Timing System compliant to JET (CTTS).

Time Stamping Specifications:
Time resolution: as low as 4ns.

Storage Capabilities:

- 4 Gbytes of data memory distributed in two blocks of four channels: 500 Mbytes per channel;

Processing Capabilities:

Two XC4VFX60-10FF1152C FPGAs for real time pulse processing.

Interface Capabilities:

- ATCA based module;
- ATCA Fabric channel 1 (x1 PCI Express) - compliant with PCIe rev1.1

8. Numerical analysis in support of the LAM/KA4 design

A series of numerical calculation activities have been carried out in support of the LAM/KA4 diagnostics design (see details in ANNEXES 2-6):

1. Evaluation of lost particle fluxes for DT experiments
2. Evaluation of expected KA4 detector response to gamma radiation for DT experiments
3. Calculation of LAM target gamma-ray emission for DT experiments
4. Evaluation of the parasitic (12C) photon flux at the location of the KA4 detector
5. MCNP calculations for the LAM Line of Sight

The results of the calculations done within the activities 3 and 4 above have lead to the conclusion that the ratio between the parasitic 4.4 MeV gamma-ray emission from the CFC tiles and the signal emission from the Be target could be as high as 10. This was one of the important motivations in the decision on the continuation of the LRM project.

8.1 Evaluation of lost particle fluxes for DT experiments. Phase I

Estimation of the flux of escaping 2-4 MeV alpha particles onto the Be LAM target due to the first orbit loss mechanism

8.1.1 LAM target placed in the LoS of the KN3 horizontal channel #10, between channels #17 and #18

Modelling:

-backward-in-time full gyroorbit-following approach

-560 uniformly distributed starting points on the modeled mushroom-type target

-9 initial pitch-angles on each starting point

-Different parabolic profiles of fusion alpha sources

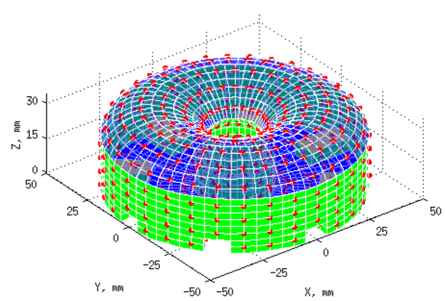

Figure 8.1: Numerical model of a Be mushroom tile with the starting points of the test trajectories marked in red

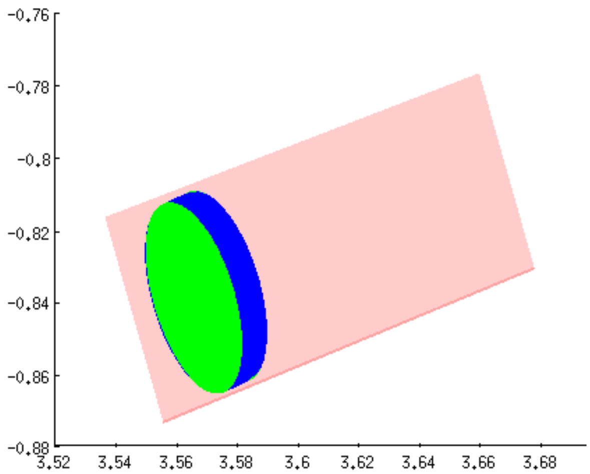

Figure 8.2: Optimal position and orientation of a disc-type LAM target (green and blue) in channel #10 FoV (pink).

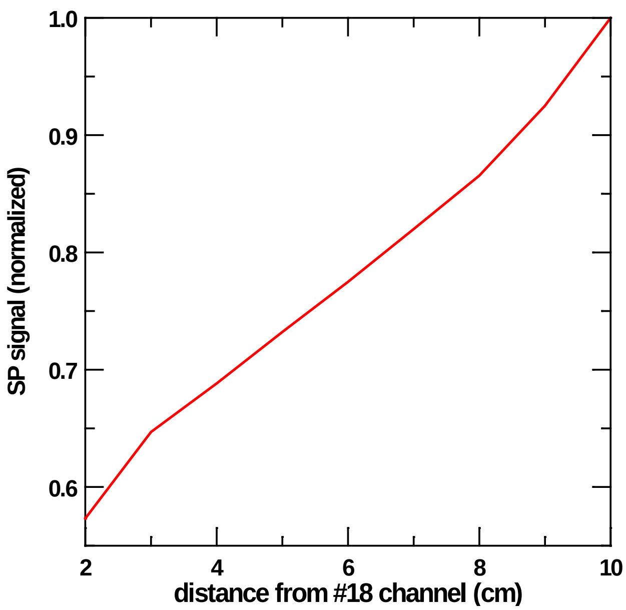

Figure 8.3: Dependence of the relative signal intensity when the LAM target moves over 10 cm away from the channel #18 LoS

8.1.2 LAM target placed in the LoS of the KJ5 channel #3 (TAE antenna protection tile)

Modelling: the same procedure as for the KN3 channel #10 case

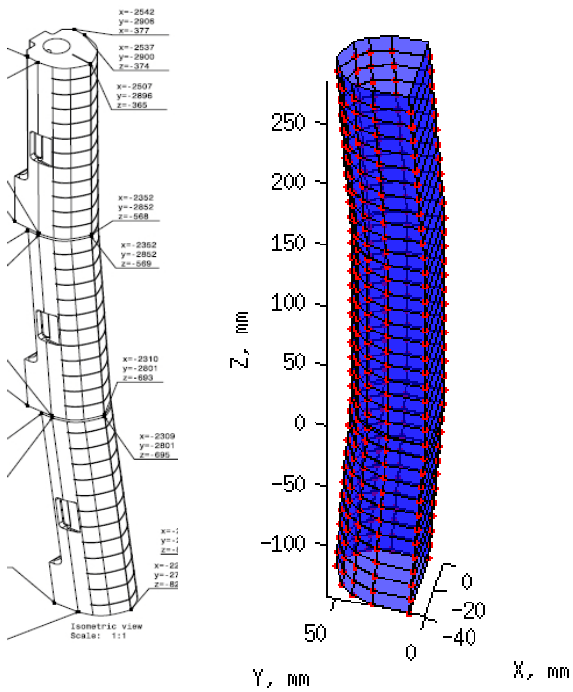

Figure 8.4: CATIA drawing of the Be TAE antenna protection tile (left) and the numerical model of the tile (right) with the starting points for test trajectories marked in red

8.2 Evaluation of expected KA4 detector response to gamma radiation for DT experiments. Phase I

KA4 detector response. Monte Carlo simulations

1. Input spectrum (provided by V. Kiptily)
   zero approximation for gamma-ray background normalised to the integral spectrum
2. 64 energy bins from 1.5 to 14.9 MeV
3. CeBr3 scintillators of a cylindrical shape
   1”×1”, 2”×2” and 3”× 3”
4. Beam of 106 parallel gamma rays
   -hitting perpendicularly a detector surface
   -collimated on a 10 mm diameter circle
5. Energy resolution 4%, independent on gamma ray energy

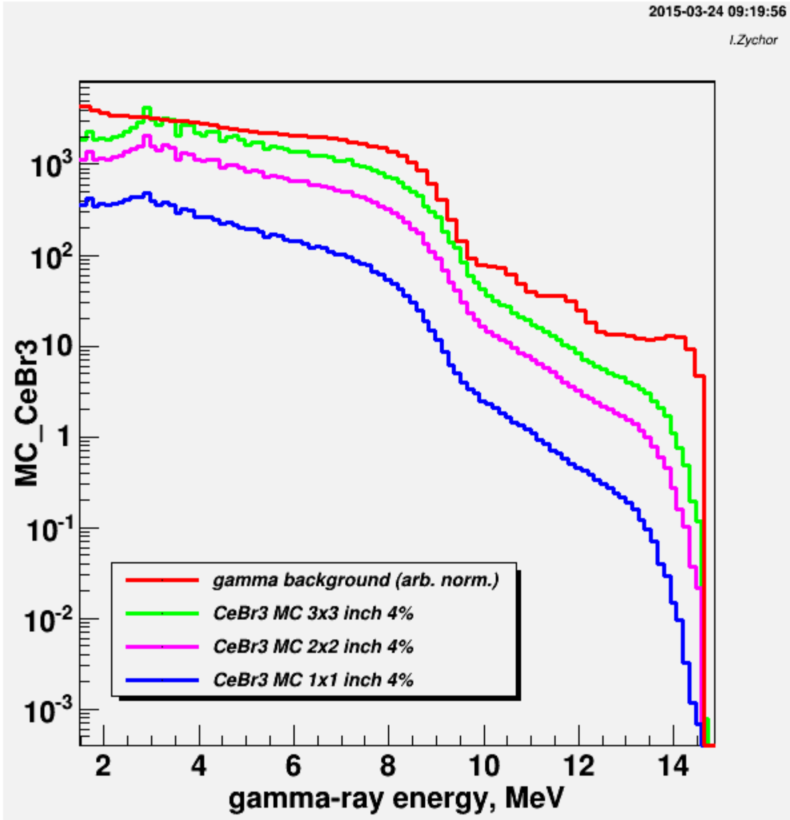

Figure 8.5: GEANT4 SIMULATIONS results

8.3 Calculation of LAM target gamma-ray emission for DT experiments. Phase I

The Be target is considered to be placed at poloidal angles $\theta=37^0-62^0$

Particle losses modelling:

In a plasma with plasma current 2.5MA<I<3MA the prompt losses (first orbit and cone losses)

$F_P \sim (0.2\text{-}0.4)*F_n$,

where "average neutron flux" is $F_n = R_n/S_{JET}$,

with $S_{JET} \sim 150\ m^2$:

$F_P \sim 1.3\text{-}2.5*10^{-3}\ m^{-2}\ s^{-1}$.

The diffusive and convective losses for $\theta>25^0$:

$F_{DC} \sim 3.1*10^{-4}\ m^{-2}\ s^{-1}$.

The 4.44-MeV gamma-emission from the Be target will be:

FO and cone loss induced gammas

$I_\gamma \sim 3.8\text{-}7.5*10^{-9}$ m^{-2} s^{-1}

and diffusive and convective

$I_\gamma \sim 9.4*10^{-10}$ m^{-2} s^{-1}.

In the case of DT-rate $R_n = 10^{19}$ s^{-1} the total Be target 4.44-MeV gamma-emission will be

$I_\gamma \sim 4.7\text{-}8.4*10^{10}$ m^{-2} s^{-1}

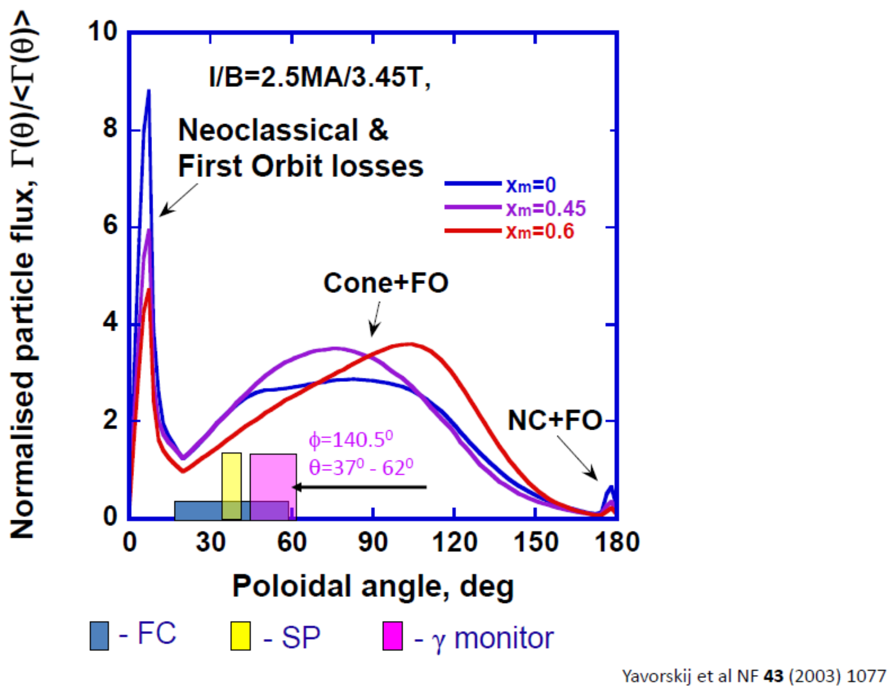

Figure 8.6: Position of the Be target (γ monitor)

The background assessments show that the same emission of 4.44-MeV gammas will be obtained from the $^{12}C(n,n'\gamma)^{12}C$ reactions in a CFC divertor tile of 80-140 g.

From the estimation of the amount of CFC falling into the Field-of-View of Channel 3 at the KJ5 location it follows that ratio between the CFC emission and target emission could be as high as 10.

8.4 Evaluation of the parasitic (12C) photon flux at the location of the KA4 detector

MCNP model:
-CATIA model for the KA4 Line-of-Sight , channel 2, with radiation system cross-sections and dimensions (see Figure 5.1)
Radiation transport:
-full numerical neutron transport
-analytical gamma transport

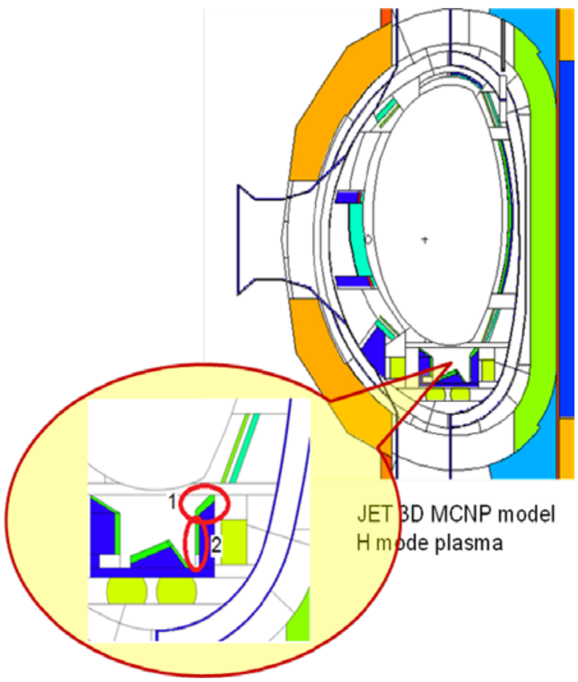

Figure 8.7: Location and numbering of the divertor cells for neutron flux and gamma production rate calculations

Evaluation of the parasitic 4.4MeV photon flux at the location of the KA4 detector.
The total neutron fluence (above 4 MeV), per source (plasma) neutron:
-cell 1 (tile 1): 6.5×10^{-07} n/cm^2
-cell 2 (tile 3): 4.0×10^{-07} n/cm^2
Average 4.4 MeV gamma emission per cm^3 of divertor material:
~10^{-8} photons per source neutron
Number of 4.4 MeV gammas reaching the detector:
~10^{-12} photons/source neutron.
At the KA4 detector location, the parasitic, neutron induced, gamma radiation is estimated to be 10-100 times higher than the alpha particle induced gamma radiation from the KA4 target.

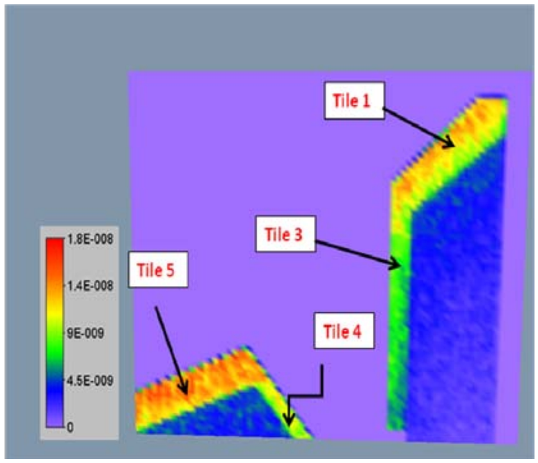

Figure 8.8: Density of prompt gamma emission in the CFC divertor (number of reactions per cm^3 of material).

8.5 MCNP calculations for the LAM Line of Sight

MCNP model
-CATIA drawing configuration shown in Figure 5.1.
-Point gamma-ray sources placed at the target position in a plane perpendicular to the axis of the detector Field-of-View (FoV).

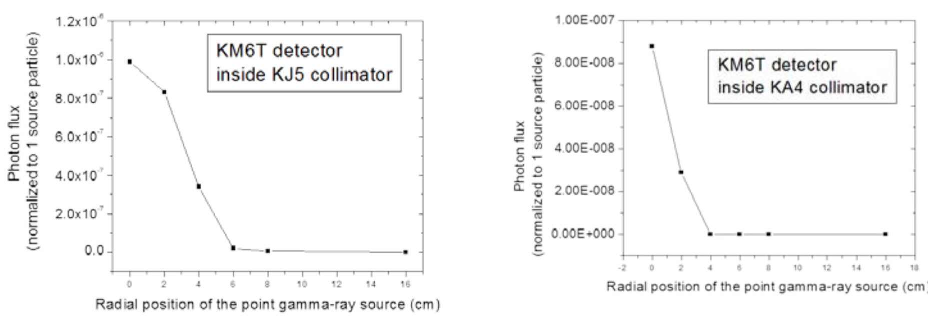

Figure 8.9: Gamma-ray source profiles: inside the KJ5 collimator (LHS), and inside the KA4 collimator (RHS)

For the KA4 detector inside the KA4 collimator the shielding factor for 4.4 MeV gamma-rays is about 100x higher than inside the KJ5 collimator.

9 Conclusions

The report on Feasibility Study and Conceptual Design, Phase I, contains detailed presentations of several technical solutions developed and evaluated for the Lost Alpha Monitor (LAM/KA4) diagnostics. Two different locations on JET were considered: one on the horizontal KN3 gamma-ray camera in Octant 1 and another on the KJ5 soft X-ray camera in Octant 4. Two design options were investigated for the KN3 location and four design options for the KJ5 location.

One of the KJ5 design options was developed up to the level of conceptual design. Its cost evaluation showed that the design and construction of such a system would have needed financial resources several times larger than those allocated to the LRM project.

The LRM project included also a first phase of numerical work done in support of the diagnostics design. The results of the numerical work had a direct impact on the design of the LAM/KA4 diagnostics. Among other things it has shown that for those design solutions in which the Field-of-View of the gamma-ray detectors included the CFC divertor tiles the ratio between the parasitic gamma-ray emission from the CFC tiles and the signal emission from the LAM target could be as high as 10.

10 References

[1] Kiptily, V.G. et al, Nuclear Fusion 42 (2002) 999

[2] Darrow, D. S., et al., Rev. Sci. Instrum. 75 (2004) 3566

[3] Baumel, S., et al., Rev. Sci. Instrum. 75 (2004) 3563

[4] Kiptily V.G. et al. Fusion Technol. 22 (1992) 454

[5] Kiptily V.G. et al., Fusion Alpha-Particle Diagnostics for DT Experiments on the Joint European Torus, International Conference on Fusion Reactor Diagnostics, Villa Monastero, Varenna (Italy), JET preprint EFDA–JET–CP(13)04/01

[6] Kiptily V.G. et al., Fusion Alpha-Particle Diagnostics for DT Experiments on the Joint European Torus, Presentation to the International Conference on Fusion Reactor Diagnostics, Villa Monastero, Varenna (Italy), September 2013.

[7] V. Yavorskij et al Physics of Plasmas 6 (1999) 3853-3867

[8] V. Yavorskij et al Nucl. Fusion 43 (2003) 1077–1090

[9] N. Hawkes et al. Plasma Phys. Control. Fusion, vol. 47, no. 9, pp. 1475-1494, 2005.

[10] V. Yavorskij et al Nucl. Fusion **50** (2010) 025002.

[11] Summary of the LRM Project Technical Meeting on March 31st, 2015.

[12] D. Falie, N.C. Zoita, V.L. Zoita, "Technique for signal processing under strong parasitic gamma radiation", Report on LRM contract NILPRP-ICIT, April 2015

[13] Horton L, “Recent Results from JET and Future Plans”, DIII-D Seminar, San Diego, February 10th, 2014.

[14] V.L. Zoita et al., "Upgrade of the JET Tangential Gamma-Ray Spectrometer. Conceptual Design", SOFE2009, Paper_09

ANNEX 1
Annex 1.1 EAG report on the KN3 location

Ref:	**EAG14/T008**	**Status: Issued**	**Issue: 1**
Date:	**26 February 2014**		**Page 1 of 102**

Project:
JET

Document Type:
Technical

Document Title:
Preliminary Assessment of KA4 Lost Alpha Target

Summary:

This note briefly summarises a preliminary assessment of a proposed Be target to be installed, if possible during the 2014 shutdown, in Octant 1C. The conclusion is that, owing to conflicts with RH equipment which has to be installed in that region, it would not be feasible to design manufacture and install such a target in this shutdown. It may be possible to engineer a solution for a later shutdown.

	Name(s)	Signature(s)	Date
Prepared by:	Vaughan Thompson		
Reviewed by:			
Approved by:	Valeria Riccardo		

DISTRIBUTION RECORD
Copies issued to:
An electronic copy of this document can be found at: N:\CCFE\CentralEng\Groups\ChiefEngr\EAG-notes\2014_EAG\EAG14_T008 KA4 Lost Alpha Preliminary I.1 .doc

DOCUMENT CHANGE CONTROL

ISSUE NO.	DATE	CHANGES FROM PREVIOUS VERSION
1 Draft A	21 May 2014	None. Original Document

INTRODUCTION

This note briefly summarises a preliminary assessment of a proposed Be target to be installed, if possible during the 2014 shutdown, in Octant 1C. The conclusion is that, owing to conflicts with RH equipment which has to be installed in that region, it would not be feasible to design manufacture and install such a target in this shutdown. It may be possible to engineer a solution for a later shutdown.

Figure 1 shows the proposal which consists of a recycled Be mushroom tile mounted in the region of the lower outer saddle coils. The tile would be mounted about 250 mm off the saddle coils in order to bring its front face in line with the WPL. Note this is the only region available for this diagnostic since in must be in direct field of view of the camera in this sector. Figure 1 shows the camera sight lines.

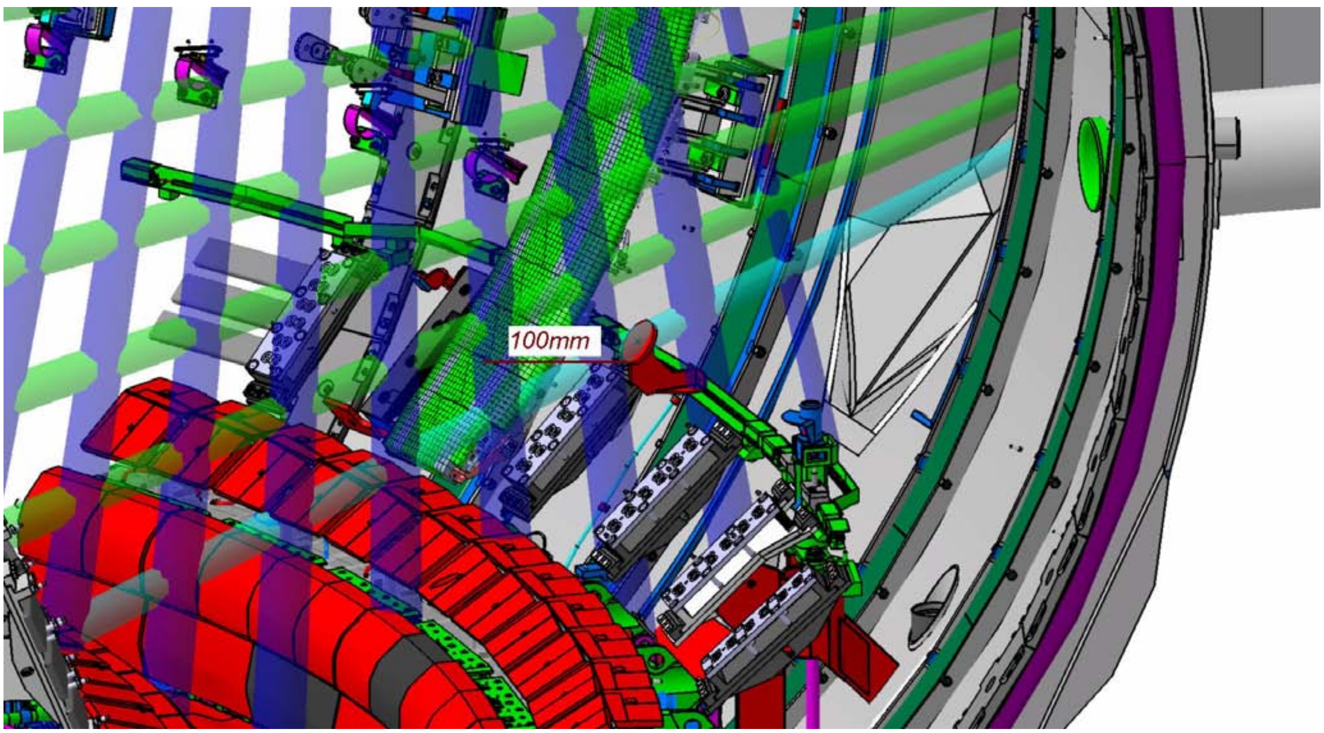

Figure 1. KA4 Lost Alpha Particle Target in Sector 1C

Appendix A contains the minutes from a meeting on 6/3/14 giving background information to the proposal and Appendix B gives notes on a preliminary structural assessment in the area. Three concepts were considered:

1. A bar clamp arrangement as shown in Figure 11.

2. A bracket mounted off two adjacent saddle coil tile carriers
3. A bracket mounted off one adjacent saddle coil carrier.

Concept 1 offers the best structural arrangement but would conflict with the RH equipment which needs to be installed through the MHP in Sector 1C at the start of each shutdown. Figure 2 and Figure 3 show this equipment in position. Similarly Concept 2 would likely clash with the RH equipment.

Concept 3 remains a possibility, although it would require complex RH tooling which would be a severe challenge to design and manufacture in time for the 2014 shutdown. The concept would work as follows:

- Install a permanent fixture under the RH SC tile carrier which does not clash with the RH equipment.
- Install a removable stalk and tile onto this fixture which would inevitably conflict with the RH equipment.
- During every shutdown, the first operation would have to be removal of the stalk and tile before the RHJ chute and wands were deployed.
- During every shutdown, the last operation would have to be re-installation of the tile and stalk after the RH chute and wands had been removed.

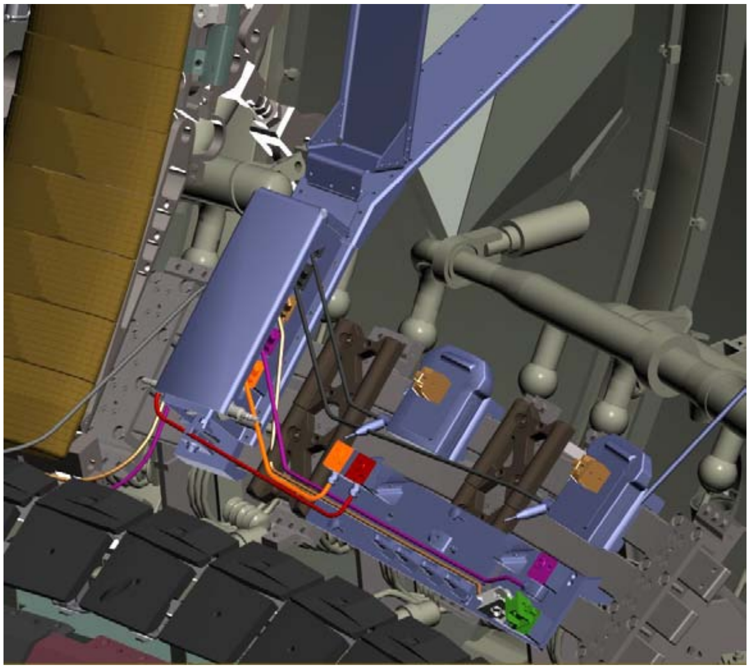

Figure 2. RH Shute and Wands in Sector 1C

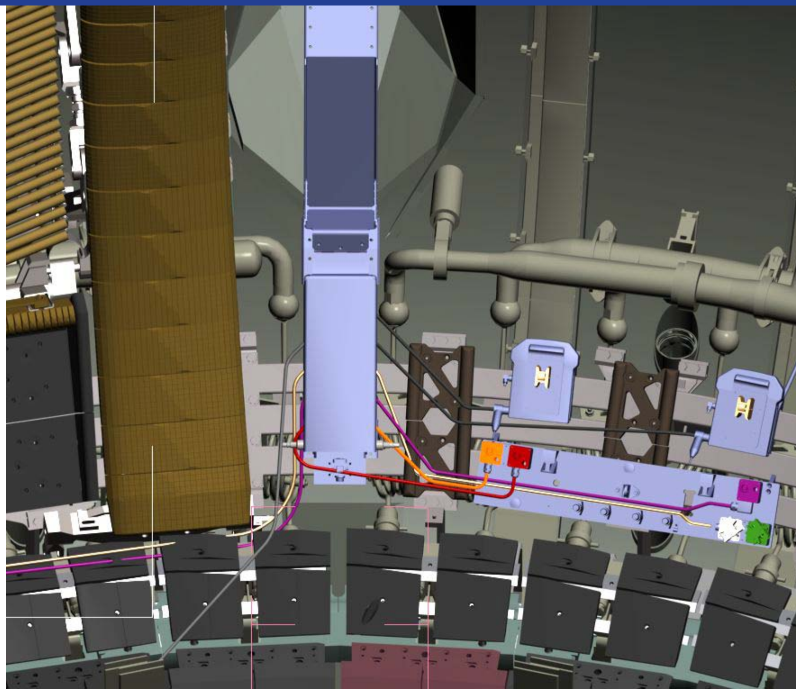
Figure 3. RH Shute and Wands in Sector 1C

For future reference, Appendix C contains details of the welds on the structure supporting the saddle coil bars in this region.

APPENDIX A: MINUTES OF MEETING ON 06.03.2014

Participants: A. Murari, J. Figueiredo, P. Lomas, V. Riccardo, V. Kiptily, S. Soare, V.L. Zoita

Summary of the main conclusions

- Space envelope & positioning:
  - The target is to be installed in the middle of the Octant 1 vacuum port. Its carrier does not span any bellows.
  - The target carrier will be a bridge to be mounted on two saddle coil brackets, figure 1. One bridge leg should be electrically insulated in order to break any induction loop.
  - The distance from the limiter apex to the innermost tip of the prototype target could be less than 100 mm, under the following conditions:
    - A. The monitor target will be made of bulk Be
    - B. Particles modeling required to asses the prototype position & geometry

  - New INCONEL saddle coil brackets have to be re-designed for the purpose, manufactured and installed; check if current bracket design is suitable unchanged
  - No electrical connections are needed

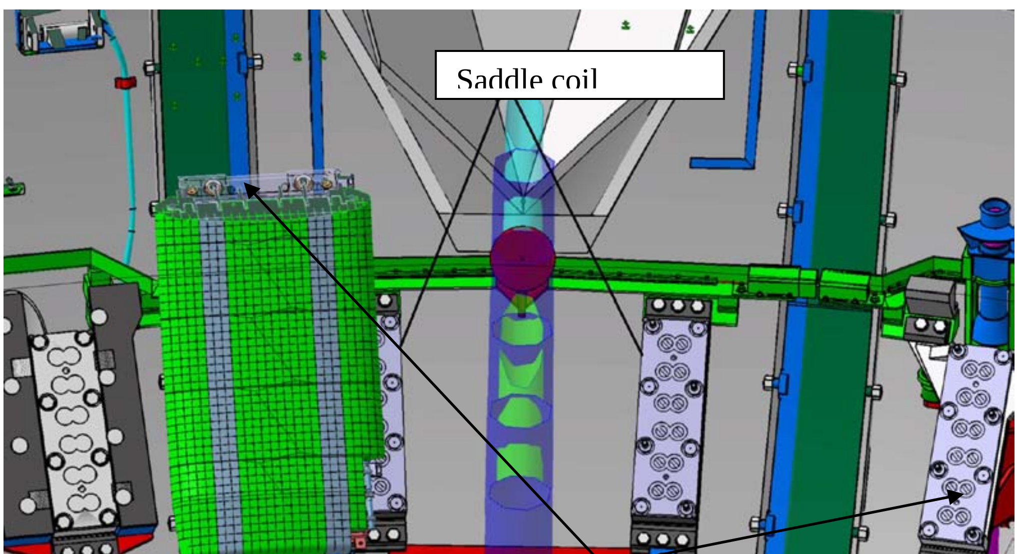

Figure 1 Target carrier is to be mounted on ... ddle coils brackets shown above; bellows on the sides

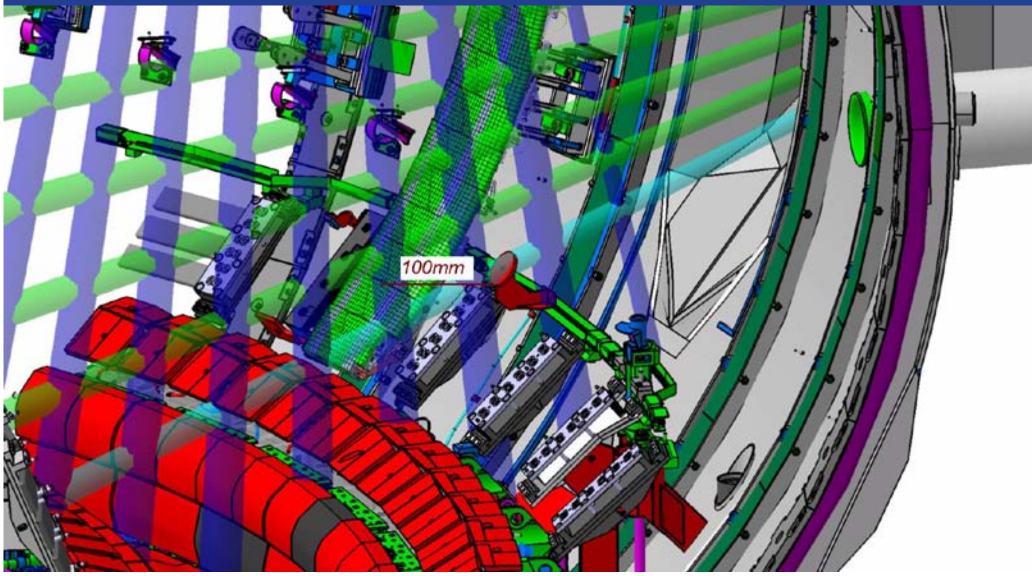

Figure 2 Distance from the limiter apex to target edge less that 100mm possible

- -In order to save time, the prototype target will be a replica of a mushroom tile, together with its INCONEL interface.
-The prototype target will be manufactured by Atmostat, France, from a Be rod made available by JOC.
The manufacture of the prototype (estimated at about 5kE) will be paid by the project. An alternative is for the order to Atmostat to be placed by JOC and the costs to be included in JOC's contribution to the project.
-The DT version of the monitor target should be designed according to the specification of an in-vessel power handling component. The design will be optimized based on the results obtained with the prototype target.

Actions:
- Recess of the mushroom tiles with respect to the dump plates/limiter: to be checked (P. Lomas)
-The mechanical limits of the connection between the saddle coil bracket and the vacuum vessel should be checked (V. Riccardo).

APPENDIX B. PRELIMINARY STRUCTURAL ASSESSMENT.

KA4 Pre-TCD-R Assessment. Lost Alpha Particle Monitor.

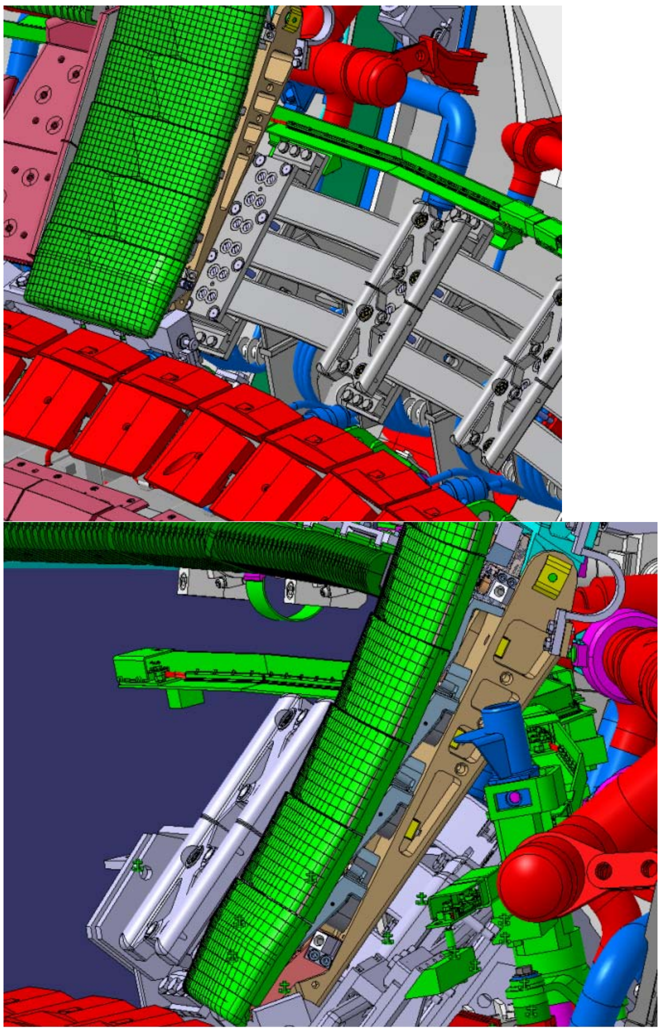

Figure 4 Sector 1C.

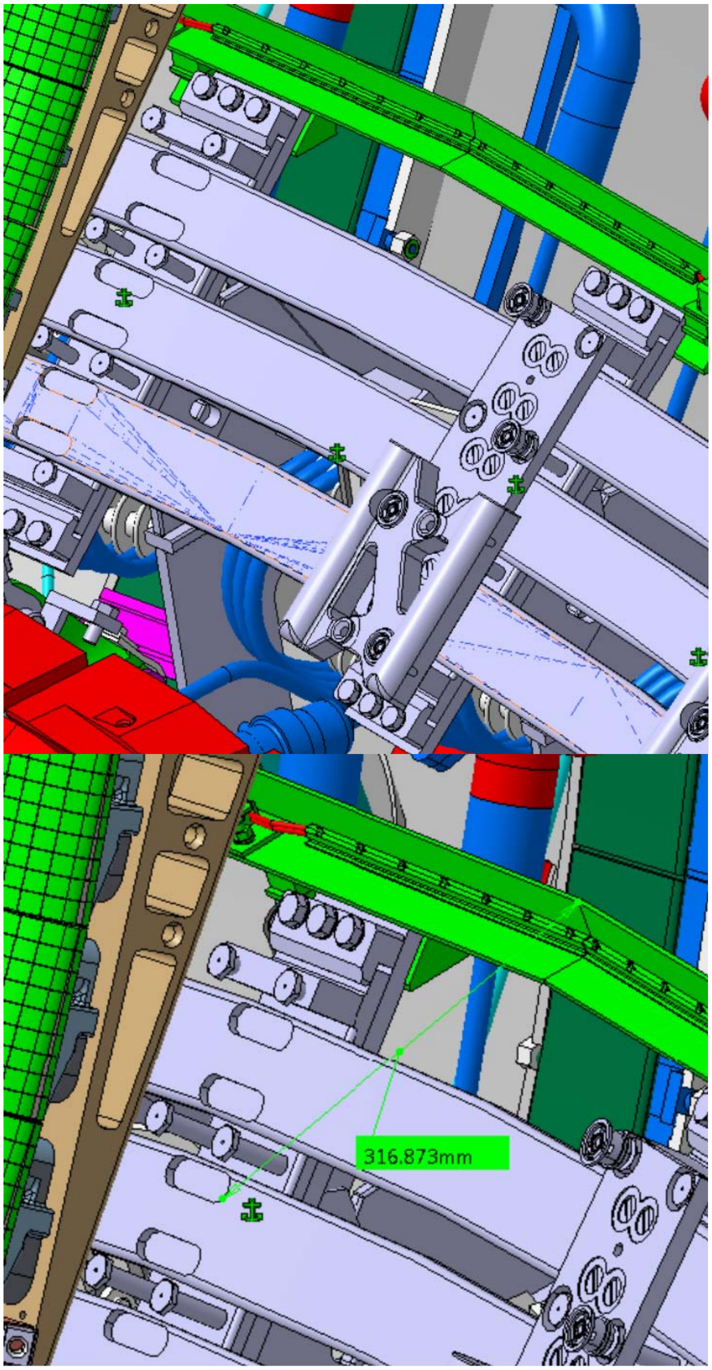

Figure 5 Sector 1C showing lower outer saddle coils where probe may be supported.

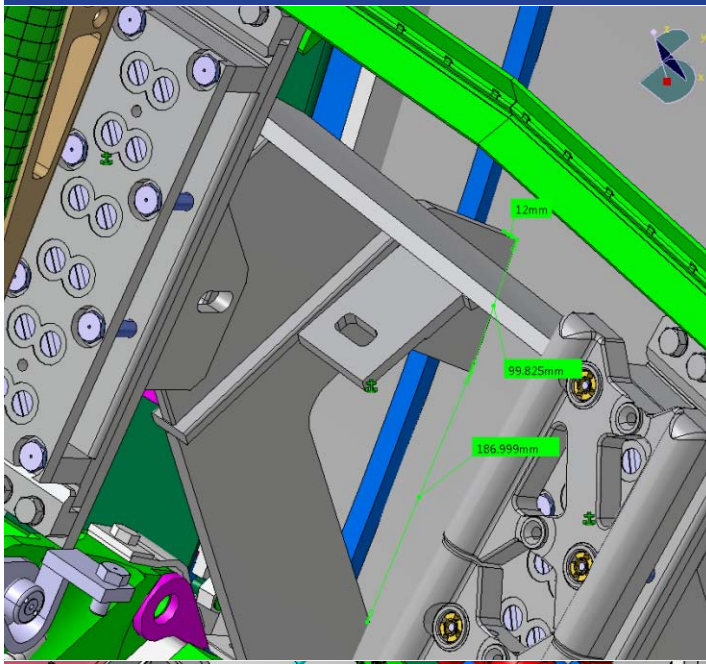
12mm
99.825mm
186.999mm

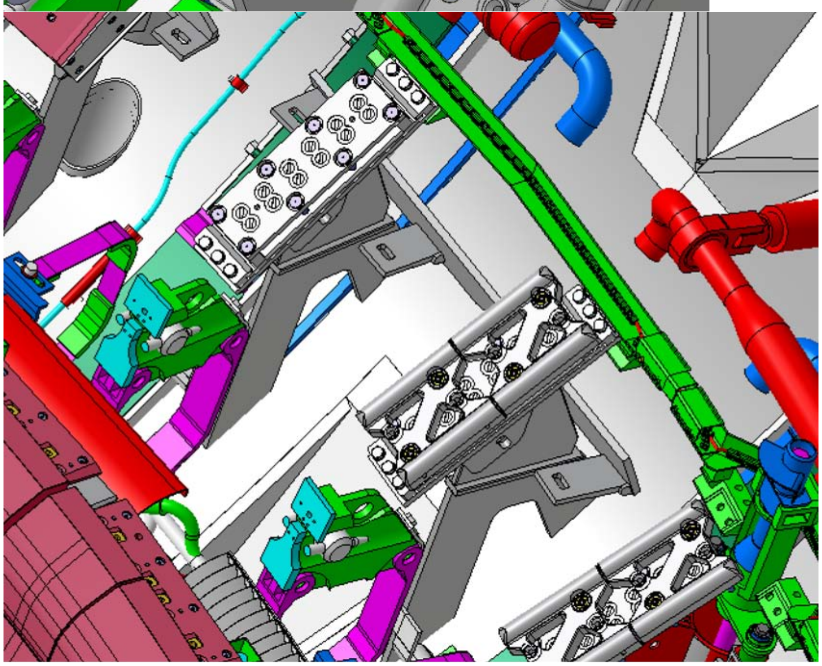

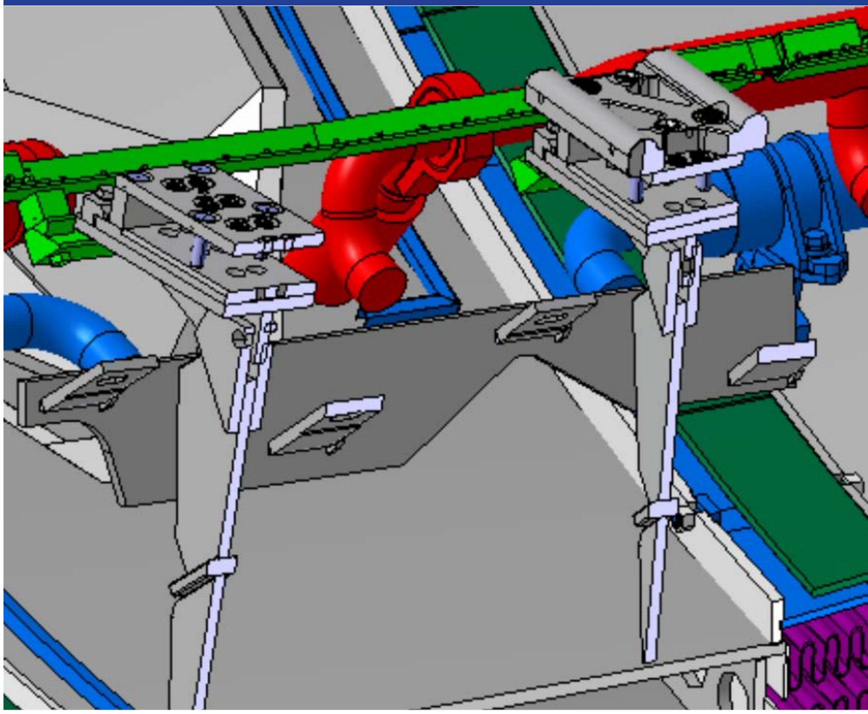

Figure 6 Sector 1C showing lower outer saddle coils where probe may be supported.

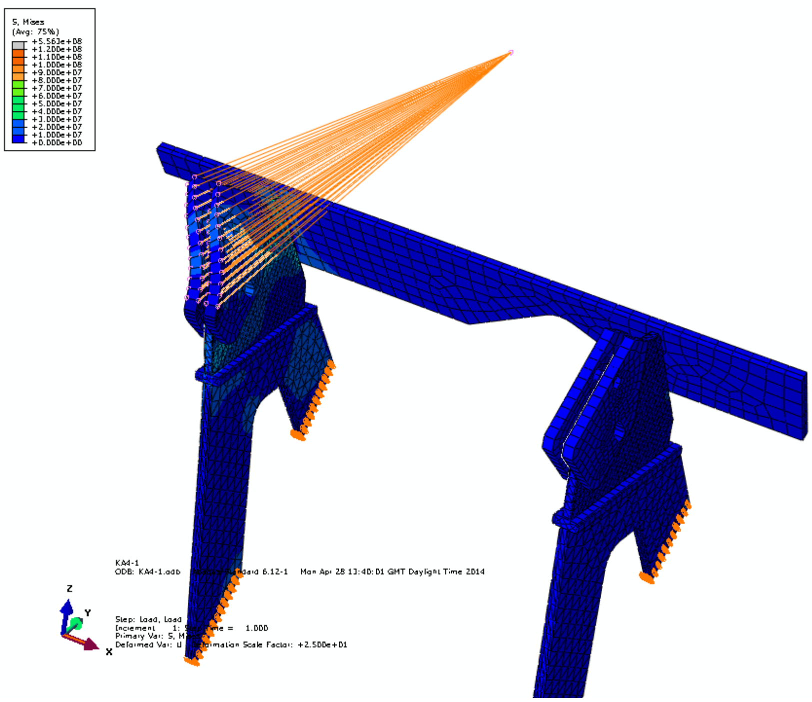

Figure 7 FE Model showing coupling from a remote point to represent a nominal halo load of 1 kN (in z). FE Ref: KA4-1b

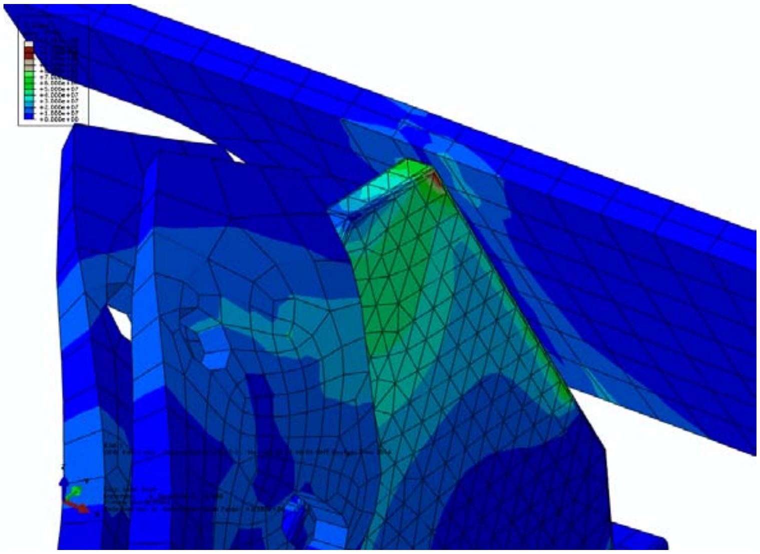

Figure 8 Close up showing that the only region is with high stress (>250 MPa) is very localised at a welded joint. FE Ref: KA4-1b

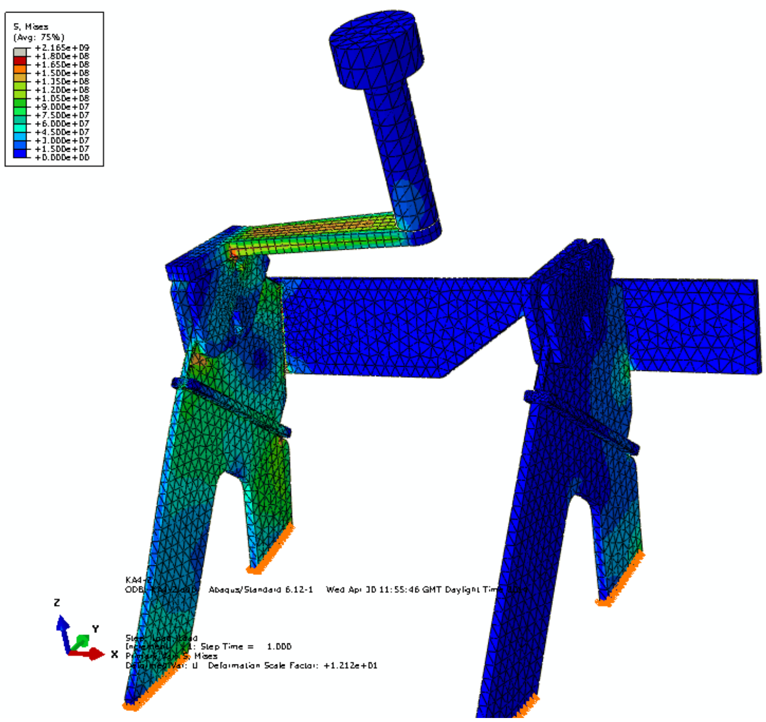

Figure 9. FE Ref: KA4-2a

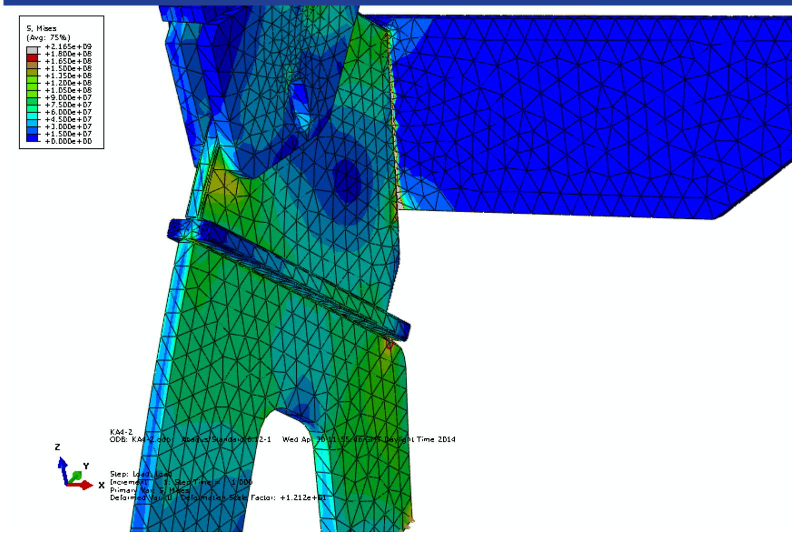

Figure 10. FE Ref: KA4-2a

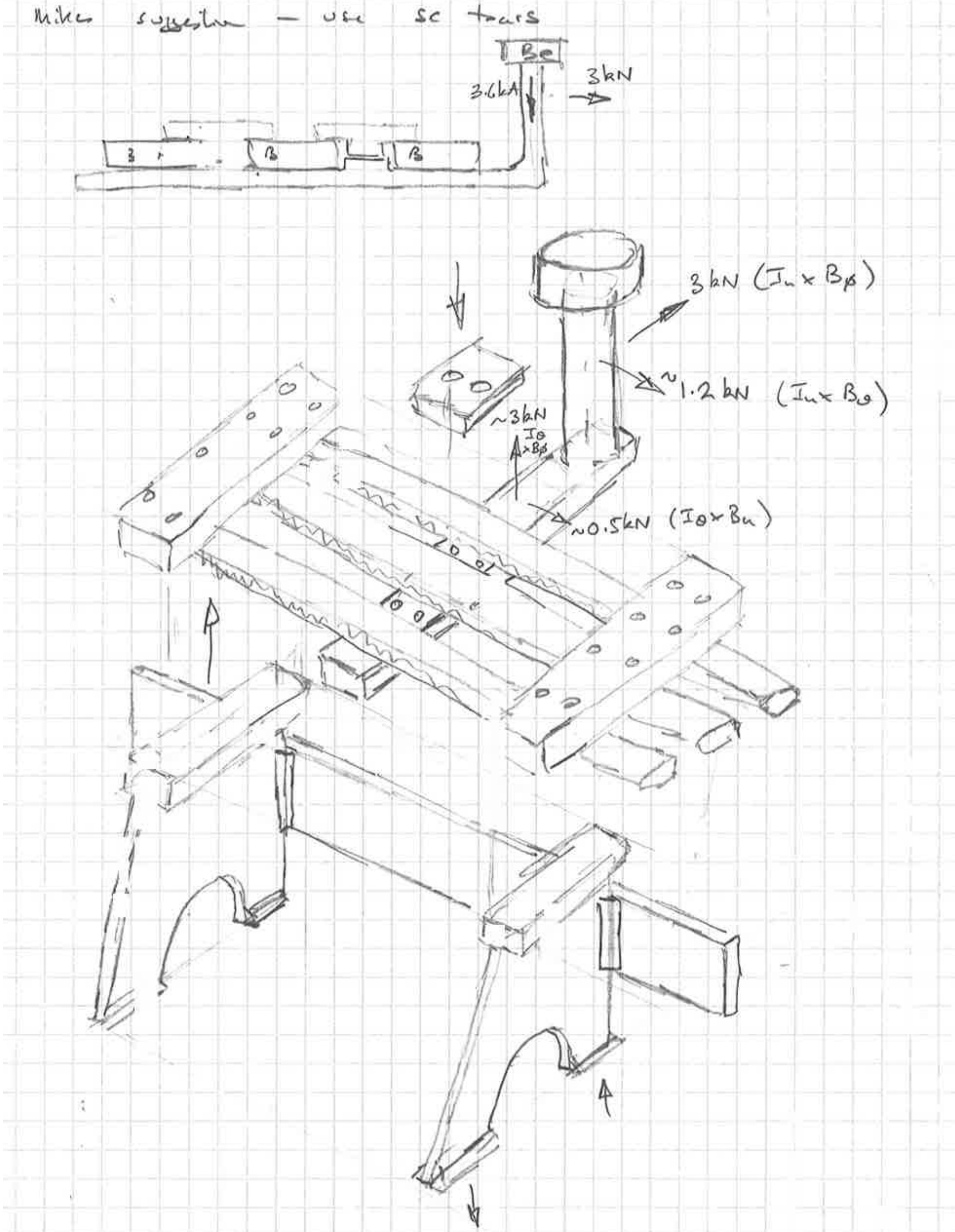

Figure 11. Bar Clamp Concept

APPENDIX C: DETAILS OF SADDLE COIL SUPPORT WELDS.

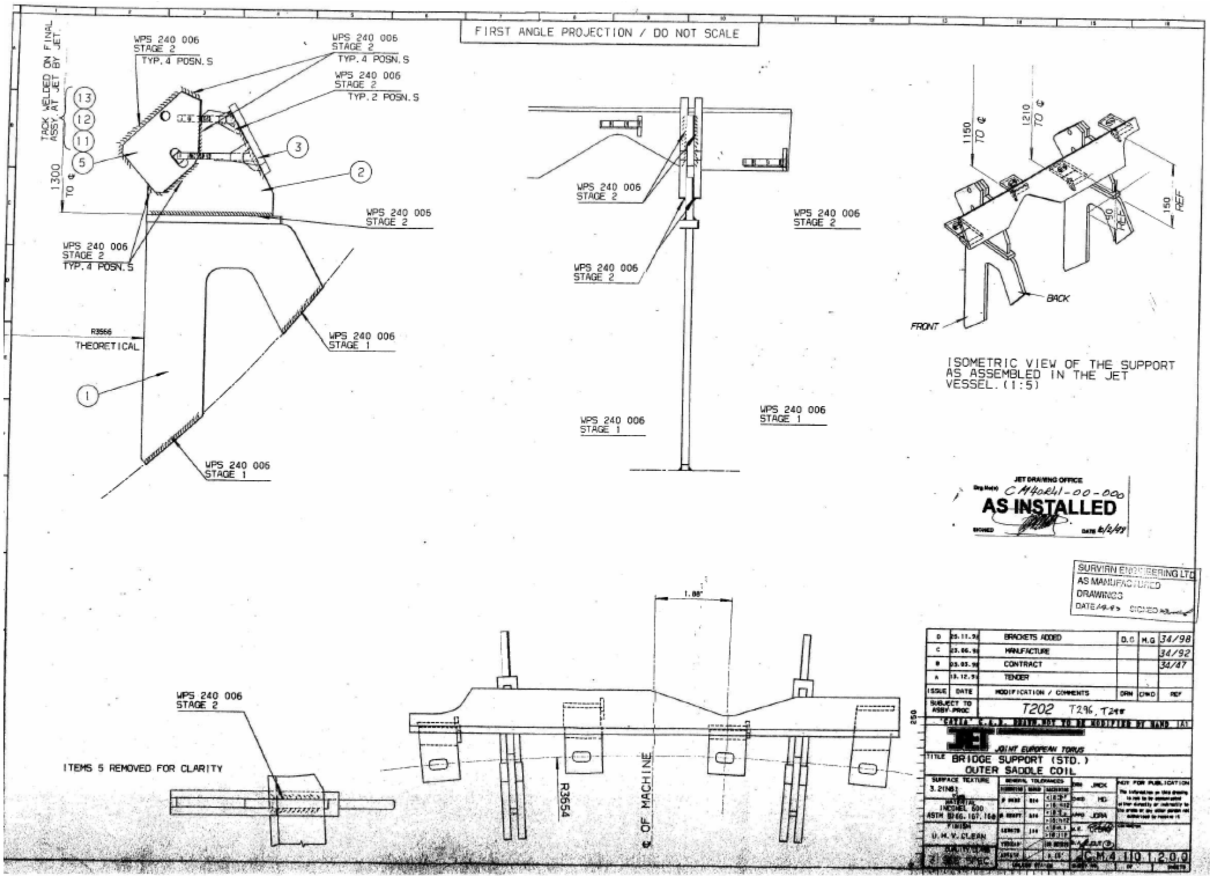

Code for Numbering of WPS

Each WPS has a six digit number.

The first three relate to material and geometry, and the last three to identification of the WPS. This is indicated in the identification box diagram below:

Identification Box

1	2	3	4	5	6

1. **Identification Box 1 : Material Type**

   2 = Inconel
   3 = Stainless Steel - Type 304 - 316
   Type 304L - 316L
   4 = Stainless Steel - Type 321
   5 = Copper
   6 = Carbon Steel

2. **Identification Box 2 : Type of Joint / Weld**

   2 = Tube butt joint - Full penetration butt weld
   3 = Plate butt joint - Full penetration butt weld
   4 = Equal fillet weld or Partial penetration fillet weld
   Tee joint - Plate to Plate or Tube to Plate
   5 = Branch joint
   6 = Lip - Plate to Plate or Tube to Tube
   7 = Tube to Flange
   8 = Lap - Plate to Plate
   9 = Others:
   - Sleeve or Socket joint
   - Full penetration fillet weld
   - Partial penetration butt weld
   - Tack welds
   - Plug weld
   - Buttering
   - Etc...

3. **Identification Box 3 : Dissimilar Material**

   0 = Similar material
   1 = Dissimilar material

Where dissimilar material is used the material type number relating to the highest nickel content is used in the first box.

4. **Identification Boxes 4,5 & 6**

The last three boxes identify the WPS starting from 001.

JET Manual Welding Procedure Specification (WPS)

240 006

SECTION A

Manual Welding Process
TIG

Joint Type
Equal Fillet Weld 6mm

Welding Position
All Positions

Base Material Spec Size
ASTM B 168 - Inconel 600
T = 6.0mm

Weld Surface Finish
As welded

Joint Sketch

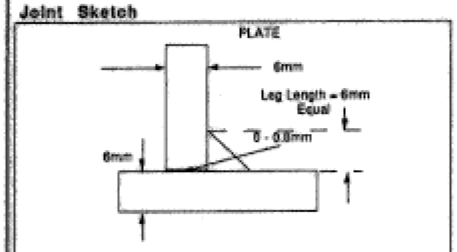

SECTION B

Standard
JET QTD 107

PQR No
006

Shielding Gas Make Type
Argon - High Purity to BS 4365

Filler Spec
SFA 5.14 ERNi Cr-3

Cleaning
Use approved solvent for distance of 50mm from weld centre line.
Use Scotch Brite on filler material.

Interpass Temperature
150°C Max

Run Sequences

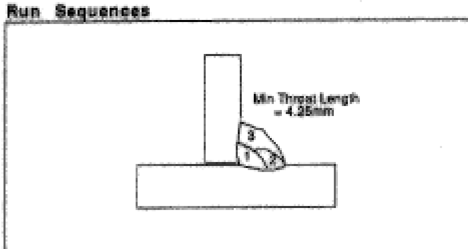

Other Information

Weaving shall not exceed 1/4 orifice diameter.

Weld run no.	Filler size (mm)	Electrode		Nozzle size (mm)	Current		Polarity of electrode (DC ONLY)	Volts	Flow rate shielding (l/min)	Flow rate purge (l/min)	Purge gas type
		Type	Dia.		Amps	AC/DC					
1	1.6	Tungsten 2%Thor	2.4	10 ID	100/120	DC	○ +ive ◉ -ive		8	N/A	
2	2.4	Tungsten 2%Thor	2.4	10 ID	100/120	DC	○ +ive ◉ -ive		8	N/A	
3	2.4	Tungsten 2%Thor	2.4	10 ID	100/120	DC	○ +ive ◉ -ive		8	N/A	
							○ +ive ○ -ive				
							○ +ive ○ -ive				
							○ +ive ○ -ive				

Replaces the 11.5.92 issue

QA Approval date
14 JUL 1993

STAMP: JET

Signature:

BEI

TPI Review date
15TH July 1993

STAMP: BRITISH ENGINE INSURANCE LTD.

Signature:

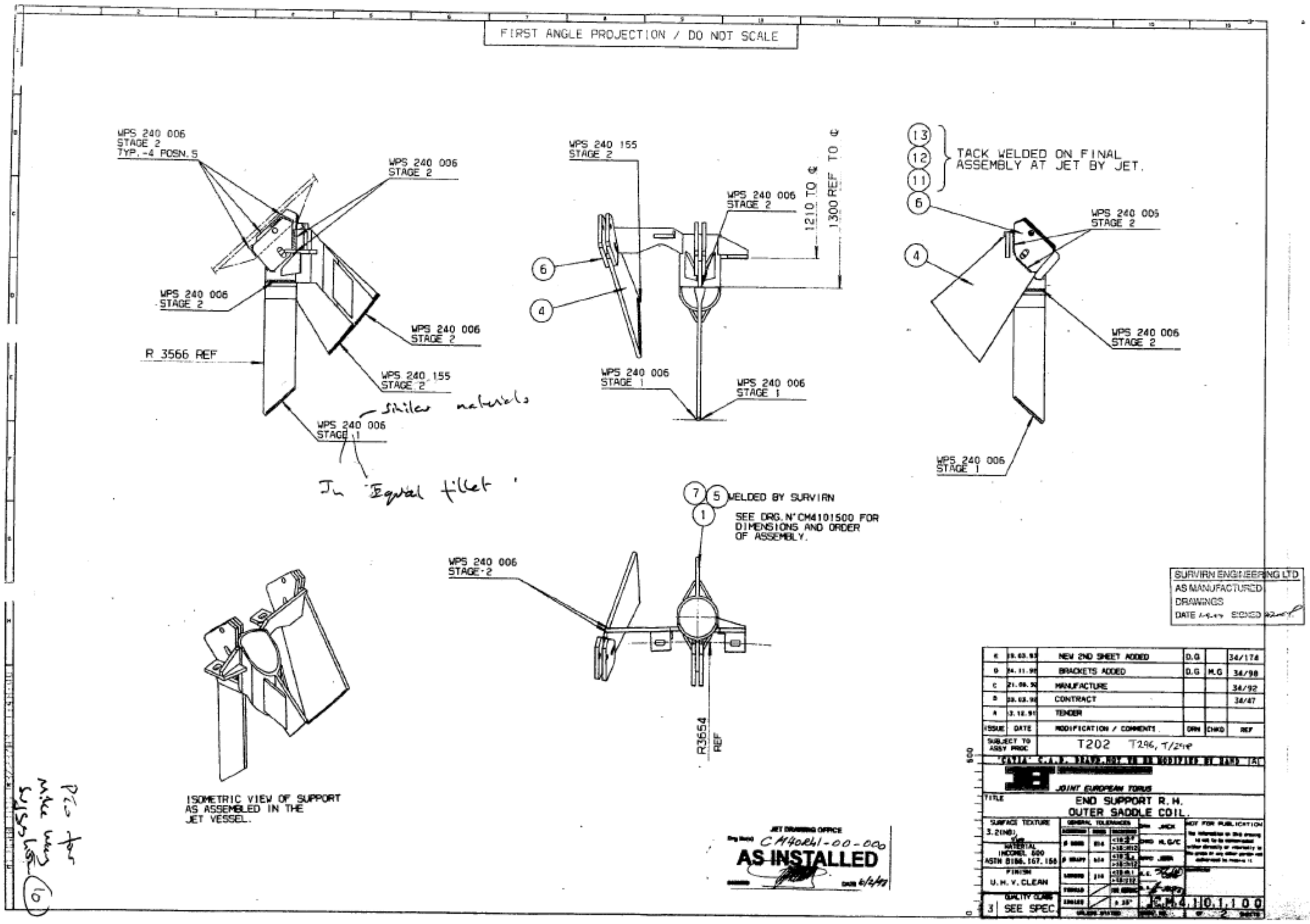

FIRST ANGLE PROJECTION / DO NOT SCALE
WPS 240 006 STAGE 2 TYP.-4 POSN.S
WPS 240 006 STAGE 2
WPS 240 155 STAGE 2
WPS 240 006 STAGE 2
1210 TO ℄
1300 REF TO ℄
TACK WELDED ON FINAL ASSEMBLY AT JET BY JET.
WPS 240 005 STAGE 2
R 3566 REF
WPS 240 155 STAGE 2
WPS 240 006 STAGE 1
WPS 240 006 STAGE 1
WPS 240 006 STAGE 2
WPS 240 006 STAGE 1
WELDED BY SURVIRN
SEE DRG. N° CM4101500 FOR DIMENSIONS AND ORDER OF ASSEMBLY.
WPS 240 006 STAGE 2
R3654 REF
ISOMETRIC VIEW OF SUPPORT AS ASSEMBLED IN THE JET VESSEL.
AS INSTALLED
SURVIRN ENGINEERING LTD AS MANUFACTURED DRAWINGS
NEW 2ND SHEET ADDED
BRACKETS ADDED
MANUFACTURE
CONTRACT
TENDER
T202
JOINT EUROPEAN TORUS
END SUPPORT R.H. OUTER SADDLE COIL
U.H.V. CLEAN
SEE SPEC

JET Manual Welding Procedure Specification (WPS)

WPS No 240 155

SECTION A

Manual Welding Process
TIG

Joint Type
Partial Penetration Fillet Weld

Welding Position
All Positions

Base Material Spec Size
ASTM B 168 - Inconel 600
T=12mm

Weld Surface Finish
As Welded

Joint Sketch

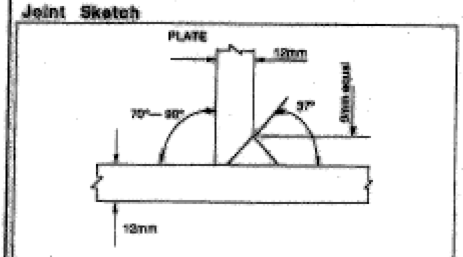

SECTION B

Standard
JET QTD 107

PQR No
012

Shielding Gas Make Type
High Purity Argon to BS 4365

Filler Spec
AWS A5.14 ERNi Cr-3

Cleaning
Use approved solvent & SS wire brush for distance of 50mm from weld centre line. Use Scotch Brite on filler material

Interpass Temperature
150° C Max.

Run Sequences

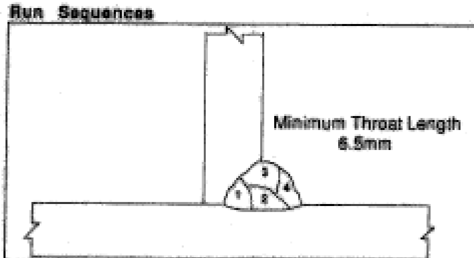

Other Information

Weaving shall not exceed 1/4 orifice diameter.

QUALITY J E T

Weld run no.	Filler size (mm)	Electrode Type	Electrode Dia.	Nozzle size (mm)	Current Amps	Current AC/DC	Polarity of electrode (DC ONLY)	Volts	Flow rate shielding (l/min)	Flow rate purge (l/min)	Purge gas type
1	1.6	Tungsten 2%Thor	2.4	10	100/120	DC	○ +ive ● -ive	—	8	N/A	—
2	2.4	Tungsten 2%Thor	2.4	10	100/120	DC	○ +ive ● -ive	—	8	N/A	—
3	2.4	Tungsten 2%Thor	2.4	10	100/120	DC	○ +ive ● -ive	—	8	N/A	—
Balance	2.4	Tungsten 2%Thor	2.4	10	100/120	DC	○ +ive ● -ive	—	8	N/A	—
							○ +ive ○ -ive				
							○ +ive ○ -ive				

QA Approval date 24 JUN 1992

STAMP: QUALITY J E T

Signature:

TPI Review date

STAMP:

Signature:

8

Annex 1.2 EAG report on the KJ5 location

Ref:	**EAG15/T007**	**Status: Draft A**	**Issue: 1**
Date:	**19 June 2015**		**Page 1 of 102**

Project:

TAE Limiter

Document Type:

Technical Note

Document Title:

Design issues and evaluations for the longer upper tile

Summary:

This note summarises the TAE design issues that require further confirmation and consideration. The electromagnetic (EM) loads were recalculated and re-evaluated for the longer tile assembly. The reserve factors (RF's) for the longer upper tile assembly were re-evaluated using the results of the previously performed analyses.

	Name(s)	**Signature(s)**	**Date**
Prepared by:	Yuri Krivchenkov		
Reviewed by:	Zsolt Vizvary		
Approved by:	Daniel Iglesias		

DISTRIBUTION RECORD
Copies issued to:
An electronic copy of this document can be found at: **N:\CCFE\CentralEng\Groups\ChiefEngr\EAG-notes\2015_EAG**

DOCUMENT CHANGE CONTROL

ISSUE NO.	DATE	CHANGES FROM PREVIOUS VERSION
1 Draft A	19 June 2015	None. Original Document

1. Background

Twice longer beryllium upper tile was suggested for the TAE vertical limiter in frame of the γ-ray experiment (Figure 1). Carrier supporting the beryllium tile was also extended in the vertical direction. However, the connection between the carrier and rail was supposed to be of the same type. In other words the extended portion of the tile assembly can be considered as a cantilever attached to the existing tile assembly. Therefore, the support system of the longer tile assembly remains the same as for the existing tile. Obviously the EM loads due to the eddy and halo current flows will be larger for the longer tile.

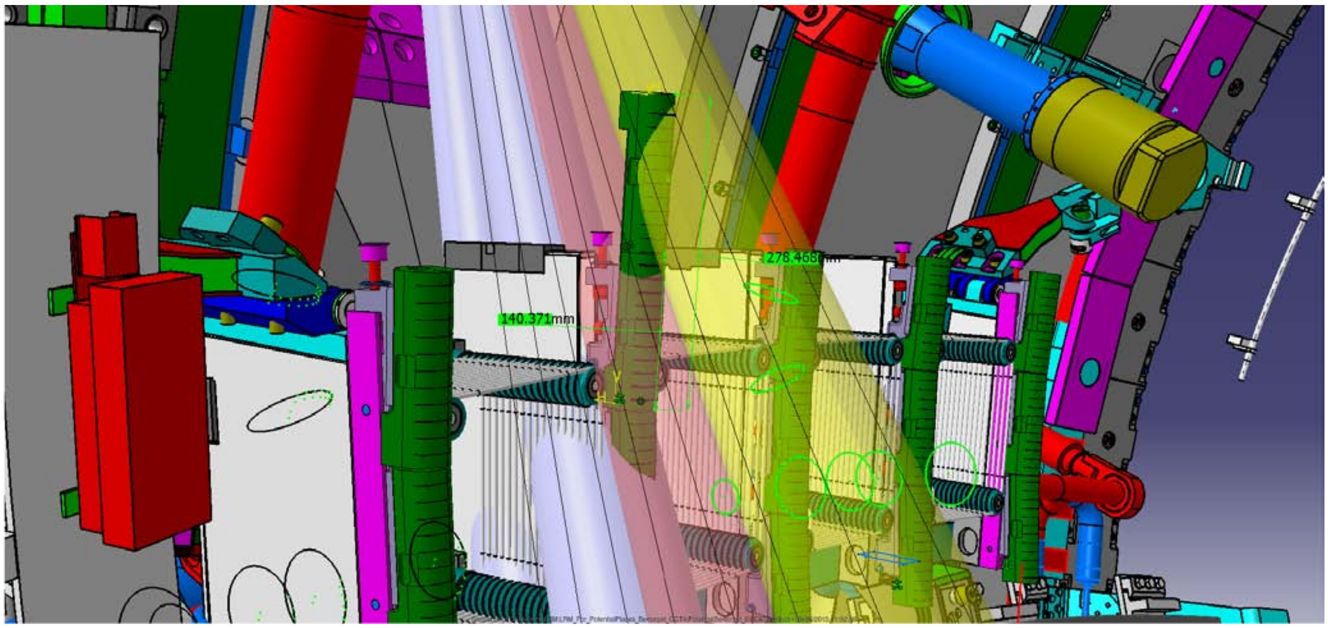

Figure 1 – Extended upper beryllium tile (middle) of the TAE limiter. Extended carrier is not shown.

2. References

[1] ILW/EDM/1215/D009 - TAE Bumper Analysis
[2] ILW/EDM/1215/D029 - FE Analysis of the TAE Tile

3. Assumptions on the evaluations

The reaction of the support system was provided by the bolted joint between the carrier and rail at one side and by the pinned joint between the carrier hook and rail at the other end. In general, reactions of the supports depend on the loads magnitude and on the load special distribution. Approximately, remaining in frame of the linear consideration and considering carrier as a rigid body and remember that supports system was not changed and the reserve factors (RF's) were calculated for the integral loads, we can assume that RF's calculated in previous reports for the components of the support system will be reduced by factor of the load magnitude increase. Therefore, the EM loads for the longer tile were evaluated first.

4. Eddy torque

The eddy torque was calculated for the new tile assembly and compared (Table 1) against that of the existing one.

$$M_{eddy\_tile} = \begin{pmatrix} 29.856 \\ 73.994 \\ 43.948 \end{pmatrix} J \qquad M_{eddy\_longer\_tile} = \begin{pmatrix} 64.564 \\ 162.367 \\ 87.897 \end{pmatrix} J$$

where vector $M = \begin{Bmatrix} Mtor \\ Mpol \\ Mrad \end{Bmatrix}$

Table 1 – EM torque ratio between longer and existing tiles.

	Mtor	Mpol	Mrad
Increase factor	2.16	2.19	2.0

Approximately we can conclude that the eddy torque was increased by factor of at least 2 for the longer tile.

5. Halo loads

The halo scenario assumed that halo current will flow from the vacuum vessel into the plasma through the TAE tiles. Assumption on the halo current flow from the vacuum vessel to the tile through the bolted joints and the back from the tile side and upper surfaces to the plasma is shown in Figure 3 for the upper longer tile. There are two bolted joints now between the carrier and beryllium tile. Some halo force components will cancel each other because currents are coming in opposite direction but some will increase.

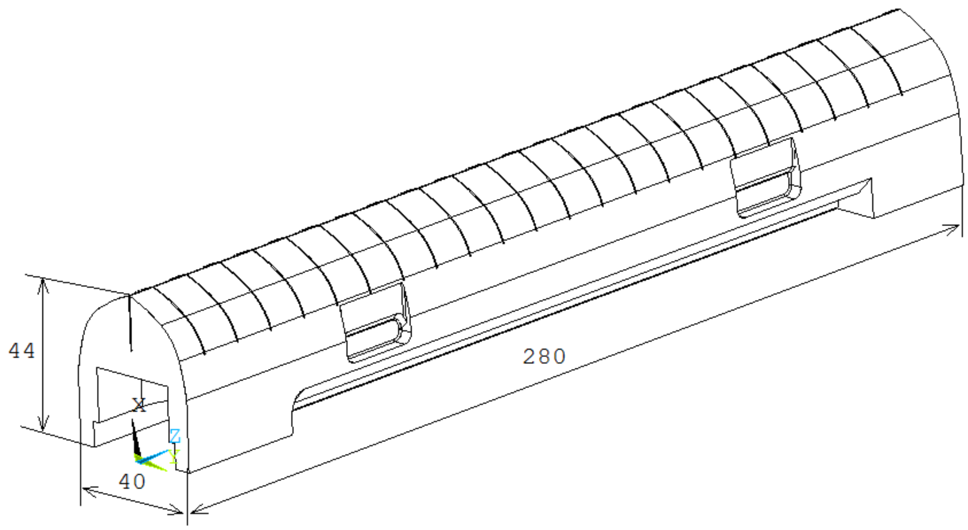

Figure 2 – Longer tile overall dimensions.

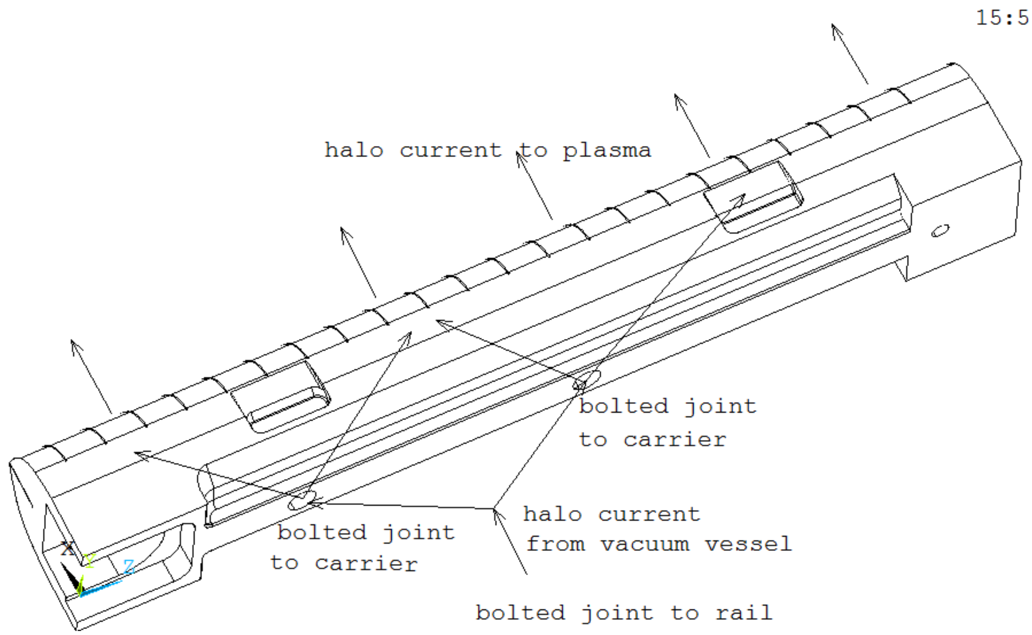

Figure 3 – Schematics on the halo current flow from the vacuum vessel back to the plasma.

The halo forces and halo moments referred to pin are the following for the existing upper tile:

$$Fhalo = \begin{Bmatrix} -0.2 \\ 0.45 \\ 0.42 \end{Bmatrix} \text{kN} \qquad Mhalo = \begin{Bmatrix} 11 \\ -4.5 \\ 13.4 \end{Bmatrix} Nm$$

Comparison between the M halo and M eddy is at least a factor of 3 with respect to the existing tile.

6. RF evaluation for the longer tile

Summarising considerations above for the eddy and halo load factors we can therefore conclude that the magnitude of the load factors on the support system, both eddy and halo, will increase by at least a factor of 2.
In this case the reserve factors calculated in [1] can be reduced by factor of 2.

In particular the important RF's are the following:

- The RF for the bearing of the pin and the carrier (poor fit) was less than 0.8 and would become less than 0.4.
- The RF of the top M10 bolt attaching the carrier to the rail was 0.94 and would become less than 0.5.
- The RF for the carrier in torsion was 0.98 and would become less than 0.5; the material is already Inconel 625 so no improvement is possible.
- There is an uncertainty on the RF of the pin (supporting the tile assembly on the rail). This could be as low as 0.23 (scaling of analytical RF) if the carrier is a gap fit or much larger for finite element analysis with the interference fit [2].
- There is also concern that the thermal bending of the twice longer tile is proportional to second order of the tile length, i.e. thermal bending will increase by factor of 4. Further analysis for the bolt attachments and Be tile is required to determine this RF.
- The other reserve factors remain unchanged assuming that the carrier as well as the tile will double in poloidal extent and that the tile and carrier are joined by two bolts (one to be engineered to allow relative thermal expansion).

- As there are at least three RF (reserve factors) less than 0.5 (ideally we should have more than 1, but 0.8-1 range could be acceptable), this modification is not viable.

7. Conclusions

- As there are at least three RF (reserve factors) less than 0.5 (ideally we should have more than 1, but 0.8-1 range could be acceptable), this modification is not viable.

ANNEX 2
Evaluation of lost particle fluxes for DT experiments. Phase I
(OEAW Report)

Deliverable D-2.01
Evaluation of lost particle fluxes for DT experiments. Phase I.

Evaluation of loss fluxes and gamma emission in the alpha-particle mimicking experiments

One of the main arguments for the Be target position is the poloidal and toroidal distribution of high energy (E>2MeV) alphas escaping from the plasma. According to previous studies [1] the maximum first orbit (FO) loss of fusion alphas is expected at poloidal angles 60°-90° below the mid-plane, where the flux of lost alphas exceeds the DT neutron flux for plasma currents I < 2.25MA and typically is about 50-100% of the neutron flux at plasma currents 2.5MA < I < 3MA. RF heated alphas with E > 2MeV, observed in JET with gamma-ray diagnostic [2,3], are expected to be lost at poloidal angles well above the poloidal angles of maximum FO loss. According to our qualitative estimate, based on the results of analysis of [3], the RF heated alphas should be lost at poloidal angles ~ $(5\div10)\cdot(\tau_b/\tau_{st})^{1/4}$, where τ_b and τ_{st} are the bounce time and, respectively, the time spent to heat alphas to E>2MeV. According to this estimation the ICRF accelerated alphas are lost roughly at poloidal angles 10°-20° below the mid-plane. Note that losses of ICRF accelerated MeV protons and deuterons were detected at the scintillator probe (SP) located at 31° below the mid-plane [4]. For obtaining more reliable poloidal angles of lost RF heated alphas we plan to perform an appropriate Monte-Carlo simulation using our code DOLFI, which is especially designed for the treatment of fast ion loss distributions. Finally we note that our recent analysis of the MHD-mode induced loss of DD charged fusion products, based on SP measurements in JET [5], indicates that the MHD-mode induced loss of fast alphas are expected to be localized at poloidal angles slightly below the equatorial plane as well.

The present investigation is focused on the optimization of the LRM beryllium target position, size and orientation to achieve a maximum gamma emission from nuclear reactions of lost fast alphas with the target beryllium. As an example, the Be target was placed between the vertical gamma-camera channels #17 and #18 field of view (FoV) of the horizontal channel #10 (see Fig.1), where the FO losses are expected. Our analysis was then devoted to the gamma emission associated with the prompt loss of fusion alphas.

Because of the insignificant impact of collisions and weak perturbations of the magnetic field on the FO losses we have used a backward-in-time full orbit-following alpha particle trajectory calculation in axisymmetric approximation, as exemplified in Fig. 2. For that we start from 560 uniformly distributed points on the LRM pellet with 9 different directions of starting velocities at each point. This is illustrated in Fig. 3. Alpha particle fluxes to the LRM target were calculated for various target positions in the FoV of the horizontal channel #10 as well as for several target sizes and orientations. The most favorable equatorial inclination of the target symmetry axis is found to be about 30 deg with respect to the channel #10 LoS (Fig. 4) and the optimum LRM target position is shown to be close to the channel #17 LoS (Fig. 5).

LRM report summary

- The efficacy of gamma emission induced by 2-4 MeV alpha particles escaping from the JET plasma onto the beryllium LRM target due to the first orbit loss mechanism was investigated.
- The modeling was based on a backward-in-time full gyroorbit-following approach assuming that the LRM target is placed between the vertical gamma camera channels #17 and #18 in the LoS of the horizontal channel #10. The calculations were performed for 560 uniformly distributed starting points on the modeled pellet-type target with 9 initial pitch-angles in each starting point. Different parabolic profiles of fusion alpha sources were considered.
- The optimum target diameter for gamma measurements is found to be less than 12 cm.
- Referring to the now disregarded previous LRM target location, it was demonstrated that the optimum position would have been close to the channel #17 LoS with the most favorable equatorial inclination of the target symmetry axis towards the channel #10 LoS of about 30 deg.
- A Beryllium Mushroom Tile was modeled and examined (see Fig. 6) as one of the possible LRM target designs.
- Recently, the TAE antenna protection tile in Octant 4 was chosen as a new LRM Be target [6]. The shape of this target has been digitized and the starting positions of test trajectories have been determined, which is shown in Fig.7.

- Our numerical tools, which have been developed so far in this context, may be used to consider any other positions of the target.

References

[1] V. Yavorskij, V. Goloborod'ko, K. Schoepf, S.E. Sharapov, C.D. Challis, S. Reznik and D. Stork. Confinement of fusion alpha-particles in JET hollow current equilibrium, 2003 *Nucl. Fusion* 43 1077 doi:10.1088/0029-5515/43/10/009

[2] V.G. Kiptily, J.M. Adams, L. Bertalot, A. Murari, S.E. Sharapov, V. Yavorskij et al Gamma-ray imaging of D and ^{4}He ions accelerated by ion-cyclotron-resonance heating in JET plasmas, *Nucl. Fusion* 45 (2005) L21–L25 doi:10.1088/0029-5515/45/5/L01

[3] M. J. Mantsinen, M.-L. Mayoral, V. G. Kiptily, S. E. Sharapov, B. Alper et al., Alpha-Tail Production with Ion-Cyclotron-Resonance Heating of 4He-Beam Ions in JET Plasmas, 2002 Phys. Rev. Lett. 88 105002. DOI: 10.1103/PhysRevLett.88.105002

[4] V. G. Kiptily, C.P. Perez von Thun, S.D. Pinches, S. E. Sharapov, D. Borbaet al., Recent progress in fast ion studies on JET, 2009 *Nucl. Fusion* 49 065030 (12pp) doi:10.1088/0029-5515/49/6/065030

[5] C.P. Perez von Thun, V G Kiptily, S Popovichev, V Yavorskij, V Goloborod'ko et al., Fast ion losses in JET hybrid scenarios - MHD sources overview, 41st EPS Conference on Plasma Physics, 23 - 27 June 2014, Berlin, Germany, P.1.007.

[6] V. Zoita, S. Soare, Lost Alpha monitor (KA4), New diagnostic location, *LRM project meeting*: JET, 22nd October, 2014.

Figures

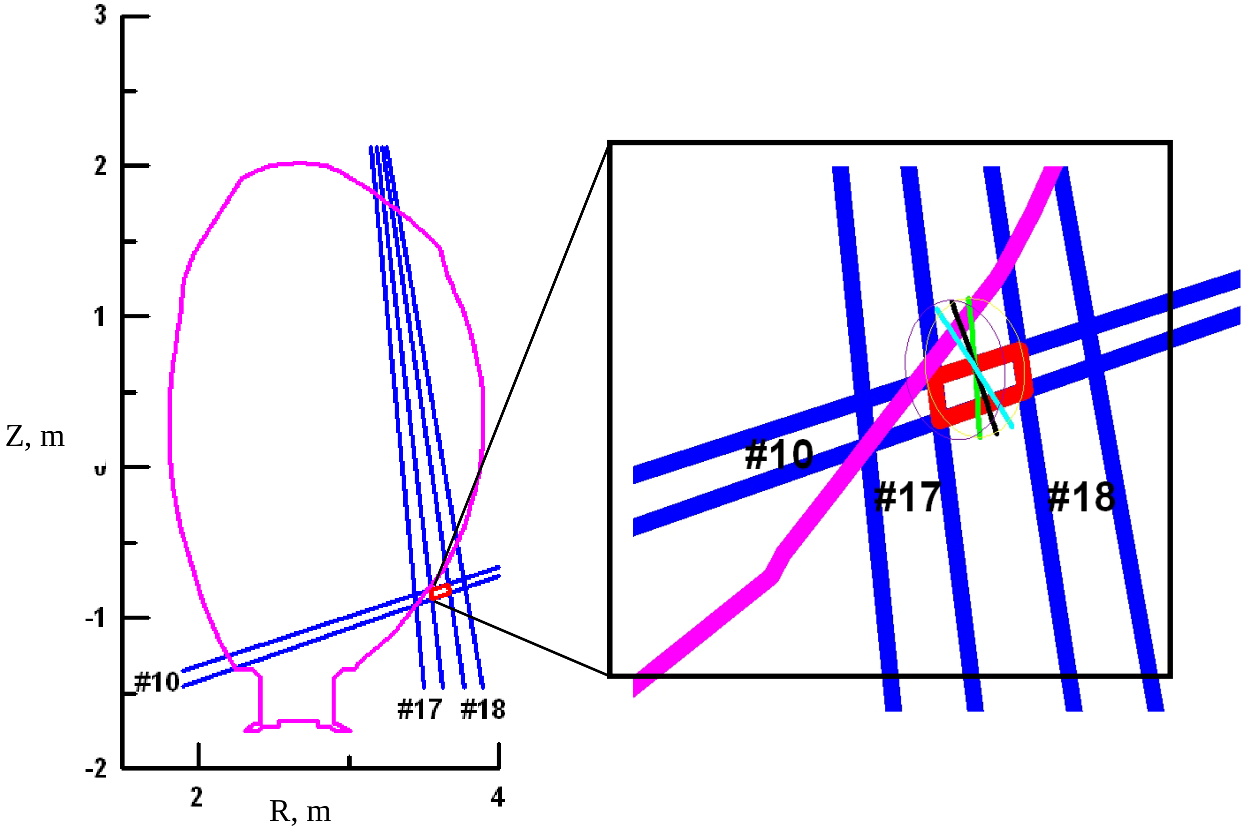

Fig.1. Expected LRM target position. Blue: gamma channels LOS. Red: possible Field of View (FOV) origin of gamma signal from LRM target. Black, green, light green: different LRM target orientations.

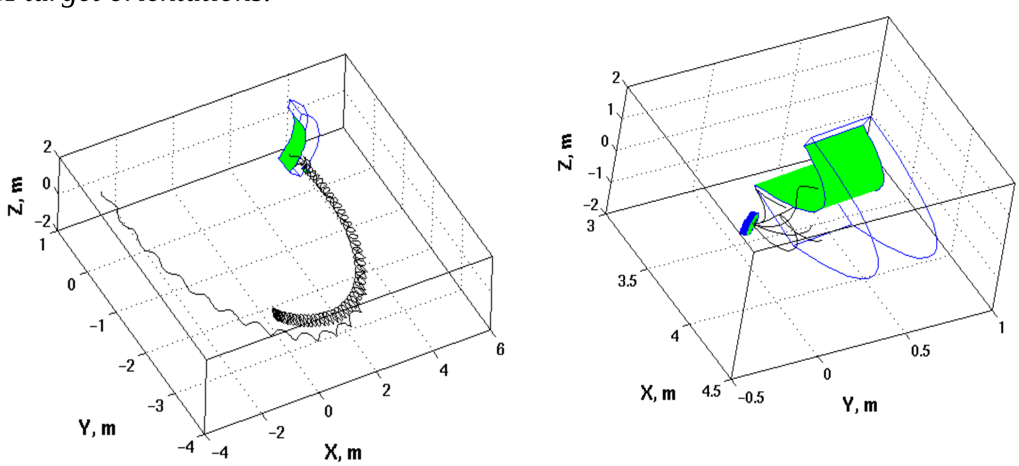

Fig.2. Example of backward-in-time trajectory calculations starting from one point on the LRM target (left) and a subset of the trajectories hitting the wide poloidal limiter (right). The target pellet is blue-colored.

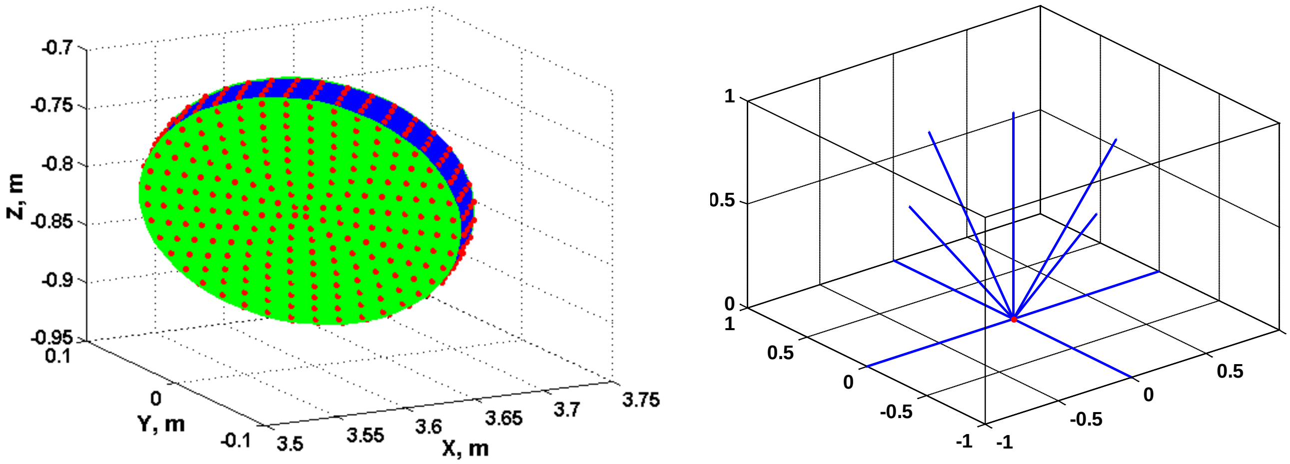

Fig.3. Left: Pellet-like LRM target with the starting points of test trajectories marked in red. Right: Starting unit velocity vectors for each starting point.

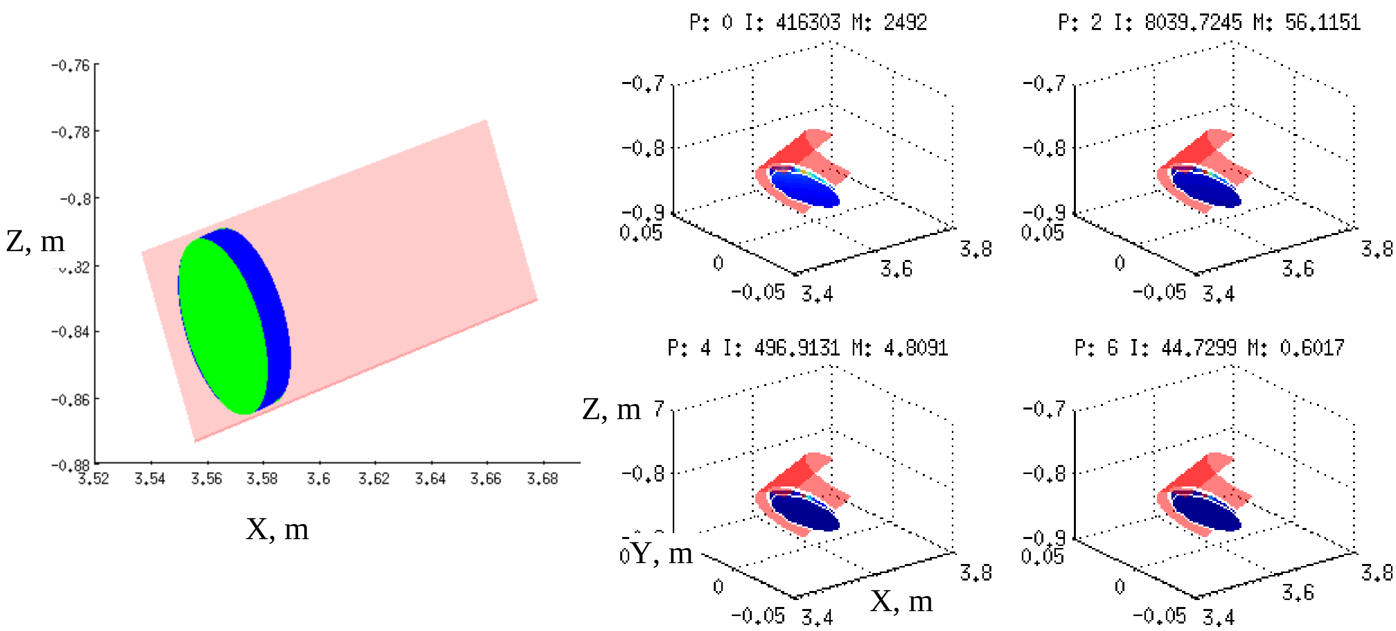

Fig.4. Left: Optimal position and orientation of a pellet-type LRM target (green and blue) in the channel #10 FoV (pink). On the RHS are shown the relative alpha flux distributions over the LRM target for different parabolic distributions of alphas in the plasma (P specifies the power of the parabolic distribution, I is the relative total alpha flux to the target and M denotes the maximum intensity of the flux).

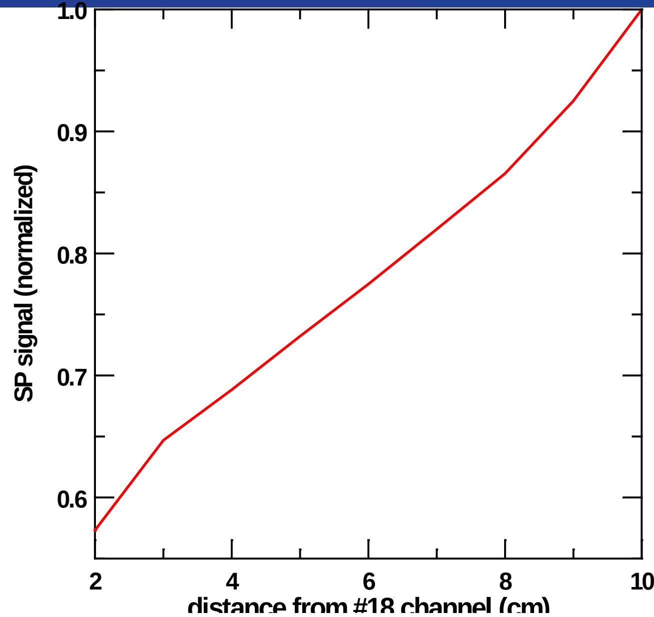

Fig.5. Dependence of the relative signal intensity when the LRM target is moved from a position 2cm apart from the channel #18 Line of Sight towards a 10 cm distance (close to channel #17). Normalization is to the maximum value.

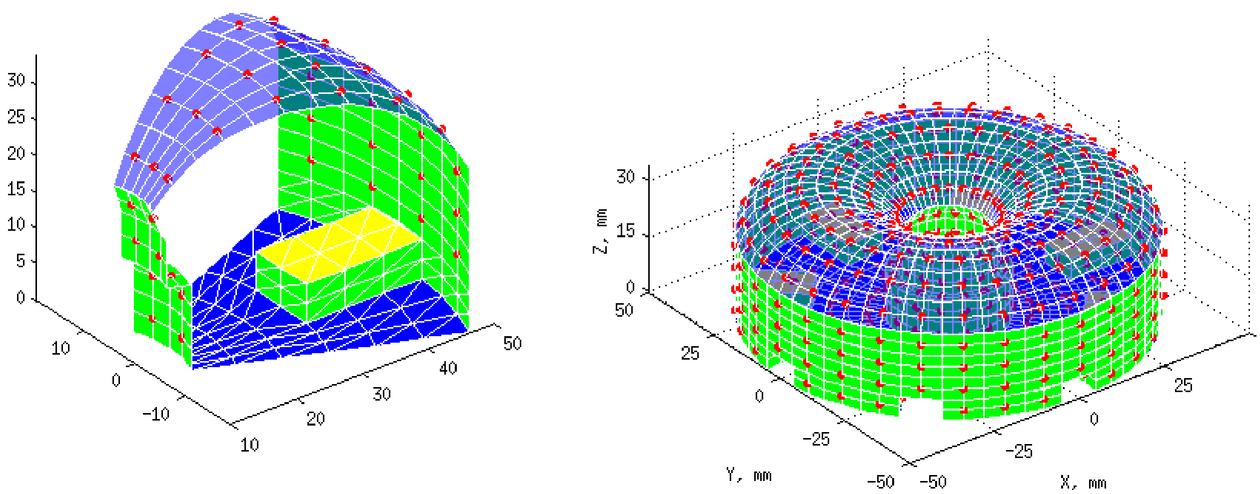

*Fig.6. Numerical model of a Be mushroom tile (1/8 element on the left) with the starting points of the test trajectories marked in red***.**

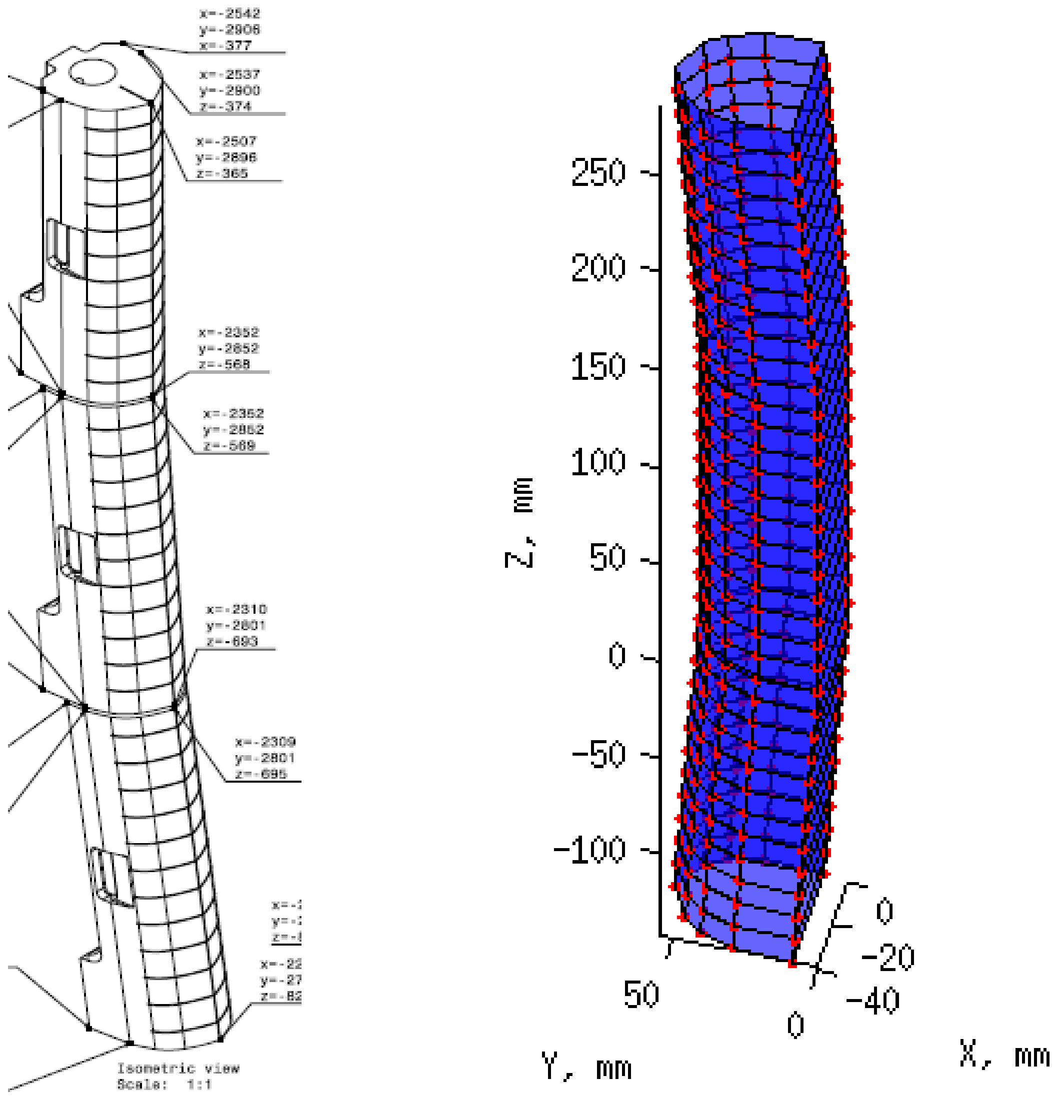

Fig.7. Drawing of the Be TAE antenna protection tile (left) and the numerical model of the tile (right) with the starting points of test trajectories marked again in red.

ANNEX 3
Evaluation of expected KA4 detector response to gamma radiation for DT experiments. Phase I
(IPPLM Report)

Lost Alpha Gamma Rays Monitor (LRM) Project
D4.01, *Report on detector response in DT experiments*

1. Evaluation of expected KA4 detector response to gamma radiation for DT experiments. Phase I

Monte Carlo simulations were performed for a 0-approx. gamma-ray background normalised to the integral spectrum provided by V.Kiptily. The spectrum, covering a range of gamma ray energy from 1.5 to 14.9 MeV, was an input to Geant4 simulations done for three $CeBr_3$ scintillators of a cylindrical shape with a diameter of 1”, 2” and 3” and a length of 1”, 2” and 3”, respectively. A beam of 10^6 parallel gamma rays, hitting perpendicularly a detector surface, was collimated on a 10 mm diameter circle. Simulations were performed for 64 gamma ray energies from the above defined gamma ray energy range. An energy resolution for each scintillator was assumed to be 4%, independent on gamma ray energy. Monte Carlo could be later repeated using an experimental energy resolution measured with a dedicated scintillator.

In Fig.1, see below, a comparison of simulated detector response is presented. The 0-approx. gamma-ray background spectrum was used to normalised number of events for each of 64 energy bins. The (red) input spectrum, labelled as “gamma background”, is arbitrary included in Fig. 1.

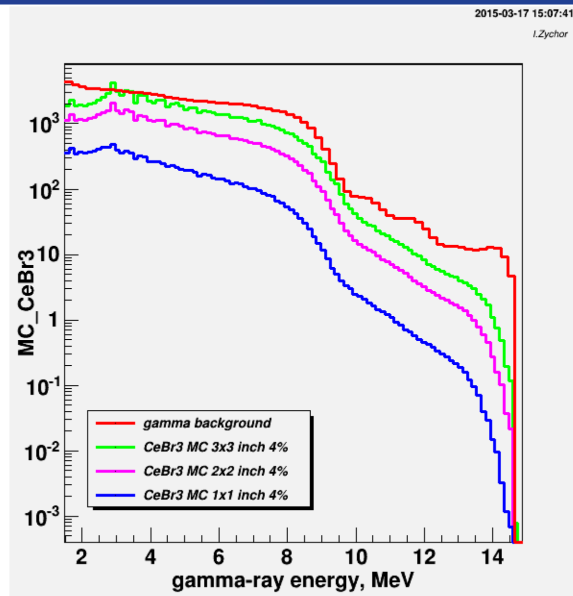

Fig. 1. *A comparison of Monte Carlo simulated detector response for $CeBr_3$ scintillators for the 0-approx. gamma-ray background used as input.*

In Table 1 a comparison of event numbers for three specific gamma ray energies is presented together with an average event number for full energy range (from 1.5 to 14.9 MeV) for three $CeBr_3$ with indicated dimensions. Numbers are normalised to those obtained for the 1”x1” $CeBr_3$ scintillator.

Table 1. *A comparison of normalised event numbers obtained from Monte Carlo simulations.*

$CeBr_3$ scintillator	average event number	event number at 1.5 MeV	**event number at 4.4 MeV**	event number at 6.1 MeV
1”x1”	1.0	1.0	**1.0**	1.0
2”x2”	4.1	4.3	**4.6**	5.0
3”x3”	8.1	8.8	**9.4**	10.8

As it was expected, bigger scintillators have a higher detection efficiency for gamma ray energies around 4.4 MeV.

2. Cost estimations for the detector options as input for the Feasibility Study Phase I.

PMT and **MPPC** photodetectors are the best candidates for light readout for scintillators in the LRM project.

PMT properties

1. Advantages
   - fast response (fast rise time, small time jitter) enabling measurements at high counting rates
   - high gain and extremely low excess noise factor resulting in good energy resolution
   - large photosensitive area (especially useful with 2” diameter scintillators)
   - fair quantum efficiency (QE) in broad light spectrum
   - large linear dynamic range in which an output signal is proportional to a registered energy
2. Drawbacks
   - sensitivity to a magnetic field (see below Figure 1 from ref. [1])

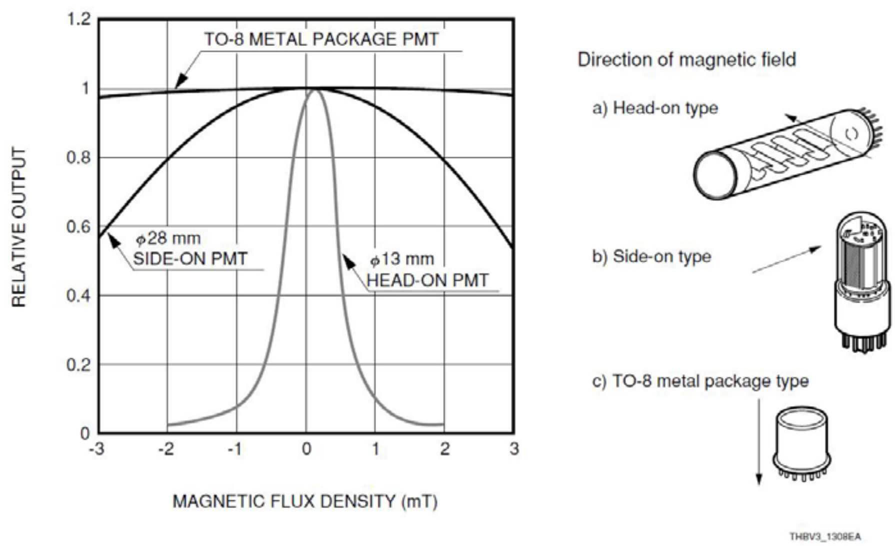

Figure 1: Magnetic characteristics of typical photomultiplier tubes

MPPC properties

1. Advantages
   - fast response enabling measurements at high counting rates
   - high gain resulting in good energy resolution
   - immunity to magnetic field

2. Drawbacks
   - gain sensitivity to temperature and voltage bias (need for gain monitoring, possible with temperature control and/or radioactive source, e.g. ^{137}Cs or ^{60}Co)
   - susceptibility to neutron damage (will be studied in 2015)

- small photosensitive area but it is not a major limitation with bright crystals like $CeBr_3$
- limited dynamic range
- a new technology, still in progress
- more challenging as there are more problems to be solved

PMT is therefore a better and more reliable solution.
It should be a first choice photodetector for LRM – but MPPC is still an alternative.

There are 2 types of PMTs that offer a reduced sensitivity to magnetic field
1. fine mesh (FM-PMT) dynode,
2. metal channel (MC-PMT) dynode (we have it at our lab).

FM-PMTs are offered in a cylindrical shape, with an outer diameter of 26 mm, 39 mm, 52 mm and a photosensitive area of 18 mm, 27 mm, 39 mm, respectively.
The FM-PMTs with outer diameter of 39 mm or 52 mm are well suited for $CeBr_3$ crystals with a diameter of 1”-2”.

MC-PMTs are usually offered in a cuboid shape, with an outer cover size of 30×30 mm, a photosensitive area is about 18×18 mm and it suites for 1” diameter $CeBr_3$ crystals.

In both cases, PMTs should be shielded with a thick layer of soft iron, e.g., Permalloy, like in the Magnetic Proton Recoil (MPR) spectrometer where 2.1 cm of soft iron was used to additionally shield the PMT [2]. The additional magnetic shielding can be constructed as a part of the holder/carrier for the detector.

To decide about a magnetic shielding, data on magnetic field in a place of an installation are needed. It is also important to know a direction of magnetic field in the detector tunnel.

From technical drawings available, e.g., from Hamamatsu, we estimate that the length of the detector with housing and space for cable input will be between 100 mm for 1” $CeBr_3$ coupled to MC-PMT and 120 mm for 1” $CeBr_3$ coupled to FM-PMT.

After necessary tests, it will be decided which PMT is better.

<u>We propose that we could participate in the updated LRM project by</u>:
1. procuring and characterizing both FM-PMT and MC-PMT coupled to $CeBr_3$. Measurements in a magnetic field could be realized in a similar way like in ref. [2] – a necessary magnetic coil must be purchased.

2. design of a detector consisting of a scintillator and PMT, based on above described measurements and Monte Carlo simulations. A possible use of a fiber optics should be discussed with our Italian partners.
3. procuring, probably at SCIONIX, a full detector setup according to the final design,
4. selecting and procuring a dedicated high voltage power supply,
5. evaluating a detector response,
6. participation in a new KA4 detector installation at JET and preparation of the documentation.

We are not able:

1. to find information about a magnetic field at the JET. Such data are necessary to design a magnetic shielding.
2. to prepare a holder/carrier for a new KA4 detector – please keep in mind that the additional magnetic shielding can be constructed as a part of the holder/carrier for the detector.

Cost estimates

1) $CeBr_3$ scintillators
    - 1”×1” – 3 kEUR
    - 2”×2” – 12 kEUR
2) PMTs for testing and final installation
    - FM-PMT – 6 kEUR
    - MC-PMT – 2 kEUR
3) HV power supply – 4 kEUR
4) final detector manufacturing (housing, magnetic shielding, voltage divider, connectors etc.) – estimated costs for one $CeBr_3$+PMT detector module: 14 – 33 kEUR. The total price depends on a scintillator size and a PMT type as well as the number of detector modules. In addition, a price of the HV power supply for each detector module must be added.
5) a coil and gaussmeter (if tests at a magnetic field should be done) – 3 kEUR

We accept a time schedule as it is now in the LRM project to manufacture a new KA4 detector by Q3 2016.

References:

[1] “Photomultiplier tubes. Basics and applications”, page 240, Hamamatsu Photonics K.K., Edition 3a, Aug. 2007

[2] F. Binda – “High Count Rate Neutron Detector Installation at JET”, Sept. 2011

ANNEX 4
Calculation of LAM target gamma-ray emission for DT experiments. Phase I
(CCFE Report)
(Double click to view the document in pdf format)


EUROfusion

Be-target γ-ray emission
in JET DT experiments (Phase I)

V G Kiptily et al

CCFE
CULHAM CENTRE FOR FUSION ENERGY

CCFE is the fusion research arm of the United Kingdom Atomic Energy Authority. This work was part-funded by the RCUK Energy Programme [grant number EP/I501045] and the European Union's Horizon 2020 research and innovation programme

ANNEX 5
Evaluation of the parasitic (12C) photon flux at the location of the KA4 detector.
(SFA/MESCS report)

KA4, divertor induced gamma transmission - Preliminary calculations

Igor Lengar, Žiga Štancar, Aljaž Čufar

Calculation with MCNP 3D model of JET
Plasma used: H mode, major radius 305 cm, v-shift 30cm

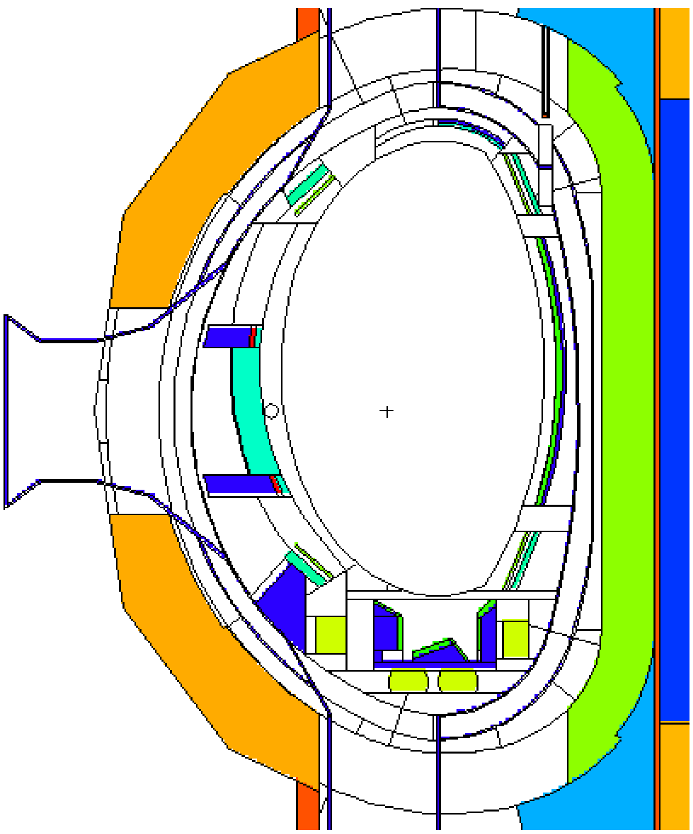

Fig. 1: Used model, 3D MCNP model of JET, H mode plasma

The full neutron transport has been performed in all calculations, the gamma transport has been calculated analytically. It was found, that in a full neutron-gamma run with MCNP, the statistics of gammas reaching the detector region behind the collimators was too low for quality results. In future runs variance reduction will be applied. Nevertheless by calculating the source of gammas in the divertor with MCNP and estimating their transport in a secondary run with a simpler model, relatively representative estimates of the gamma flux, reaching the detectors could be made.

CATIA model of the line of sight was available including two drawings:

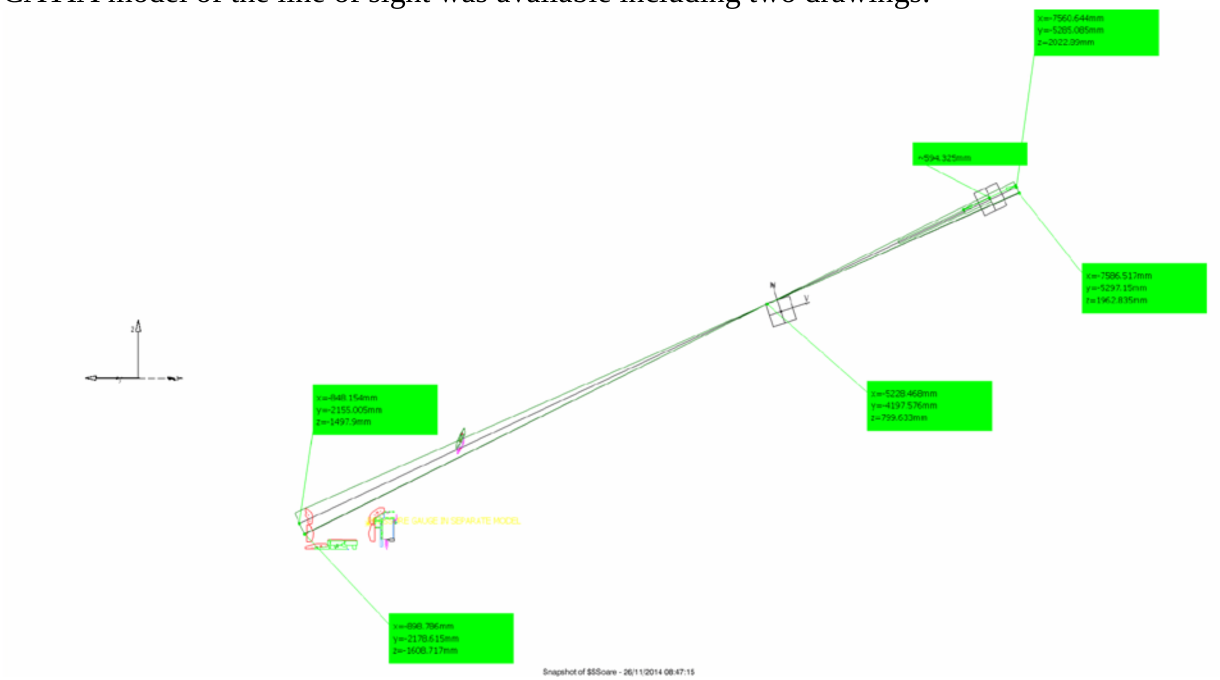

Fig. 2: The line of sight with dimensions.

Neutron transport and gamma production in divertor

The gammas at an energy of 4.439 MeV are produced in carbon via the ^{12}C (n, n’ $1^{st\ excited\ state}$) γ . The branching ration for the of 4.439 MeV gamma line from 1^{st} excited state is 100%. The neutron threshold energy for the reaction is 4.81 MeV. The cross section for neutrons is in the range of a few tenths of a barn, presented in Fig. 4.

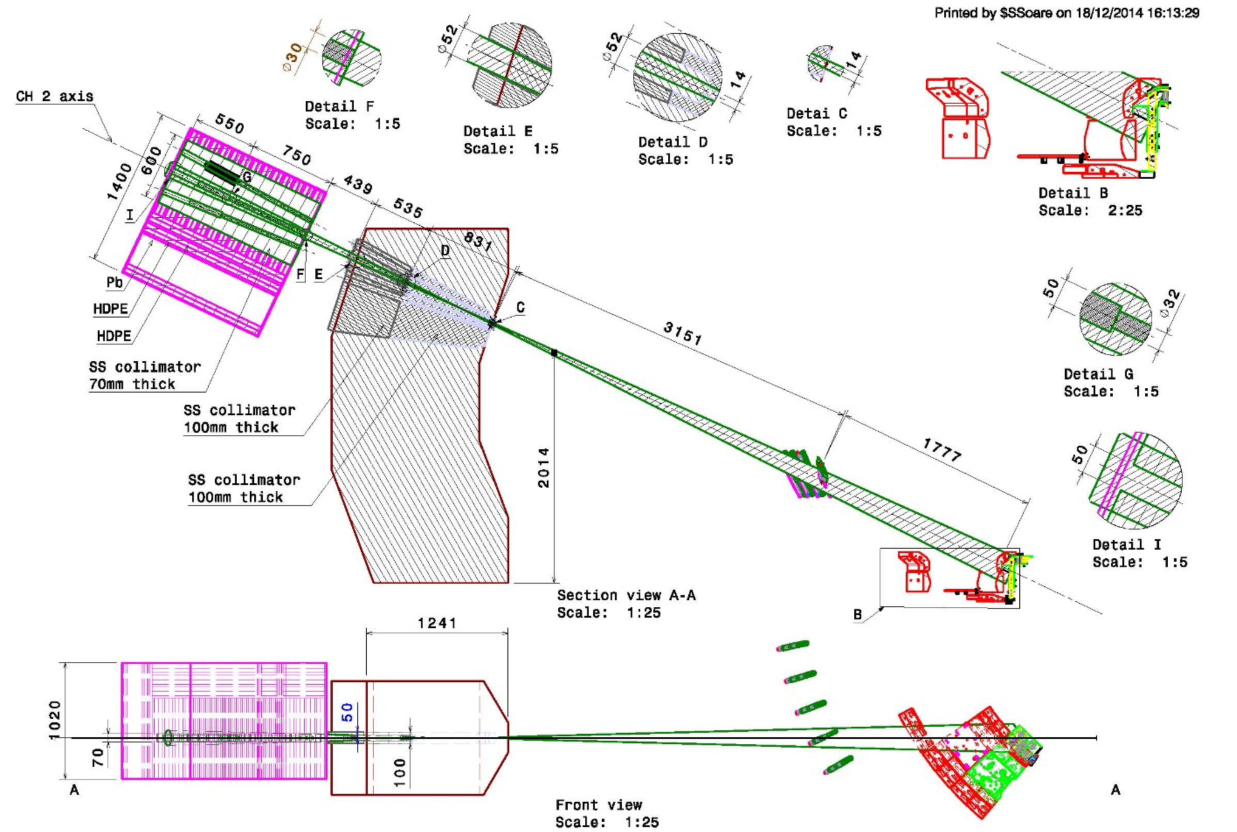

Fig. 3: The line of sight and cross-sections of the collimators with dimensions.

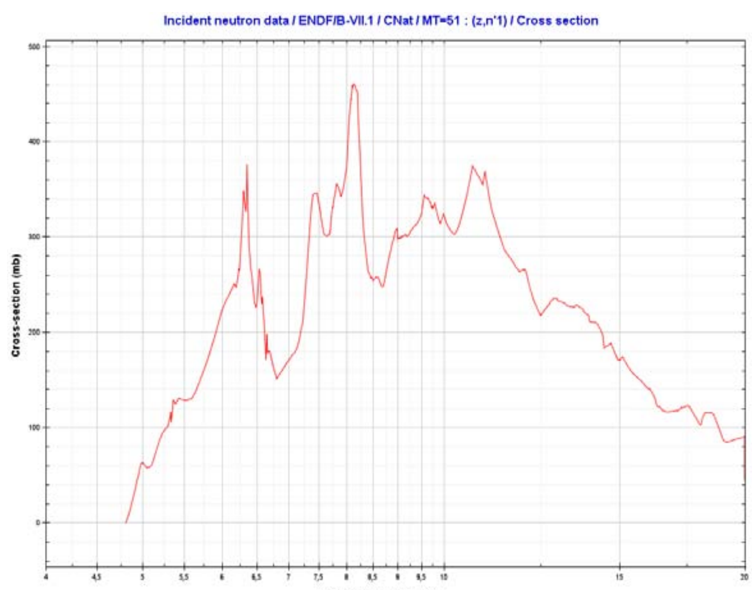

Fig. 4: Cross section for neutrons in C^{nat} for 4.439 MeV gamma production.

The spectrum in two divertor cells, within the line of sight of the KA4, channel 2 collimator, has been calculated, Fig. 5.

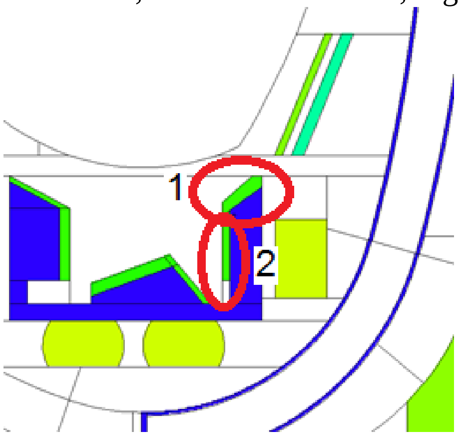

Fig. 5: Location and numbering of the divertor cells for flux and gamma production rate calculations.

The average spectra in cells 1 and 2 are presented in Figs. 6. The neutron cut-off in calculations has been set to 4 MeV. The most important component is the 14 MeV plasma peak. The average flux in cell 1 (the upper divertor cell) is approximately two times larger than in the lower cell. The values are presented /per source neutron /per MeV.

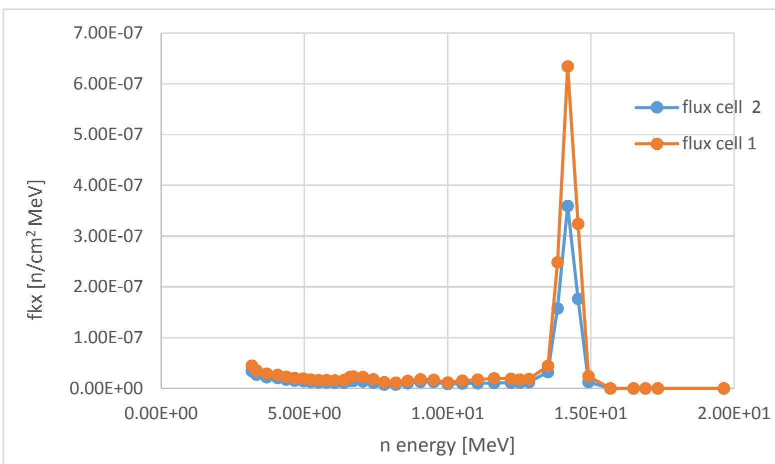

The corresponding total fluences above 4 MeV are 6.47E-07 n/cm^2 for cell 1 and 3.96E-07 n/cm^2 for cell 2 per source neutron in the plasma.

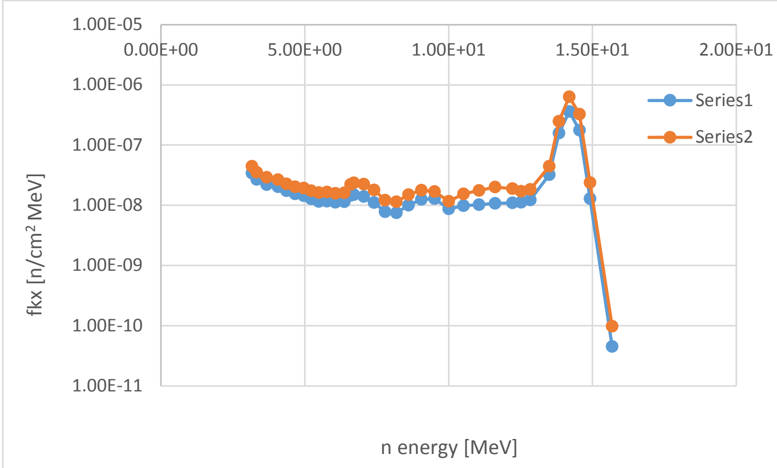

Fig. 6: Average spectra in cells 1 and 2, lin scale - upper picture, log scale – lower picture.

The neutron spectra are within MCNP convoluted with the values of the cross-section for the 4.439 MeV gamma production (Fig. 4).

The probability for gamma production /per source neutron /per C atom is

1.21E-31 for cell 1 and

7.29E-32 for cell 2 .

In order to obtain the gamma production per cm^3, the above values are multiplied by the atomic density of C atoms (within 1 cm^3, i.e. by $N_{Avogadro}$ · density / M ; for a density of CFC of 1.8 g/cm^3 and molar mass 12 g/mol), which gives the factor of 0.09 .

The graphical presentation of the density of the (n, n’ 1$^{st\ excited\ state}$) γ reaction is shown in Fig. 7 .

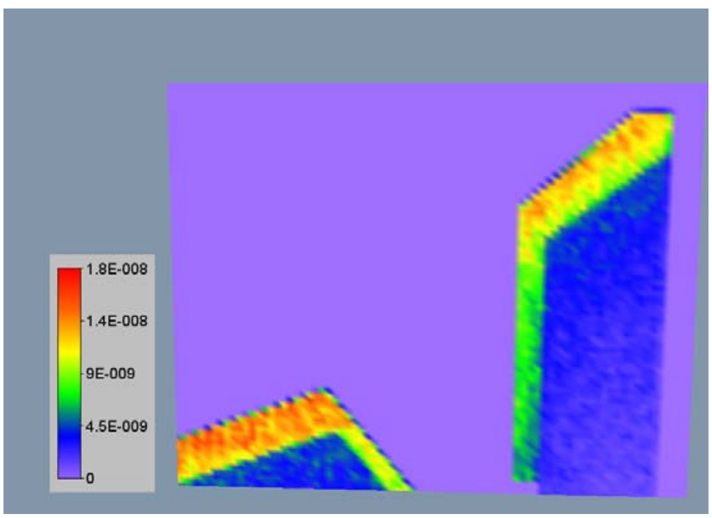

Fig. 7: Graphical presentation of the density of the (n, n’ 1$^{st\ excited\ state}$) γ reaction in the divertor. Presented as the number of reactions per cm^3 of material.

The reaction is found in carbon with a gamma energy of 4.439 MeV – visible with the most intensity in the figure – and also in the underlying Inconel – less intensity in the figure. The latter reactions (in Inconel, Cr, Mn, Fe, Ni, Cu) result in gammas of different energies and are not important since they can be discriminated from the gamma line in question; besides that, their intensity is lower, as seen from the figure. As seen, the average reaction density is approximately 1E-8 gammas / cm^3 of divertor / source neutron

Estimation of gamma rays passing through the collimator

The gammas are assumed to be produced isotropic with respect to the angle, what is a reasonable approximation. The transmission through the system of collimators has been done by using a simple MCNP model of the collimator and checked by analytical calculations.
The provided cone, representing the line of sight (Fig. 2), has been found to not adequately mimic all neutrons, passing through the collimators, since the cone is partly obstructed by the collimator structure, in particularly by the second collimator.
The ratio of the neutrons, passing from the divertor position through the collimators, has been estimated on the assumptions that the collimators are black (do not transmit gammas) and that the gamma absorption within the divertor (for gammas produced in the lower layers of the divertor), can be neglected. The last assumptions gives a conservative, slight overestimation of the gammas exiting the divertor since the transmition for 4.4 MeV gammas in carbon is 74% for a 6 cm carbon thickness. The average transmission is however much closer to 100% since the intensity of gamma production is higher in the upper layers of the divertor, i.e. the average transmission would be around 0.9 .
The limiting apertures from Fig. 2 and 3 have been found to amount to and be positioned at a distance from the divertor of :

distance from divertor (cm)	aperture diameter (mm)
492.8	14
575.9	14
673.3	30
748.3	32

The simple MCNP model of the collimator is presented in Fig. 8.

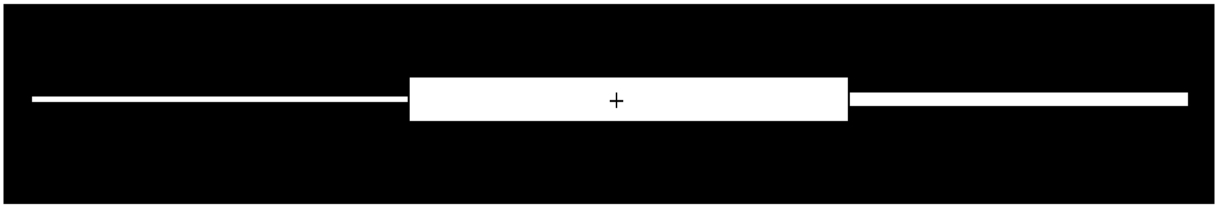

Fig. 8: Simple MCNP model of the collimator line of signt; presented is only the collimator and not the origin of the divertor gammas, located 5m from the collimator to the left.

The number of the gammas, passing through the collimator from an infinite layer at the position of the divertor with an surface strength of 1 gamma produced per 1cm^2 of source surface isotropic with respect to the angle at the distance of 492.8 m from the opening (thus at the surface of the divertor) has been found to amount to 1.32E-05 .
The number of gammas produced in the divertor per 1 DT neutron from the plasma has been previously discussed and the average number has been found to be 9.0E-09.
The average thickness of the divertor in the line of sight, from which the gammas are emitted, is found to be 6 cm.
The final number of gammas, reaching the detector through the collimator is the multiplier of all the three above numbers and found to be 7.1E-13 and rounded to 1 significant digit to be:

1E-12 $\gamma^{4.44MeV}$/source neutron.

More accurate calculations will be performed with a coupled neutron-gamma run. Prior to that variance reduction techniques will have to be accordingly adjusted and applied since in a direct MC run the statistics for the result of the number of gammas at the desired position is too low.

ANNEX 6
MCNP calculations for the LAM Line of Sight
(IAP Report)

Lost Alpha Gamma Rays Monitor (LRM)

MCNP calculations for the LAM Line of Sight

T. Craciunescu[1], S. Soare[2], V.L. Zoita[2]

[1] IAP EUROfusion Research Unit, National Institute for Laser, Plasma and Radiation Physics (NILPRP), Magurele, Ilfov, Romania

[2] IAP EUROfusion Research Unit, National Institute for Cryogenics and Isotopic Technologies (ICIT), Rm. Valcea, Romania

SUMMARY

In order to assess the operational features of the Lost Alpha Monitor (LAM/KA4) radiation system an evaluation of its collimation and shielding characteristics was required. The evaluation has been performed by means of Monte Carlo numerical simulations using the MCNP-6.1 code using point gamma-ray sources emitting within a defined narrow solid angle which ensures the coverage of the structures of interest. The point gamma-ray sources are placed at positions equivalent to KA4 target, the TAE antenna protection tile. The MCNP model takes into account both the existing KJ5 radiation shield and the newly designed LAM/KA4 radiation collimator and shield.

The MCNP numerical results show that the combination of the two radiation shields (KJ5 and KA4) provides adequate shielding and collimation for the KA4 detector, and that shielding factors of about 10^3 can be obtained. On the other hand, the designed KA4 configuration has to be improved in order to allow a larger area of the beryllium target to be seen by the KA4 detector.

CONTENTS

1. Introduction.

A new gamma-ray technique to measure escaped alpha-particles in JET was proposed to be developed within the EUROfusion Lost Alpha Gamma Rays Monitor (LRM) project. This new JET KA4 diagnostics was proposed [1-2] to be based on the nuclear reaction $^{9}Be(\alpha,\gamma n)^{12}C$ presently used for the JET gamma-ray spectrometers. Escaped alpha particles with energies in excess of 1.7 MeV interacting with a bulk beryllium target will produce 4.44-MeV gamma-radiation. Measurements of the gamma radiation will provide the rate of fast alpha particle losses. Eventually the alpha particle monitor will provide a local value of the lost fast particle flux (number of lost particles per unit surface and time).

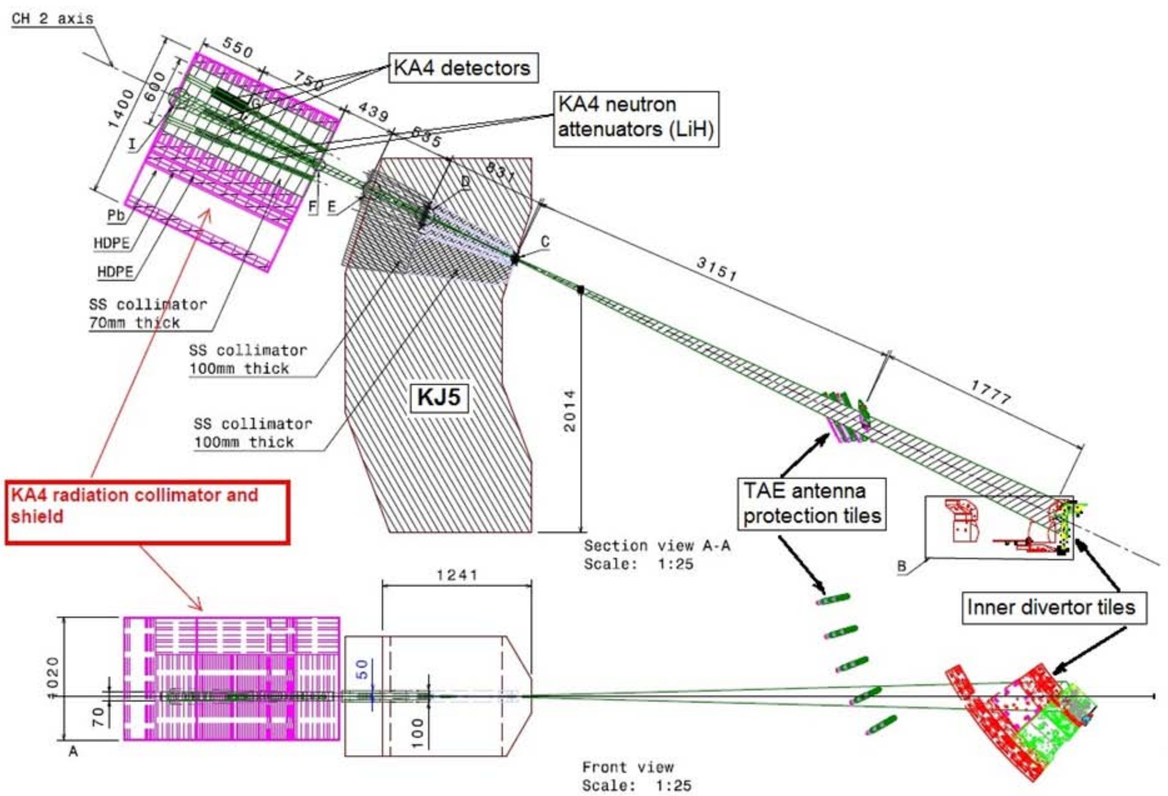

Figure 1: Overall view of the LAM/KA4 radiation system

A conceptual design for the KA4 diagnostics has been developed and it resulted in a complex radiation system. An overall view of the LAM/KA4 radiation system is shown in Figure 1, including the following main components, from left to right:

-KA4 radiation collimator and shield

-KJ5 radiation collimator and shield

-TAE antenna protection tiles
The KA4 radiation collimator and shield houses the KA4 detectors and the KA4 neutron attenuators having lithium hydride (LiH) as the neutron attenuating medium. The KJ5 radiation collimator and shield operates as a pre-collimator and shield for the LAM/KA4 diagnostics. One of the TAE antenna protection tiles represents the KA4 beryllium target that will emit the gamma radiation from the nuclear reaction $^{9}Be(\alpha, n\gamma)^{12}C$.

2. Gamma-ray transport calculations: MCNP model

In order to assess the operational features of the KA4 radiation system an evaluation of its collimation and shielding characteristics was required. The evaluation has been performed by means of Monte Carlo numerical simulations using the MCNP-6.1 code [3]. A full description of the radiation field at the specific positions of interest would involve complex and long duration calculations which are much beyond the possibilities (resources) of this project. It was therefore decided to use the Monte Carlo simulation for the evaluation of the photon flux at the desired locations in a simplified geometry that uses point photon sources emitting within a defined narrow solid angle which ensures the coverage of the structures of interest. The gamma-ray emission is characterized by a Gaussian shape - mean energy at E = 4.4MeV and a full width at half maximum (FWHM) of 0.1 MeV. The photon source has been placed at the position of the KA4 target (the TAE protection tile, see Figure 1), both on the LAM/KA4 diagnostics symmetry axis and at several off-axis positions obtained by displacements on a direction perpendicular to the symmetry axis (Figure 2). The photon source displacements from the symmetry axis are given in Table 1.

Table 1: Source positions displacements from the LAM/KA4 symmetry axis

Displacements (mm)
20
40
60
80.5
161

Table 2: Displacements of the virtual detector positions

Displacements (mm)	
KJ5 shield	**KA4 shield**
23.5	52.5
35.0	105

At the location of interest the photon flux has been calculated in a specific cell (called *virtual detector*). Figure 2 shows the position of the virtual detector inside the KA4 radiation shield. For the MCNP configuration model, the virtual detector positions are illustrated in Figures 3 and 4. For both KJ5 and KA4 radiation shields one virtual detector is located on the channel symmetry axis. For the KA4 radiation shield the virtual detector is located immediately after the attenuator. The other virtual detectors are displaced, along a perpendicular direction. The values of the displacements are given in Table 2. The virtual detectors located inside the KJ5 radiation shield have a cylindrical shape with radius R = 0.25 cm and height H = 0.9 cm. The virtual detectors located inside the KA4 radiation shield are also cylinders with radius R = 1.05 cm and height H = 0.9 cm.

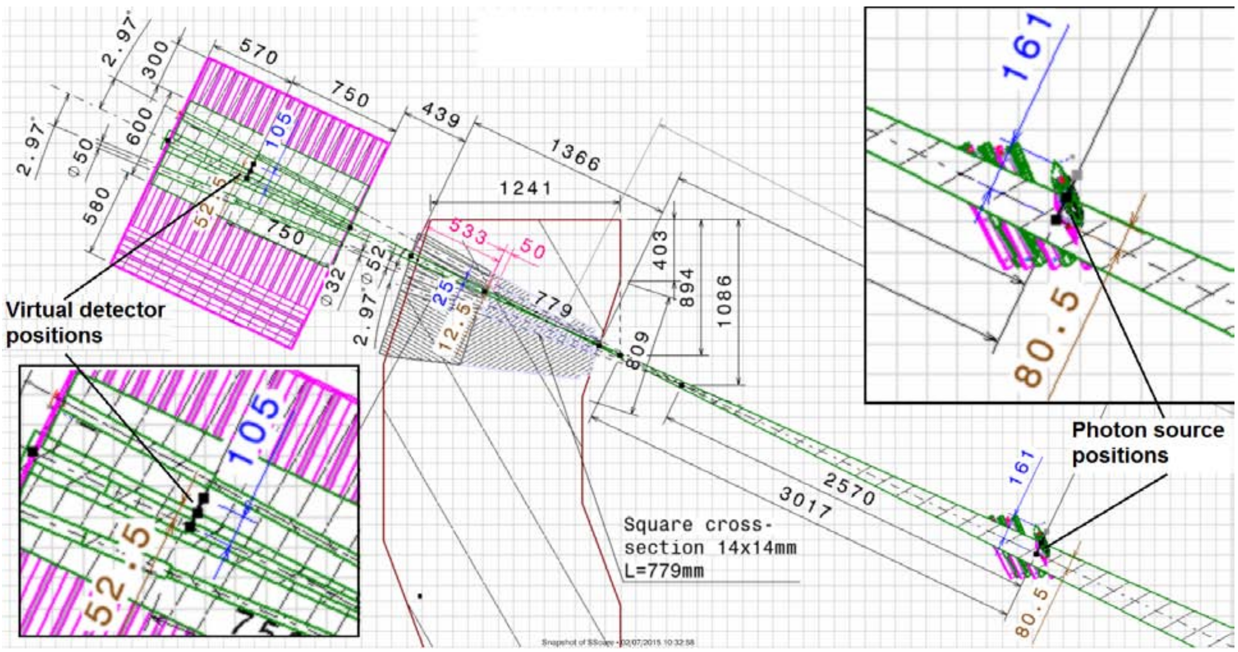

Figure 2: Positions of the photon source and virtual detector. The inserts are zoomed-in views of the target region (photon source) and detector region, with the detector inside the KA4 radiation collimator and shield.

3. Gamma-ray transport calculations: MCNP results

The results of the simulations together with their uncertainties are given in Table 3. The total number of photons generated ensures a good enough statistics except for the cases of large source position displacement and displaced detectors for KA4 radiation shield. In these cases the cumulative effect of the radiation shields located between source and detector lead to a very high attenuation. For a number of cases no photons arrived at the detector location. However this does not impede the physical interpretation.

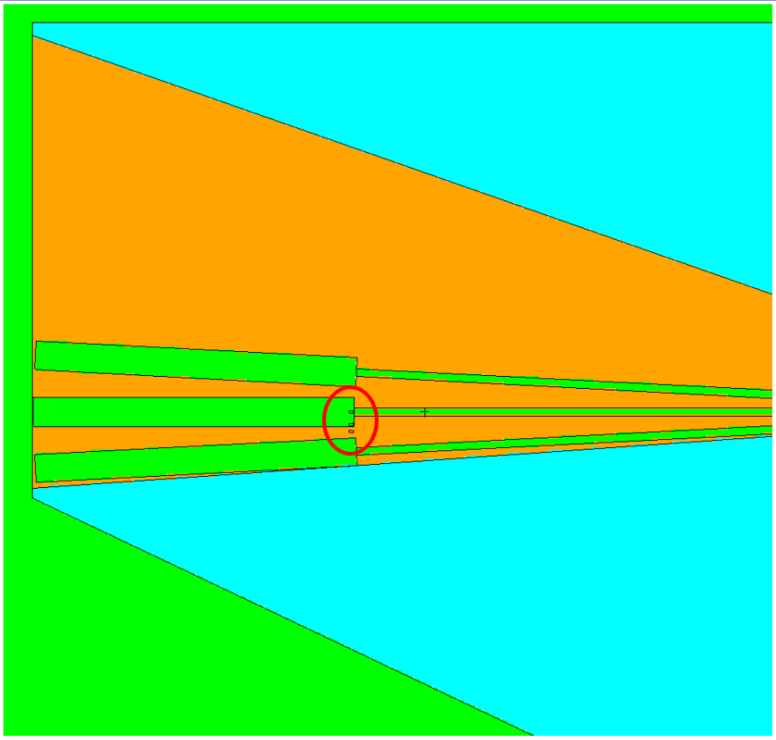

Figure 3 – MNCP geometry detail showing the location of the virtual detectors inside the KJ5 radiation shield (circled in red)

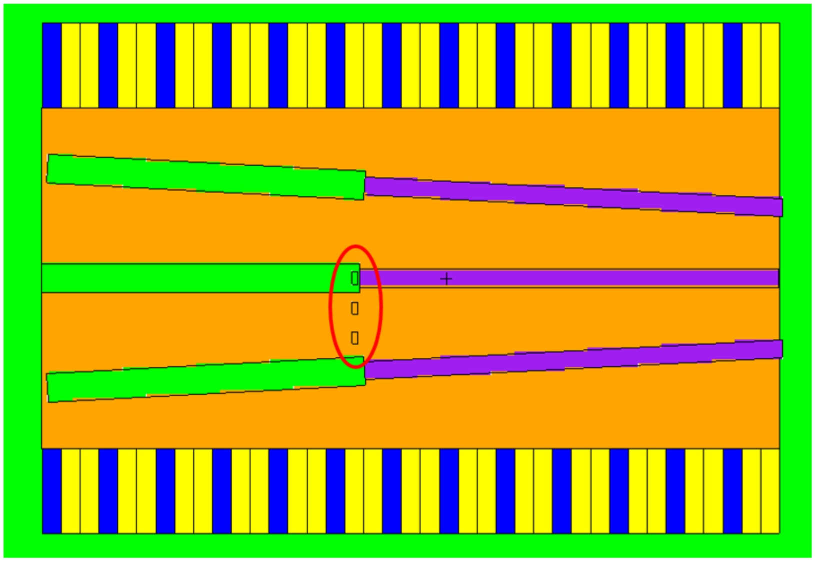

Figure 4 – MNCP geometry detail showing the location of the virtual detectors inside the KA4 radiation shield (circled in red)

Table 3

Radiation shield	Virtual detector Position			Source Position	No of generated photons
	on axis	at 2.3 cm	at 3.5 cm		
KJ5	Gamma-ray flux and associated uncertainty (relative to one source particle)				
	9.9 E-07 0.2 %	1.2 E-09 4.7 %	5.6 E-10 6.8 %	on axis	3.0 E+09
	8.3 E-07 0.3%	1.2 E-09 5.7%	5.6 E-10 6.0%	2.0 cm displacement	2.0 E+09
	3.4 E-07 0.4%	1.0 E-09 4.7%	5.6 E-10 6.3%	4.0 cm displacement	2.0 E+09
	2.1 E-08 1.3%	0.7 E-09 3.1%	5.4 E-10 4.5%	6.0 cm displacement	3.0 E+09
	6.7 E-09 2.6%	8.2 E-10 6.1%	5.6 E-10 4.4%	8.05 cm displacement	3.0 E+09
	8.1 E-10 2.8%	1.9 E-10 3.1%	3.4E-10 5.2%	16.1 cm displacement	3.0 E+09
KA4	8.8 E-08 0.2%	1.5 E-10 4.8%	1.1 E-11 17.7%	on axis	3.0 E+09
	2.9 E-08 0.4%	1.1 E-10 7.3%	7.3 E-12 27%	2.0 cm displacement	2.0 E+09
	6.1 E-11 7.5%	1.8 E-12 45.8%	6.5 E-13 90%	4.0 cm displacement	2.0 E+09
	4.3 E-12 21.8%	*No particles recorded*	*No particles recorded*	6.0 cm displacement	3.0 E+09
	2.8 E-12 31.6%	*No particles recorded*	*No particles recorded*	8.5 cm displacement	3.0 E+09
	2.3 E-12 16.9%	*No particles recorded*	*No particles recorded*	16.1 cm displacement	3.0 E+09

The dependence of the photon flux on the source position is illustrated in Fig. 5 for the detectors located on the diagnostics axis of symmetry.

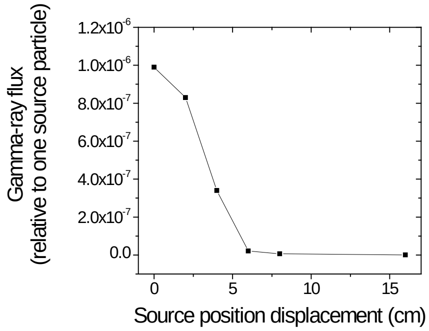

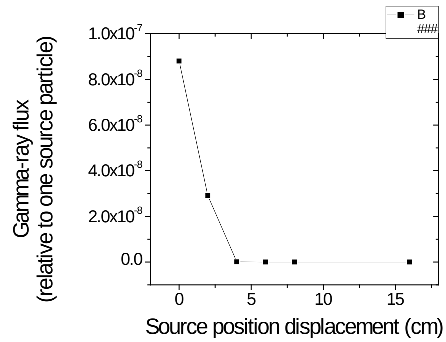

Figure 5: The dependence of the photon flux on the source position for the detectors located on the KA4 diagnostics axis of symmetry in case of KJ5 (left) and KA4 (right) radiation shields.

The numerical results show the following:

-The combination of the two radiation shields (KJ5 and KA4) provides adequate shielding and collimation for the KA4 detector. By comparing the values of the gamma-ray flux inside the KA4 shield with the virtual detectors on the axis and at radius of 4cm one can see that a shielding factor of about 10^3 is obtained. A similar comparison for the detector placed inside the KJ5 shield shows that he KJ5 shield alone would not provide sufficient shielding and collimation for the KA4 detector.

-With the designed KA4 configuration a target of only about 5 cm diameter would be seen by the gamma-ray detector. This is about 25% of the minimum recommended beryllium emission surface for an acceptable level of the signal-to-background ratio.

4. Conclusions

In order to assess the operational features of the Lost Alpha Monitor (LAM/KA4) radiation system an evaluation of its collimation and shielding characteristics was required. The evaluation has been performed by means of Monte Carlo numerical simulations using the MCNP-6.1 code using point gamma-ray sources emitting within a defined narrow solid angle which ensures the coverage of the structures of interest. The point gamma-ray sources are placed at positions equivalent to KA4 target, the TAE antenna protection tile. The MCNP model takes into account both the existing KJ5 radiation shield and the newly designed LAM/KA4 radiation collimator and shield.
The MCNP numerical results show that the combination of the two radiation shields (KJ5 and KA4) provides adequate shielding and collimation for the KA4 detector, and that shielding factors of about 10^3 can be obtained. On the other hand, the designed KA4 configuration has to be improved in order to allow a larger area of the beryllium target to be seen by the KA4 detector.

References

[1] Kiptily V.G. et al. Fusion Technol. 22 (1992) 454

[2] Kiptily V.G. et al., Fusion Alpha-Particle Diagnostics for DT Experiments on the Joint European Torus, Presentation to the International Conference on Fusion Reactor Diagnostics, Villa Monastero, Varenna (Italy), September 2013.

[3] *** MNCP 6.1, Monte Carlo N–Particle Transport Code System, https://mcnp.lanl.gov/

EUROfusion

Be-target γ-ray emission in JET DT experiments (Phase I)

V G Kiptily et al

CCFE CULHAM CENTRE FOR FUSION ENERGY

CCFE is the fusion research arm of the **United Kingdom Atomic Energy Authority.** This work was part-funded by the RCUK Energy Programme [grant number EP/I501045] and the European Union's Horizon 2020 research and innovation programme

This work has been carried out within the framework of the EUROfusion Consortium and has received funding from the European Union's Horizon 2020 research and innovation programme under grant agreement number 633053. The views and opinions expressed herein do not necessarily reflect those of the European Commission.

JET Lost Alphas γ-ray Monitor

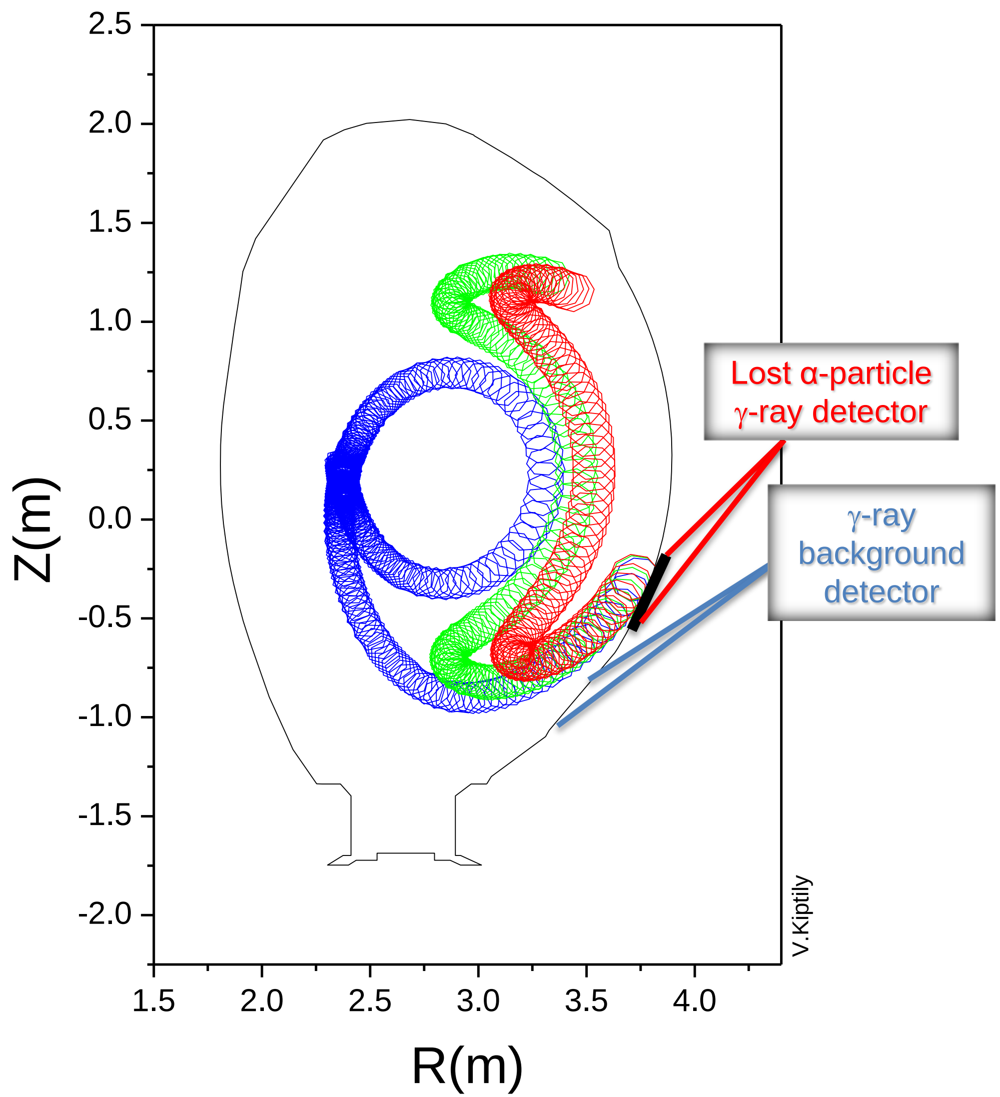

Technique:

- Escaped alphas strike **a solid target**
- Measurement of **gammas** from the alpha-induced nuclear reaction
- A thick **target** is placed in field of view of a gamma-detector, avoiding observation of W-CFC tiles
- A separate detector for background measurements is needed

Kiptily et al Fusion Technology 22 (1992) 454

Nuclear reaction for α-particle measurements

$$^{9}Be + \alpha \rightarrow {}^{13}C^{*} \xrightarrow{n} {}^{12}C^{*} \xrightarrow{\gamma} {}^{12}C$$

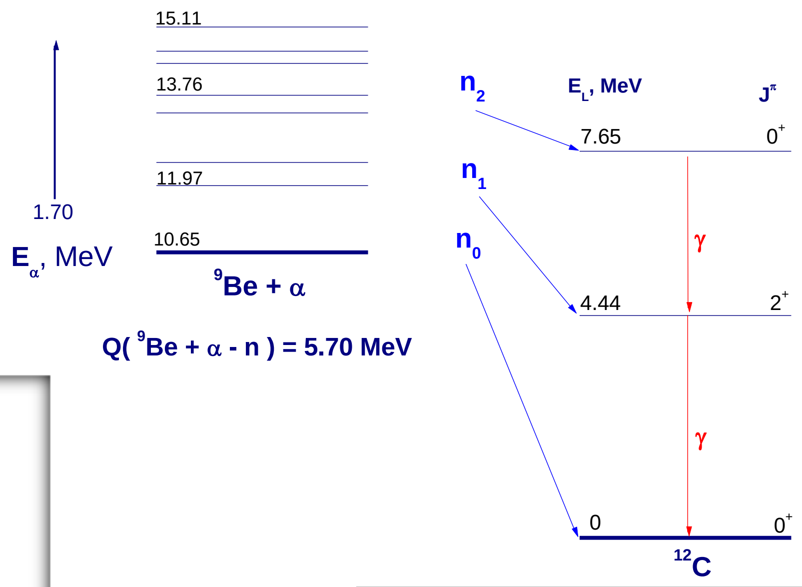

The nuclear reaction between fast α and ^{9}Be impurity leads to:

- Excitation of high-energy levels in $^{13}C^*$ nucleus
- De-excitation by emitting neutrons with population of the low-lying levels in $^{12}C^*$
- Further de-excitation by γ3.21 MeV and γ4.44 MeV to the ground state of ^{12}C nucleus:
  - ✓ γ4.44 MeV (1st level) are produced by $E_\alpha > 1.7$ MeV
  - ✓ γ3.21 MeV (2nd level) are produced by $E_\alpha > 4$ MeV

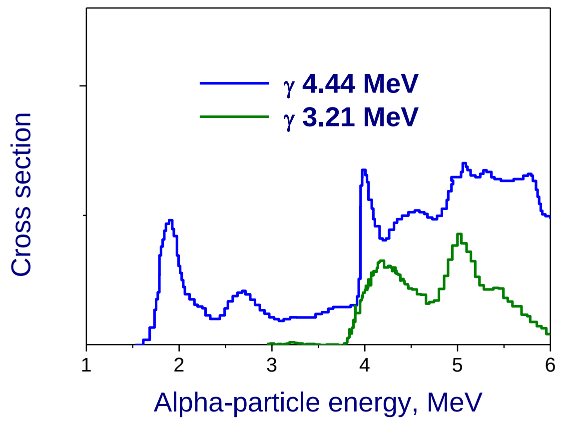

JET

JET Lost Alphas γ-ray Monitor rates

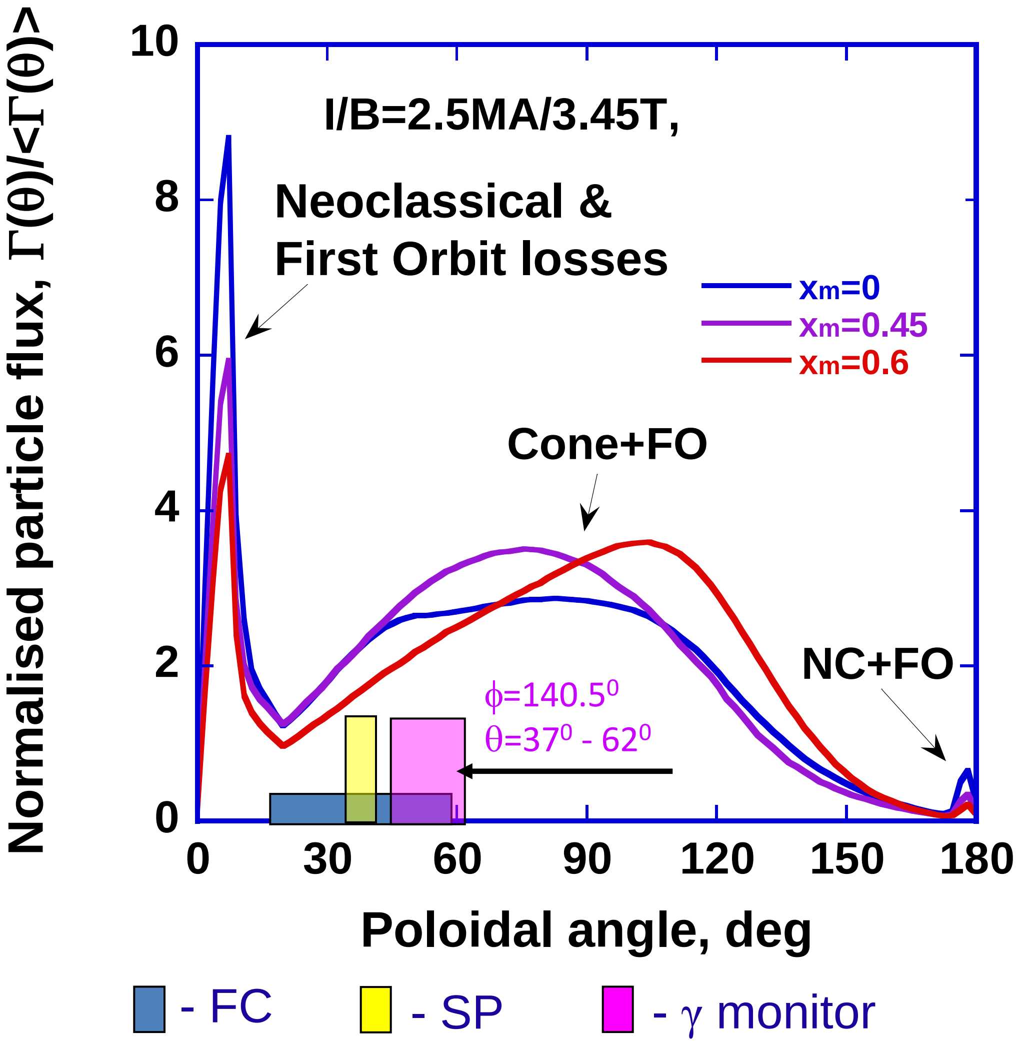

Yavorskij et al NF **43** (2003) 1077

Alpha-particle losses at $\theta=37^0-62^0$

First Orbit & Cone losses

α-loss flux :

- @ I_p= 2.5-3MA => ~ 1.3-2.5*10^{-3} $m^{-2}s^{-1}$

Diffusive/Convective type of losses

α-loss flux for $\theta>25^0$:

- ~ 3.1*10^{-4} m^{-2} s^{-1} @ I_p= 2.5MA

see Yavorskij's talk

JET

γ-ray monitor & background emission

$^9Be(\alpha,n\gamma)^{12}C$ reaction-rate per DT-neutron:

- ~ 3.8 – 7.5*10^{-09} m^{-2} s^{-1} @ I_p= 2.5-3MA

& diffusive/convective for $\theta>25^0$:

- ~ 9.4*10^{-10} m^{-2} s^{-1} @ I_p= 2.5MA

@ DT neutron-rate = 10^{19} s^{-1}

4.44-MeV Be-target γ-emission:

- ~ 4.7 – 8.4*10^{10} m^{-2} s^{-1} (@ I_p= 2.5-3MA)

4.44-MeV background γ-emission of 4-kg CFC-tile:
According to Igor's Cells #1,2 ~ 1.5 – 2.4*10^{14} s^{-1}
Independent assessments ~ 4*10^{14} s^{-1}

JET

An alternative nuclear reaction for α-particle measurements

$$^{10}B + \alpha \rightarrow {}^{14}N^* \xrightarrow{p} {}^{13}C^* \xrightarrow{\gamma} {}^{13}C$$

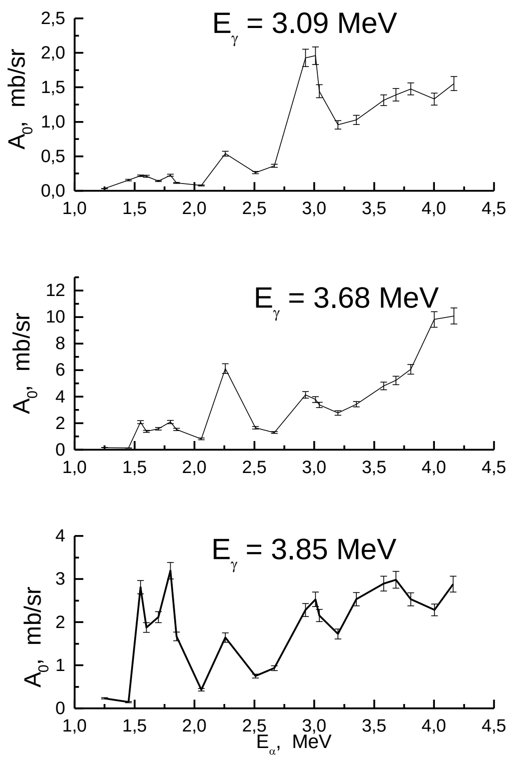

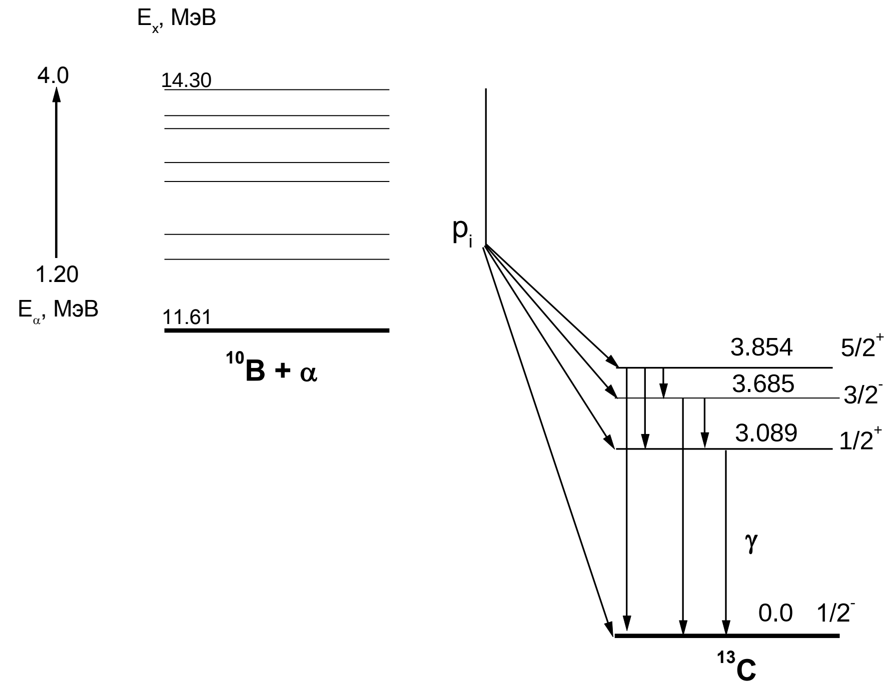

Kiptily V.G et al, Bull. Rus. Acad Sci **63** no.5 (1999) 898-909

Kiptily V.G et al, "Gamma Ray Spectrometry in ITER: Conceptual Design" in: Diagnostics for Experimental Thermonuclear Fusion Reactors 2, P.E.Stott, G.Gorini, E.Sindoni, eds., Plenum Press, New York&London, 1998.

The nuclear reaction between fast α and ^{10}B impurity leads to:

- Excitation of high-energy levels in $^{14}N^*$ nucleus
- De-excitation by emitting protons with population of the low-lying levels in $^{13}C^*$
- Further de-excitation by γ3.09 MeV, 3.68 MeV and γ3.85 MeV to the ground state of ^{13}C nucleus

JET

An alternative nuclear reaction for α-particle measurements

$^{9}Be(\alpha,n)^{12}C$ neutron measurements:

- ✓ 2-MeV alphas produce neutrons $E_0 \approx 7.6$ MeV, $E_1 \approx 2.8$ MeV
- ✓ 3.5-MeV alphas produce $E_0 \approx 7.6 - 9.0$ MeV, $E_1 \approx 2.8 - 4.2$ MeV
- ✓ Due to the alpha slowing down, the neutron spectrum is continuous, which cannot be separated from the DT-neutron background

$^{10}B(\alpha,p\gamma)^{13}C$

- ✓ Cross-sections ~ 2 times less than $^{9}Be(\alpha,n\gamma)^{12}C$ rate
- ✓ A lost alphas energy resolution – 3 energy levels
- ✓ A possible test in D-plasma with $^{10}B(t,n\gamma)^{12}C$ reaction
- ✓ $^{10}B(n,\gamma)^{11}B$ thermal capture generates γ4.4-MeV
- ✓ $^{10}B(n,\alpha\gamma)^{7}Li$ with a huge γ0.478-MeV gamma-rate
- ✓ CFC-problem is not solved: $(n,n'\gamma)$ 4.44-MeV gammas produce a terrible background conditions for 3.1, 3.68 and 3.85-MeV gammas of ^{13}C.